TÉCNICO LISBOA

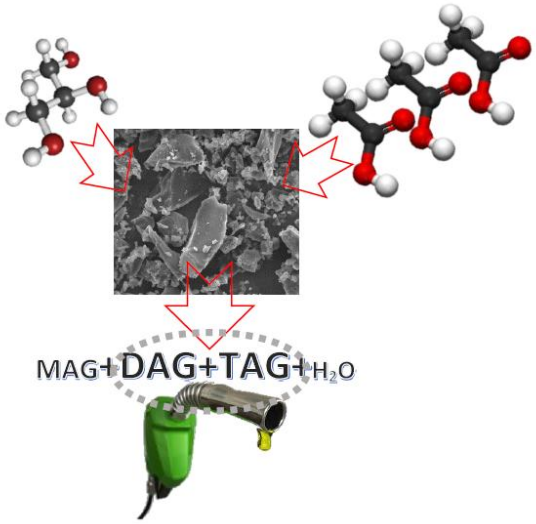

Glycerin from Biodiesel

Valorization by Acetylation

Tânia Filipa Pereira Cordeiro

Thesis to obtain the Master of Science Degree in

Chemical Engineering

Supervisor(s): Prof.ª Doutora Ana Paula Vieira Soares Pereira Dias

Eng. Sandra Marina Reis do Couto Ferreira dos Santos

Examination Committee

Chairperson: Prof. Carlos Manuel Faria de Barros Henriques

Supervisor: Prof.ª Ana Paula Vieira Soares Pereira Dias

Member of the Committee: Prof. Jaime Filipe Borges Puna

June 2017

Agradecimentos

Em primeiro lugar quero agradecer à minha orientadora Ana Paula Soares Dias, pela belíssima oportunidade de me ter dado um tema desafiante e bastante fascinante. Além do mais, quero agradecer-lhe todo o apoio, esforço, carinho e simpatia que teve para comigo ao longo desta tese.

Aos meus colegas de laboratório obrigada pela recepção e companhia.

À professora Norberta Pinho agradeço pela disponibilidade do equipamento GC, bem como aos engenheiros Nuno Simões e Alexandre Júlio pela paciência que tiveram comigo durante o funcionamento do equipamento. Obrigada à engenheira Marina Reis pela disponibilidade da glicerina bem como em esclarecer dúvidas.

Muito obrigada Marta, Célia, Dani, Filipe, Vera, Ricardo, Fred e João, por me apoiarem sempre nos bons e maus momentos.

Aos mais importantes de todo o Universo, quero agradecer aos meus pais Joaquim e Teresa por todos os sacrifícios que fizeram por mim sem nunca duvidarem das minhas capacidades. Meu irmão Daniel Filipe que adoro tanto! e nunca perde o optimismo. À Sissi pela ternura e carinho. E por fim ao Nuno Miguel, amor da minha vida, que me incentiva e desafia a querer sempre mais.

Resumo

De modo a melhorar a competitividade do biodiesel, face ao diesel origem fóssil, a glicerina coproduzida tem que ser valorizada. Num contexto de mercado saturado devido à crescente indústria do biodiesel, a produção de aditivos oxigenados para o diesel é apontada como uma aplicação viável para a glicerina.

Estudou-se a produção de acetatos de glicerol (acetinas) por acetilação da glicerina com ácido acético sobre catalisadores heterogéneos ácidos. Montmorilonites comerciais (K10, K30 e KSF) e carvões, com ativação ácida, foram usados na acetilação da glicerina pura (99.9 %) e crude (82%). A glicerina não refinada glicerina demonstrou um efeito negativo nas performances dos catalisadores maioritariamente devido ao alto teor em água. De modo a melhorar o desempenho catalítico a argila K10 foi tratada com ácidos inorgânicos (clorídrico, sulfúrico e fosfórico) e orgânicos (propiónico, acético, láctico, cítrico, tartárico e oxálico). Pretendeu-se a remoção parcial do alumínio de modo a aumentar a acidez e melhorar as suas características morfológicas.

A reação acetilação foi efetuada à temperatura de refluxo com 10 % (mássico) de catalisador e um rácio molar de ácido acético/glicerina de 9.6. O catalisador obtido por ativação da argila K10 com ácido sulfúrico apresentou as melhores *performances* com uma seletividade em triacetina de 33% ao fim de 5h de reação. As performances catalíticas parecem resultar dum efeito combinado, ou sinergético, entre a acidez e a morfologia.

Os catalisadores à base de carvões com ativação ácida mostram ser mais ativos que qualquer das argilas testadas.

Palavras-chave: valorização da glicerina, acetilação, catalisador argila, carvões activados, acetinas, aditivos

Abstract

To improve the competitiveness of biodiesel the glycerin by-product must be valorized. Fuel oxygenate additives manufactured from such poliol is envisaged as a relevant usage of the glycerin glut arising from a growing biodiesel industry.

Acetins, glycerol acetates, were produced by glycerin acetylation with acetic acid over acid treated montmorillonite catalysts. The maximum triacetin yield was envisaged. Commercial K10, K30 and KSF montmorillonite as well as sugar catalysts were used to catalyze the acetylation of pure (99.9%) and crude (80%) glycerines. Crude glycerin had a slight negative effect on the catalysts performances. In order to improve the catalytic activity of commercial K10 clay acid treatments were performed using inorganic (hydrochloric, sulfuric and phosphoric) and organic (propionic, acetic, lactic, citric, tartaric and oxalic) acids.

The surface morphology and chemical composition of fresh and post reaction catalysts was examined by SEM-EDS. The crystallographic changes promoted by the acid treatment were evaluated by XRD. Also, the post reaction catalysts were characterized by XRD to detect crystallographic changes occurred during reaction. The surface acidity of the acid treated clay materials was assessed through the skeletal isomerization of 1-butene.

The acetylation, solvent free, catalytic tests were carried out at reflux temperature using 10% (W/W) of catalyst and an acetic acid/glycerin molar ratio around 9.6. The sulfuric acid was the most effective leading to a triacetin selectivity of 33.0% after 5h of reaction. The citric and oxalic acids were the best among the organic acids, leading to 27.2% and 25.6 % of TAG selectivity. Sugar catalysts exhibited the best performance achieving around 47 % in 2.5 hours.

Keywords: Glycerin valorization, acetylation, clay catalysts, sugar catalyst, acetins, oxygenate additives, green fuels

Contents

List of Abbreviations

Acronym	Meaning
Mt	Montmorillonite
TAG	Triacetin
DAG	Diacetin
MAG	Monoacetin
HAc	acetic acid
Ac_2O	acetic anhydride
Gly	glycerin
BD	Biodiesel
FAME	Fatty acid methyl esters
FTIR	Fourier Transformation Spectroscopy
ATR	Attenuated Total Reflectance
SEM	Scanning Electron Microscopy
FEG	Field Emission Gun
SE	Secondary Electrons
BSE	Backscattering Electrons
EDS	Energy Dispersive Spectroscopy
XRD	X-Ray Powder Diffraction
T	Temperature
GC	Gas Chromatography
TGA	Thermal Analysis
BTL	Biomass to Liquid

List of Figures

List of Tables

1 Introduction

1.1 Contextualization

1.1.1 Worldwide energy scenario

The current global energy sector is mostly driven by fossil fuels such as oil, coal, and natural gas. Prior to the discovery of inexpensive fossil fuels, our society was dependent on plant biomass to meet its energy demands (Figure 1). Then came the industrial revolution in the 18th century and coal took the lead until the middle of the 20th century, the start of the age of oil, which remains dominant today. The discovery of crude oil created an inexpensive liquid fuel source that accelerated the world's industrialization and improved the standards of living. Due to its extraction and consequent supply shortages, a global energy crisis emerged in the 1970s, leading researchers to focus on renewable energy sources and alternative fuels[1][2].

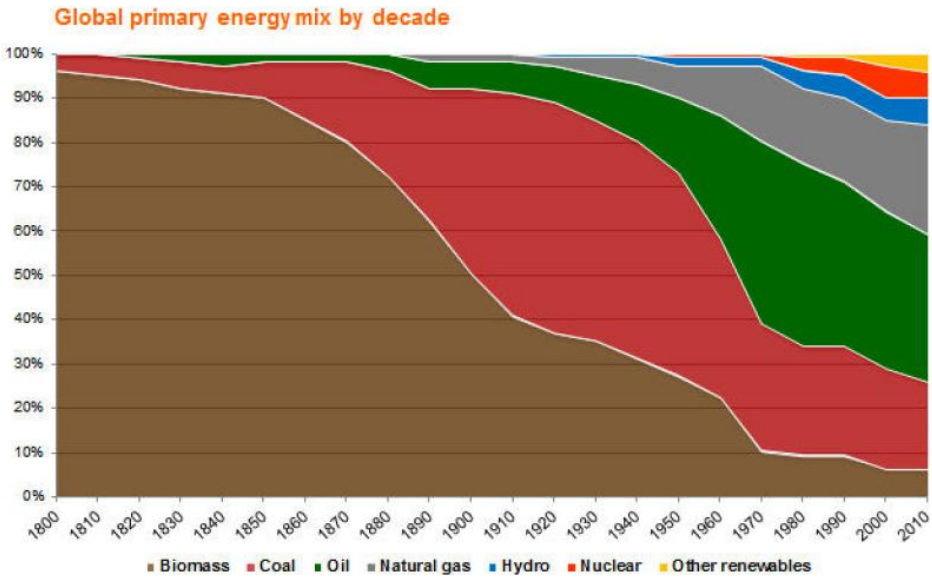

Figure 1 – Mooc "Sustainable Mobility 3, 2016", adapted from Exxon energy Outlook 2013.

Biofuels are, currently, a sustainable source for liquid fuels that generate significantly less greenhouse gas emissions during their life-cycle, consequentially having a lower impact on the environment [2].

According to the Biofuels Directive of the European Union Commission it will be requested, by 2020,to have 10% of the transport fuel of every EU country come from renewable sources such as Biofuels [3].

1.1.2 Biodiesel (Production)

Similarly to BioEthanol, Biodiesel (BD) is a promising biofuel, derived from renewable resources (such as agricultural crops, woody and herbaceous biomass, and waste materials), economically viable and environmentally accepted, especially for the transportation industry. Its use as a fuel substitute is especially beneficial, since BD has a low aromatic compound content and has no Sulphur. Traditionally, the manufacturing process of BD, composed by methyl esters, involves the reaction of triglycerides (from seed oils) with an alcohol, in a basic catalyst environment (Figure 2).

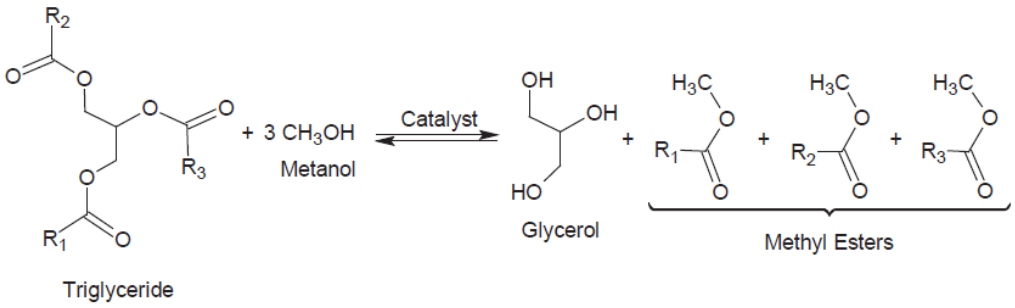

Figure 2 – Overall chemistry reaction for transesterification process [4]

However, though BD is a good answer to some important challenges such as reduction of pollution (including greenhouse gas emissions), there are also some disadvantages associated such as its high viscosity (leading to the reduced atomization quality and the increase in the average droplet diameter), longer combustion duration, lower rate of heat release, engine power losses, lower volatility, 12 % lower heating value and lower energy density [5].

Several generations of feedstocks have been used for Biofuel production. For Diesel engines, the 1st generation is called Biodiesel, or *FAME* (fatty acid methyl esters). These are produced from rapeseed, soya, sunflower or palm, consequently competing with food production and raising its prices.

Due to this problem, a *2nd generation* of BD feedstocks was developed out of non-edible by-products (such as cereal straw, bagasse, and forest residues, among others), waste vegetable oil and animal fats. Nevertheless, large areas could be used for their growth and it could lead to a risk of biodiversity.

The 3rd generation of biofuels is based on improvements in the production of biomass, namely algae and cyanobacteria, as they possess exclusive advantages in the Global Carbon Balance and Oxygen Generation, in which they're responsible for almost half of total CO_2 sequestration and half of total O_2 genesis in the world [6].

Additionally, they aren't in competition with food and they're cultured to act as a low-cost, high energy and entirely renewable feedstock. Yields can be higher than for 1st and 2nd generations but the process chain is not economically viable yet.

A new hypothetic definition has been given by many researchers that claim the next generation is, in fact, the photoautotrophic conversion of CO_2 into oil or algal biomass [7][8][9]**.** The 4th generation, photobiological solar fuels and electrofuels, aims not only to produce sustainable energy but also to capture and store the CO_2 gas, using processes such as oxy-fuel combustion. Technology for production of solar Biofuels in an emerging field based on direct conversion of solar energy into fuel using cheap raw materials such as algaes [7][9].

In 2011, nearly 65% of glycerin risings were from Biodiesel production and it was estimated that the global production of BD was2015 of $3.1x10^{10}$ L and it was projected to increase by $11x10^{10}$ by the year of 2020 [10]. This implies that glycerin market will follow BD's grow, since it strongly depends on the BD industry [11].

In terms of BD blends, the common range is between 5 to 20 % of BD's concentration in petroleum diesel, where 5 % of BD is considered B5 and pure BD (100 %) is B100. The most common type is B20, especially in the USA, representing a good balance of cost, emissions performance and materials capability. Overall, all different types of blends mentioned must be in agreement with the standards specifications, approved by the American Society for Testing and Materials (ASTM) [11].

1.1.3 The Glycerin market

In 2005, the major glycerin global suppliers were *Procter & Gamble*, *Cognis* and *Croda*, which together owned more than *1/3* of the market stake, whereas years later the main glycerin suppliers were BD and oleo chemical companies mainly situated in Southeast Asia. In fact, it's reported that between 2005 and 2007, several major factories ceased activities due to the exponential growth of BD market, like the Dow Chemical plant in Texas(60 kton/year), Procter & Gamble's in London (12.5 kton/year)and Solvay's in France [12].

Nowadays, the market is controlled by four major companies – *IOI Group, Wilmar It, KL Kepong* and *Emery Oleochemicals*, that control over 65 % of global glycerin market (2.47 billion dollars) [13]].The increasing global demand for BD has created a glycerin glut, affecting its market. Glycerin is mainly produced as a by-product of BD production, as10 kg of glycerin are produced for every 100 kg of BD. The global production of glycerin increased from 200 kton in 2003 to 600 kton in 2006, with the BD boom [12] causing its rapid price decline and led to an historic low of50 $/ton as of mid-2006 for unrefined glycerin.

Prior to the expansion of BD production, the price of refined and crude glycerin was 1543 $/ton and 551 $/ton, respectively, depreciating to 660 $/ton and 110 $/ton of refined and crude glycerin by 2007[14].In 2013, the cost of refined crude glycerin was around 900-965$/ton, depending on the raw material used in BD production, in contrast with the unrefined glycerin at approximately 240 $/ton in 2014[15].

It was reported that since BD's boom, crude glycerin was often disposed of at negative prices, with suppliers paying customers to get rid of unwanted crude glycerin. The continuously increasing flood of glycerin from BD has been further supplemented by oleochemical glycerin and in early 2015,

refined glycerin was sold at 600–650 $/ton in Southeast Asia, whereas crude glycerin was priced at 225–235 $/ton [10]

In late 2016, spot prices of crude glycerin cargoes going to China were assesses at 190 – 200$ per ton[16], as can be seen in Figure 3, where the price highly depends on macro factors, namely seasonals, decreasing substantially during the harvesting months of palm oil and other edible and non-edible oils.

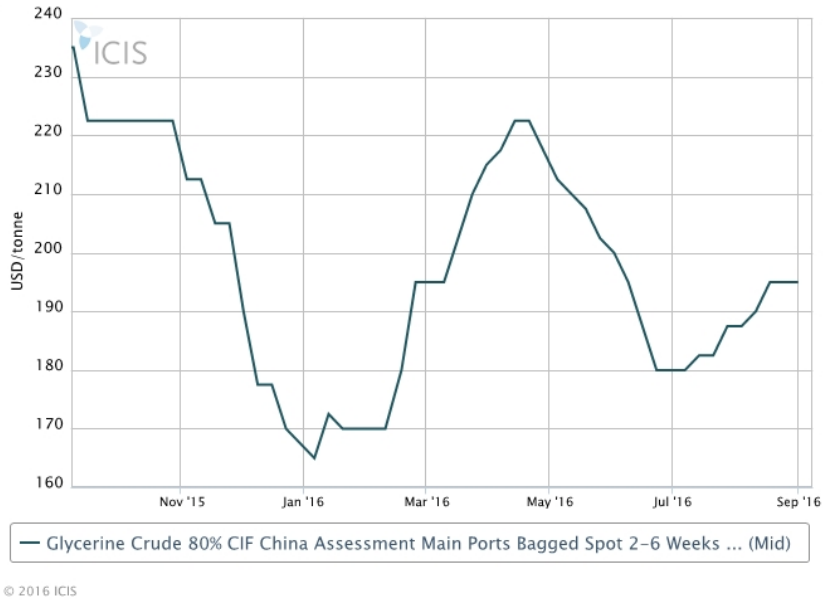

Figure 3 – Market scenario for glycerin crude 80 %, CIF prices in China, between November 2015 and September 2016.[16]

As for Europe, at the end of January of 2017, the prices of crude 80 % glycerin veg-oil based were approximately 220 €/ton, and when mixed with feedstock the price lowered by 40 € [17]. In fact, the decreasing price of unrefined glycerin and the high cost of BD production require novel approaches of glycerin application to minimize the net energy requirement for BD production, compensating the cost differences between BD and fossil diesel, and increasing the market viability of BD[12].

It was demonstrated that the net production costs of B100 can be reduced from 0.63 $/L to 0.35 $/L, by adding value to the glycerin by-product[18]. Due to the need to lower costs and increase competitiveness of their main product, many BD manufacturers have started to include new glycerin refineries in the last couple of years.

However, there are some concerns due to the fact that the glycerin market depends on two major factors: the way the main BD suppliers implement and execute the legislated BD policies/mandates in their countries (Biofuel Laws: blending a percentage of BD in their vehicles) and the market price of crude oil (when this reaches a price below stable/standard, many BD producers start reporting losses on BD) [18]. There's some resistance to policy changes, impacting the first of the factors in many countries, Thailand being an example since last year the Thai government conceded and reduced its BD blending mandate from B5 (5%) to B3 [19].

1.1.4 Glycerin Purification

Glycerin (1,2,3-propanetriol) is a trihydric alcohol (Figure 4) and a colourless, odourless, viscous and nontoxic liquid. Due to the three hydrophilic alcoholic hydroxyl groups, glycerin is hygroscopic and soluble in water. The overall properties of glycerin can be seen on Table 1.

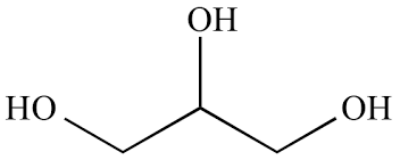

Figure 4 – Structure of glycerin.

Nowadays, the majority of BD plants use a homogeneous catalyst system operated in either batch or continuous mode, using typical basic catalysts such as *NaOH* or other alkali metal hydroxides. The main problem of the process is the contamination of the catalyst on the solution and the difficulty of full extraction [4].

During the transesterification reaction, the excess of alcohol (the most used/abundant is methanol) ends up in the bioglycerin layer, increasing the purification's cost and difficulty (mainly unfeasible for small and medium scale plants). During the purification, most of the expensive methanol is recovered from the glycerin layer, and salt-grade bio glycerin is produced [4]**.**

Table 1 – Summary of the properties of glycerin [4].

Properties	**Values**
Molecular Formula	$C_3H_5(OH)_3$
Molar Mass (g.mol^{-1})	92.09
Melting Point (ºC)	18.2
Boiling Point (ºC)	290
Density$^{20\ ºC}$ (g.cm^{-3})	1.2375
Viscosity (Pa.s)	1.5
Flash Point (ºC)	176
Auto-ignition temperature (ºC)	400
Vapor pressure$^{20\ ºC}$ (mmHg)	< 1
Food energy (kcal.g^{-1})	4.32

There have been several attempts to eliminate these problems, one of which being the use of heterogeneous catalysts as they are easy to separate from the solution and to regenerate. However, problems with external diffusion and leaching of the catalysts have increased the difficulty of their implementation in the industry.

Usually, crude glycerin is 70 – 80 % pure and generally contains several components beyond glycerin, such as methanol, water, soap, FAMEs, glycerides and ash; thus, it is usually purified prior to its commercial sale at 95.5 – 99.7 % purity [20].

Refined glycerin is classified into three main classes, as can be seen in Table 2:

- Technical grade– used as a building block in chemicals, not used for food or drug formulation;
- USP glycerin from animal fat or plant oil sources, suitable for food products, pharmaceuticals;
- Kosher glycerin from plant oil sources, suitable for use in kosher foods [12].

Table 2 – Refined Glycerin grades' purity.

Refined Glycerin	Purity %
technical grade	95.5
USP	USP 96, vegetable -base
USP	99.5, tallow -based
USP/FCC-Kosher	99.5
USP/FCC-Kosher	99.7

Traditional purification of raw glycerin employs high temperatures and starts with neutralization with hydrochloric acid, followed by filtration and centrifugation, and distillation under vacuum in order to avoid decomposition or oxidation.

The final step involves the reduction/elimination of minor components like residual color and fatty acids, with the help of activated carbons [21].

1.1.5 Glycerin Applications

Normally, the non-distillated glycerin by-product is discharged as a waste or burned, which in turn may lead to environmental problems, as noted in a USA river water analysis where high, poisonous levels of glycerin residue were detected – at the vicinity of a BD plant [22]. Since 1 ton of glycerin is produced for every 10 tons of BD, this problem needs to be solved, creating the need to exploit the unique properties of glycerin.

1.1.5.1 Traditional Uses

Traditional applications of glycerin have always been present in daily activities, since it's used as food, a skin care product (shaving cream, hair care products and soaps), tobacco, drug additive or for alkyd resins. Nowadays, its main application is still personal care and pharmaceutics, where glycerin acts as ingredient, acting firstly as a moisturizer, retaining moisture and preventing skin dryness while providing softness, and it is projected to remain the leader until 2022, as can be seen in Figure 5 [4].

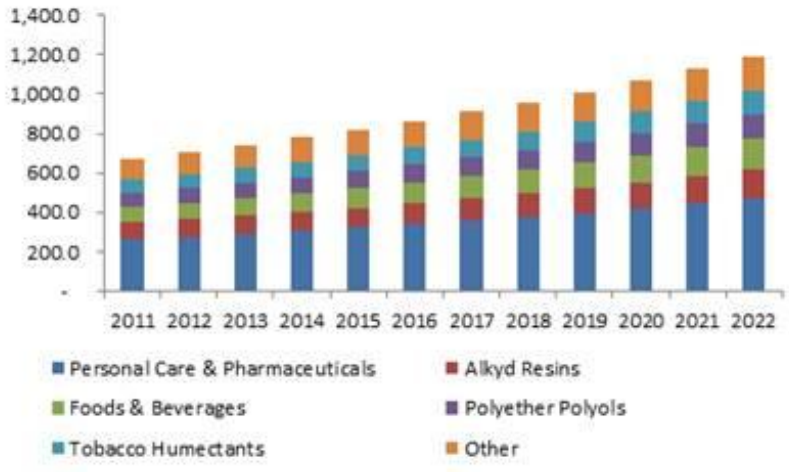

Figure 5 – Europe Glycerin market size by application, 2012-2020 (kton) [23]

Recently, the industry has focused on upgrading glycerin into fine chemicals, through several reactions, namely Acetylation, Epicerol, Steam Reforming, Hydrogenolysis and Etherification, among others, that already have been implemented in a large scale for glycerin's conversion into higher value-added chemicals. There are few applications that use glycerin in a large scale for its conversion into higher value-added chemicals.

1.1.5.2 Epicerol

Available and patented since 2007 by Solvay with an initial production plant of 10kton per year, in this process glycerin reacts with hydrohydrochloric acid over a catalyst, forming Epychlorohydrin, a chemical product largely used in the than conventional manufacture of plastics, epoxy and phenoxy resins [23][24].

1.1.5.3 Reforming

When glycerin is used in the Reforming process, hydrogen and carbon monoxide are formed, known as Syngas, which is then reformed at high pressure and temperature to form Methanol. The Syngas can also be used in the Fischer-Tropsch process (to produce alkanes). The Reforming reaction is proceeded under temperatures between 225 and 300 ºC with a Pt-Re catalyst in a single reactor. This process gives high yields of hydrogen fuel at low CO concentrations, and lower energy consumption than conventional methane reforming. The company BioMCN, in Netherland, reports the use of200 kton/year of glycerin in Reforming [18][21][25]

1.1.5.4 Oxidation

Oxidation of the second hydroxyl group of glycerin with the help of carbon-supported Pt, Pd or gold catalysts, forms Dihydroxyacetone (DHA), an important ingredient in the cosmetic industry, namely in sunless tanning formulations, with a global market of 1.8 kton per year [22][26].

1.1.5.5 Selective Reduction

Two important glycols can be produced through selective reduction, 1,2propanediol (or propylene glycol, PG) and 1,3propanediol (PDO).PG is traditionally derived from propylene oxide, in turn produced from propylene, and used as a safer replacement for ethylene glycol-based products such as antifreeze and aircraft devices, with a global market of 2 Mton in 2007.PDO is an important diol in polymer production of polyesters, polycarbonates and polyurethanes.

Using glycerin in the Hydrogenolysis process, in the presence of metallic catalysts (such as Ru/TiO_2 or Cu/ZnO) and hydrogen, PG and PDO are formed. It was reported that, since 2008, PG is commercialized by Synergy Chemicals, obtained through the reduction process of glycerin and, in 2010, the company Archer Daniels Midland implemented this process with a capacity of 100 kton per year [27] [4] [28]

1.1.5.6 Dehydration

Acrolein and Hydroxyacetone are important derivatives of catalytic and thermal dehydration of glycerin. Acrolein is formed in the presence of acid catalysts such asH_2SO_4, $Zn(SO_4)_3$ or WO/ZrO_2,

and is a precursor to acrylic acid, which has an annual production of 1.2 Mton, as reported in 2010[22].

1.1.5.7 Etherification

Glycerin ethers are reported to be implemented as fuel oxygenated additives. These ethers are formed due to the reaction of glycerin with, for example, isobutylene, producing mono, di and tri tertiary butyl ethers (GTBE) which can be used as a diesel fuel additive, greatly reducing the emissions of particulate matter [29].They have already been implemented in the industry, such as in the US-based company CPS.

Another product is polyglycerin, a popular polyol, known to be applied not only in cosmetics but also in controlled drug release products. It is already commercialized by Hyperpolymers GmbH, from Germany [4].

1.1.5.8 Esterification

Esterification of Glycerin with carboxilic acids results in the formation of monoacylglycerins (or monoacetin, MAG), diacylglycerins (diacetin, DAG) and triacylglycerins (triacetin, TAG).

Monoacetin (MAG) is used as a food additive, employed in the production of explosives and smokeless powder and is an emulsifier, corresponding to 10% (in a total of 400 kton) of the world market of food emulsifiers in 2006 [30].

Diacetin (DAG), or glycerin diacetate, has several applications, ranging from its use as a cocoa butter bloomer to an intermediate in the synthesis of structural lipids and to a plasticizer and a softening agent[31]. It was reported that DAG is present inedible fats and oils, as a minor component, existing either as 1,3 – DAG or 1,2 (2,3) – DAG. In terms of industry application, since 1999, the japanese company Kao Econa has been manufacturing cooking oils containing 80 % of DAG, which is produced from soybean and canola using a lipase.

Triacetin (TAG) is one of the most promising derivatives, also known as glycerin triacetate or triacetyglycerin. It's used as a fuel additive, which allows the increase in octane numbers in diesel or biodiesel and prevents the crystallization of BD, caused by changes in temperature, preventing blockages in the engine. TAG can also be used as a solvent or biocide, appealing for the cosmetic industry, but also as an anti-knocking and hardening agent for cellulose acetate fibers, also known as "filter tow" in the tobacco industry [32][33].

According to [34] the mix of DAG and TAG as fuel additives, improves some fuel properties, increasing viscosity, flash point and pour point to a certain degree and decreasing CO_2 emissions.

In terms of TAG addition to BD, it's reported that the addition of 5 to 10% (% m/m), leads to a maximum reduction of 50 % of CO emissions, and this blending of BD with 10% of TAG improves direct-injection diesel engine performance. This is due to the fact that Diesel and TAG are highly oxygenated compounds, which benefits a complete combustion [35].On the other hand, the addition of 20% or more of TAG in the fuel, not only leads to a decrease in the flash point and pour point, but also

in the cetane index in the mixture [33].

Another main product from Esterification is Nitroglycerin, an explosive agent that is formed when Glycerin is nitrated with nitric agents, such as fuming nitric acid. This product is currently commercialized by a weaponry company, the Alliant Techsystems in the USA[36].

It is also used as an antianginal drug by the pharmaceutical industry. Glycerin esterification can be supported with or without the use of catalysts, though their presence can greatly increase the rate of reaction and the product selectivity, since the solvent used in acetylation is normally acetic acid that already helps to convert glycerin into acetins but a slower rate.

Table 3, displays a summary of the above described applications above and others that are not yet fully developed to be commercialized.

Table 3 – Synthesis of the main processes of Glycerin.

Process	Product	Application
Esterification	• MAG, DAG & TAG	Fuel additives
	• Polyglcerol ester	Emulsifiers
Etherification	• Bu-ethers	Fuel additives
	• Polyglycerin ether	Polymer
	• Nitro-esters	Explosive agent
Hydrogenolysis/ Reduction	• 1,3 propanediol • 1,2 propanediol	Polyesters
Oxidation	• Dihydroxyacetone	Sunless tanning skincare
Dehydration	• Acrolein	Chemical intermediate
	• Hydroxyacetone	Acrylic fibers, resins, paints, polymers…
Reforming	• Syngas	Fischer Tropsch synthesis
Epicerol	• Epichlorohydrin	Epoxy Resins
Carboxylation	• Glycerin Carbonate	Polycarbonates, Polyurethanes
Telomerization	• C_8 chain ethers	Surfactant chemistry
Condensation	• Dioxane	Used in vented reactor, inert solvent
	• Dioxolane	Aprotic solvent, ingredient in pharmaceutical intermediates
Raw Glycerin	• Bioglycerin	Additives for Cement

1.2 Catalysts

Glycerin acetylation can be conducted using different types of acid catalysts, mainly divided between two categories: homogeneous and heterogeneous catalysts. Table 4 sums up the main characteristics of these categories.

Table 4 – Main characteristics of the two types of catalysts: heterogeneous and homogeneous.

Catalyst	Homogeneous	Heterogeneous
Thermal Stability	Low	Good
Recovery	Difficult	Easy
Profit	Expensive	Cheap
Selectivity	Very good	good
Example	Sulfuric, phosphoric acids	Amberlyst, K10, zeolites

1.2.1 Montmorillonite

Montmorillonite (Mt) was the main catalyst chosen for the acetylation of Glycerin. To understand the role of Mt as a catalyst, some background information about this special clay will be presented.

The Mt clay minerals are very common, being found in many soils and sediments and belonging to the smectite group, name given to a group of Na, Ca, Mg, Fe and Si-Al silicates, with a molecular formula $M_x(Al_{2-x}Mg_x)(Si_4)O_{10}(OH)_2.nH_2O$, (*M* - monovalent cation, *x* - degree of cations isomorphous substitution in octahedral sheets) [37][38].

Smectite is a 2:1 layer silicate (Figure 6), which has two silica tetrahedral sheets sandwiched and joined to a central octahedral sheet. Clay minerals are usually either positively or negatively charged, the main reason for their ion exchange capacity.

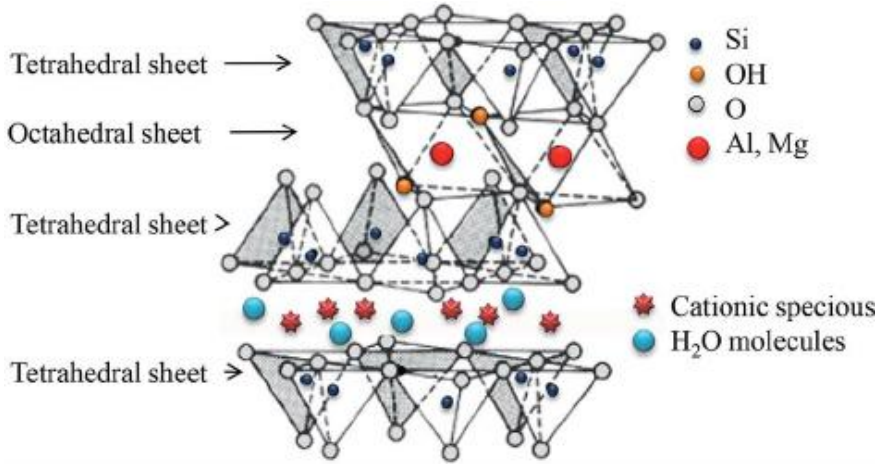

Figure 6 – Smectite structure of a 2:1 clay mineral [38]

At the layers of stacked aluminosilicates, partial isomorphous substitution of Si^{4+} ions in the tetrahedral layer by trivalent metal cations (Al^{3+}) and Al^{3+} ions by divalent metal cations (Mg^{2+}, Fe^{2+})causes a charge deficiency. In order to balance this charge deficiency, hydrated alkali and alkaline earth metal cations occupy the interlayer space of Mt [39][40][41].

The minerals of this group have an expandable lattice, which depends on the thickness of layers of water molecules between silicate layers. In fact, Mt has a high swelling capacity of the order of 10 – 15 times their clay volume when placed in water [42][43].

Catalysts *K5*,*K10*, *K20* and *K30*, are Mt treated with different concentrations of hydrochloric acid and calcined at a specific temperature, resulting in a high surface area material and porosity that contains Brønsted and Lewis acid sites (KSF is, on the other hand, treated with sulfuric acid [44][45]).Though these properties are advantageous, some drawbacks are observed, the main one being the transformation of arranged laminar sheets of Mt into disordered sheets, like amorphous silica, generally occurring due to the acid leaching [47]. Reported by Flessner [44], K30 is more acid than K10 because the Brønsted sites of K30 are a little more acidic than K10.

Accordingly to Tkác *et al*, [47], in the 1st stage of dissolution of the Mt Si atoms bearing OH groups are separated and as a result of condensation reactions of SiOH groups, amorphous silica with a 3D cross-linked SiO_4 framework is formed.

In terms of acid attack, it's reported that acid treatments dissolve central atoms from the tetrahedral and octahedral sheets at similar rates [47][48]**.** Although the smectite acid dissolution proceeds more rapidly in octahedral sheets with higher preference of octahedral Mg^{2+} than octahedral Fe^{2+} or Fe^{3+}, which makes dissolution similar too [49][50].

Additionally, though one of the disadvantages of clay minerals usage as catalysts is the long range clay layers collapse due to the elimination of water, when calcined at temperatures higher than 200 ºC, Mt doesn't contain long-range clay layers, and is, therefore, generally calcined at 500 - 600 ºC, inducing high thermal stability on the catalyst [51][52]**.**

Despite numerous studies on acid treatment of clays, the nature of the acid sites and the details of the surface chemistry of these catalysts are unknown. Although K10 is designated an acid treated Mt, this catalysts contains, besides Mt, a mixture of amorphous species (amorphous silica) contaminated with crystalline materials like quartz, mica and cristobalite, making it an inexpensive, green and efficient catalyst [53].

Table 5 presents a summary of the analytical and structural properties of the used clay catalysts.

Table 5 – Characteristics of the acid clay catalysts Mt KSF, Mt K10 and Mt K30[44][54][55].

Catalyst	Surface Area (m^2/g)	Apparent Bulk Density (g/L)	Loss on Ignition (%)	pH	Pore Volume (mL/g)		
					0 – 80 nm	0 – 24 nm	0 – 14 nm
KSF	20 – 40	800 – 850	7	1.5	0.023	0.01	0.01
K10	240	300 – 370	7	3 – 4	0.36	0.30	0.26
K30	330	450	n.r.	2.8 – 3.8	0.5	0.44	0.38

n.r – not reported

1.2.2 Sugar Catalysts

Recently, carbon-based solid acid catalysts have gained significant advantage over homogeneous catalysts since they're sustainable, eco-friendly, stable and can be reused several times without significant loss of activity. These type of catalysts can be successfully prepared using materials from biomass like wood sources [56][56], or vehicle residues (i.e. from tyre rubber) [57][58]or even from sugar molecules, having been reported the use of Glycerin, Sucrose and D-Glucose, among others [58][59][60].

The mechanism of the sugar catalysts' formation, as shown below, consists in two steps. On the first step, the dehydration of the OH groups of the compound occurs (e.g. glucose or glycerin) releasing water to the atmosphere and, consequently, carbonizing it. The introduction and functionalization of SO_3H groups in the support follows the first step, increasing the total acid site density of strong Brønsted acid sites [61] [62] .

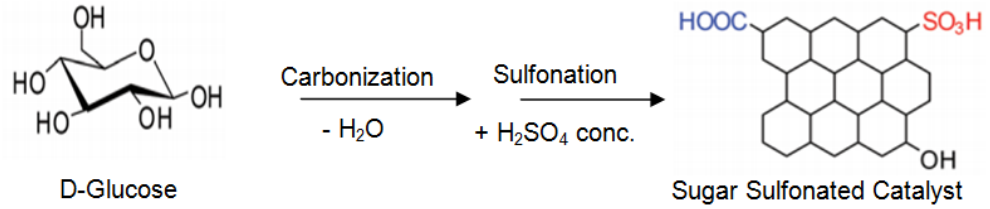

Figure 7 – Schematic formation of sugar catalyst from D-Glucose [63]

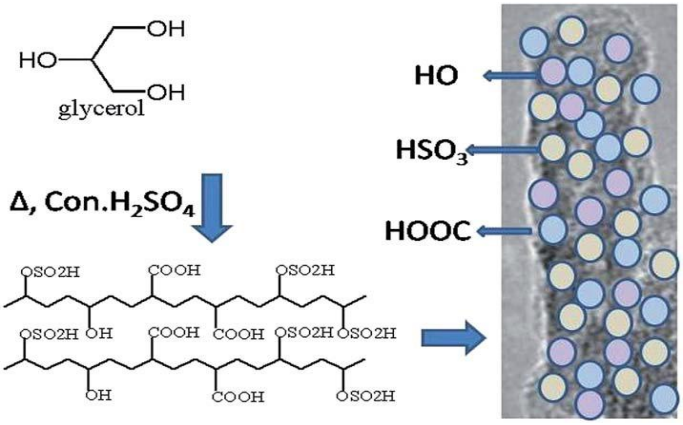

Figure 8 –Schematic representation of Glycerin carbonization and sulfonation [64]

1.2.3 Amberlyst 15 wet

Amberlyst type resins are prepared in the form of cation or anion exchange resins. The H-form of the cation resins shows acid catalytic activities. The thermal stability of Amberlyst, however, is limited up to 120 °C. One of the most popular and commercially available Amberlyst, the 15, is an acidic variation, which functions as a macro reticular type exchange resin. It's known that the hydrogen form of Amberlyst 15 displays sulfonic acid functionalities, providing a higher acidity, compared to other resin catalysts [65]. As reported by Testa *et al*. [66], Amberlyst is a resin constituted by strong acid sites, making it a catalyst adequate for glycerin's acetylation .

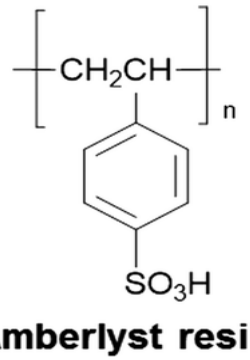

Figure 9 – Schematic representation of Amberlyst [65].

1.3 Main Goals

The purpose of this work is to study the influence of acid catalysts in the acetylation of glycerin over acetic acid as well as the stability and optimal values of performance of synthetic clays (KSF, K10 and K30). The reaction was performed at atmospheric pressure in a specific temperature range within a round flask reactor, under conventional heating.

Different configurations of the clay were tested to determine the importance of the acidity as well its textural properties, namely analyzed by X-Ray, BET and SEM. In addition, with the help of FTIR it was possible to characterize which chemical bonds corresponded to the Mt. The treatment of Mt was done using different types of acids: inorganic, organic and metal oxides.

After determining which catalyst yielded the best result, an optimization procedure of the acetylation conditions, such as temperature and molar ratio between acetic acid and glycerin, was applied.

1.4 Thesis Outline

Chapter 1 provide some general information about the major motivation of this study, some introductory basis about the subjects that were approached during this work as well as some information about the industrial applications that were or may be performed based on the valorization of glycerin.

On the following chapter, a literary revision of available similar work is presented, focusing on articles concerning Glycerin's Acetylation and the chosen catalysts.

In Chapter 3, the experimental methods used throughout the reactions performance and catalysts preparations are shown and explained. The main techniques and characterization methods used to analyze the catalysts: X-ray Diffraction (XRD), Fourier Transformation infrared Spectroscopy (FTIR), Scanning Electronic Microscopy (SEM), Catalytic Isomerization of 1-Butene, Thermal Analysis (TGA) and N_2 Adsorption-Desorption, are also mentioned.

In Chapter 4, consists on the results of the performance of the catalysts and the glycerin acetylation yields of MAG, DAG and TAG are reported, as well as a summary and integration of the main conclusions of this work and possibilities for further research represented.

On Chapter 5 an estimation of the industrial process' viability is displayed, taking into account the worst-case scenario on all the investment requirements and operational costs.

Finally, the conclusions are summed on Chapter 6.

2 State of the Art

2.1 Literary Review – Acetylation

Glycerin valorization by acetylation is currently recognized as a way to produce added-value fuel additives, with acetylation with acetic acid being one of the most important alternatives. In this reaction, the acetyl functional group from acetic acid goes into the chemical compound glycerin, substituting the hydrogen atom of a hydroxyl group of Glycerin with an acetyl group, resulting in an acetoxy group.

The main products from this reaction are MAG, DAG and TAG, whose applications were reported in *Section 1.1.5* and can be seen in Figure 10. Additionally, Diglycerol Tetraacetate (and other isomers) can also be obtained, though these compounds are of no interest for this thesis.

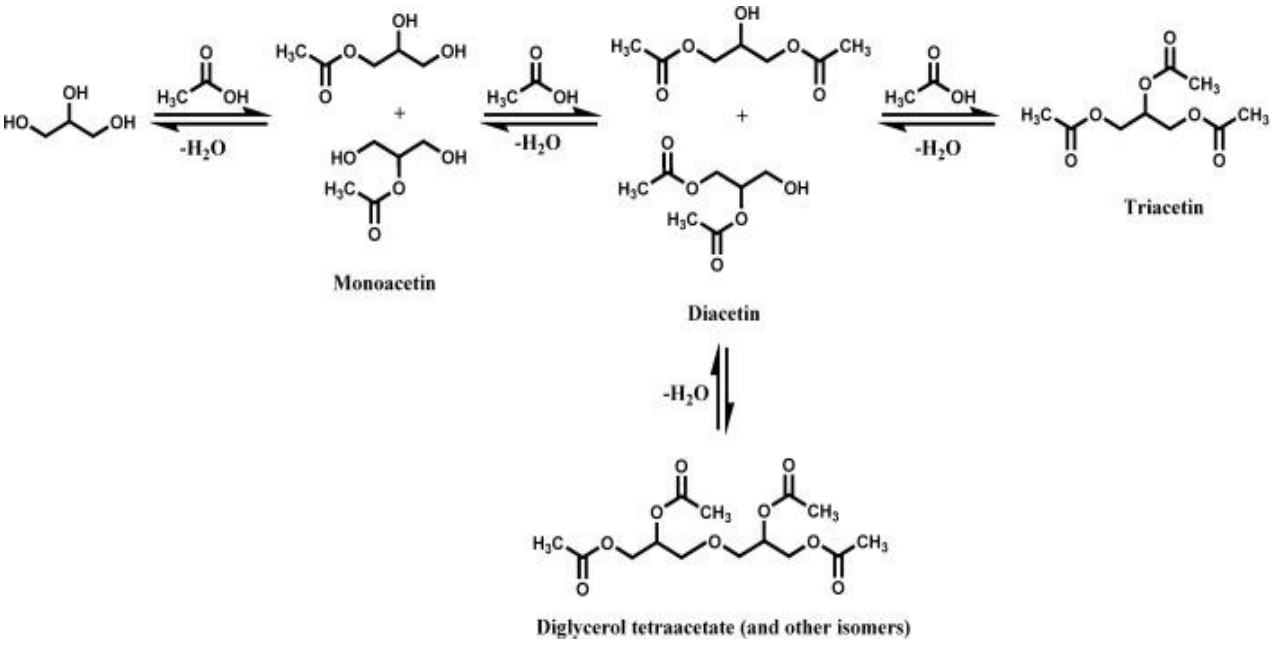

Figure 10 – Glycerin's Acetylation[67]

Acetylation occurs with or without the use of catalysts, whereas the presence of catalysts naturally increases the rate of reaction, as well as the product selectivity.

Traditionally, the acetylation of glycerin is achieved at mild temperatures with homogeneous catalysts, namely, sulfuric acid, hydrochloric and orto-phosphoric acid. In this case, the discharge of the effluent leads to negative environmental effects, due to the major difficulties in the separation of the catalyst and the solution and there is a high cost associated with the neutralization and purification steps. These issues can be mostly resolved by using heterogeneous catalysts.

Numerous studies have reported the use of acid heterogeneous catalysts for the preparation of glycerin acetates by glycerin, acetic acid and acetic anhydride. Although acetic anhydride produces the same conversion with a smaller time span, when compared with acetic acid, due to the absence of water formation (as the presence of water leads to the equilibrium shifting to favor the reagents' formation and consequently lowers the ester's yield), since it is a much more reactive and costly reaction, as well as difficult to handle/control (the reaction is highly exothermic), the use of acetic acid is generally favored instead.

The reaction tends to be mainly influenced by catalyst loading, acetylating agent molar excess, temperature, reaction time, among others, with all of these parameters favoring the most desirable products. It is claimed that the biggest challenge of glycerin acetylation is to obtain a good selectivity of TAG, above 50 %, regardless of not only the reaction conditions or catalysts used but also the similar/identical boiling points of MAG, DAG and TAG, increasing the difficulty of TAG recovery [4].

Solid acid catalysts have shown better selectivity towards the desired products when compared to conventional homogeneous acetylation. Acid-exchange resins [68][69][70], Mt [71][68][72], Activated Carbons [73][74][75], Mesoporous and modified Silica [66][76], Zeolites HZSM-5 and H-β [68], Metal Oxides [1] and Heteropolyacids [77][78][75] are several of the solid catalyst proposed in the literature.

The most common ion-exchange resins is Amberlyst, which has shown satisfactory performance on the glycerin acetylation carried out in excess of acetic acid, where the maximum temperature used is below 120 ºC, since at this temperature Amberlyst starts to degrade (its thermal limit). However, their main disadvantage is their thermal stability, their quick loss in active sites due to high polarity and low selectivity to TAG. It is published by *Liao et al*., the selectivity of 100% towards TAG, when the acetylation is proceeded in two steps. In the 1st step, the reaction carries with acetic acid to glycerin ratio of 3:1 during 4 hours, achieving 15 % of TAG's selectivity. Then, in the 2nd step, they add anhydride acetic, with a ratio of 1:1 in order of glycerin, achieving 100% of TAG's selectivity within 15 minutes.

Silica is a common precursor, known to be an inert compound, and the addition of anions has been found to enhance its acidity, providing thermal stability and porosity. The incorporation of simple anions, such as H_3PO_4, is report to have achieved a TAG selectivity of 26 % in 1 hour with a molar ratio of acetic acid to glycerin of 9:1.Testa *et al*., reported the synthesis of Propyl-SO_3H functionalized amorphous SiO_2bysol-gel technique, attaining a TAG selectivity of 49 % in 3 hours, concluding that the acid strength of the sulfonic acid groups within silica leads to an enhance in the acid strength, increasing significantly the catalytic activity in the reaction.

Organically functionalized mesoporous materials have been used as catalysts, due to their high surface areas and large ordered pores ranging from 20 to 300 Å [79]. The most used mesoporous materials are synthetized/made from silica (SBA, MCM, among others). Khayoon *et al*,

reported the synthesis of SBA with 3% of Yttrium, obtaining full conversion of glycerin and 56% of TAG´s selectivity. The catalytic performance was attributed to its strong acidity, high specific area and mesoporosity, facilitating the diffusion [80].

Activated carbon (AC) with sulfur containing groups via hydrothermal treatment with sulfuric acid is a suitable catalyst, achieving a 91% conversion of glycerin with a TAG's selectivity of 34%[73]. A new class of sulfonated carbon catalysts named "sugar catalysts" has earned consideration. They are prepared via incomplete carbonization and sulfonation of carbohydrates, such as glycerin, glucose and cellulose [59].

Zeolites are crystalline solids composed of silicon and aluminum oxides arranged in a 3D network of uniformly shaped micropores (< 2 nm) of tunable topology and composition. In the Zeolite's category, *Kownar et al*., reported the performance of Hβ, HY and HZSM-5[81], and observed that only HY was capable of achieving 100% TAG's selectivity, compared to the others in the same conditions. The explanation for this difference is due to the fact that the porous diameter of HY (1.124 nm) is higher than the critical diameter of TAG (1.021 nm), implying that the diameter of the pores is an important parameter in the aim of formation of TAG [81].

As an alternative, Heteropolyacids (HPA) have been used as acid catalysts in the acetylation of glycerin. Like ion exchange resins, HPA also exhibit poor thermal stability, regeneration ability and low specific area [82]. To increase the surface area, they're usually supported on amorphous mesoporous materials.12-Tungstophosphoric immobilized in a silica matrix and in an activated carbon is reported of having a glycerin conversion superior than 78 % [78][75]. However, this kind of support tends to limit accessibility and efficiency of the catalyst [82].

The use of metal oxide-based catalysts for the esterification reaction has drawn attention due to several advantages, as they are inexpensive, stable, and active over a wide range of temperatures and have a strong surface acidity. The presence of *Lewis* and *Brønsted* acids of metal oxide provided the required catalytic sites for esterification. Zirconia based catalysts were reported by Reddy et al [1] as well as Cerium (IV) based catalysts [82].

At last, the section of clays (or aluminosilicates, Mt) are commonly used in catalysis since cracking time [44] due to their structural modification upon acid treatments increasing notably their surface characteristics and pore diameters. In the acetylation reaction, *Venkatesha et al*.[65], reported achieving 51.1 % of TAG's selectivity when using a green organic acid – methanosulfonic acid.

In the following Table 6, a summary is presented, containing the main conditions of the best performances in the acetylation reaction of glycerin using acid catalyst.

Table 6 – Summary of the catalysts used in the acetylation of Glycerin, obtained from literature.

Section	Catalyst	HAc:Glyc (mol)	Ac_2O:Glyc (mol)	T (^oC)	t (h)	% Conversion	% S MAG	% S DAG	% S TAG	Reference
Blank	No Catalyst		5:1	100	3	100	4.3	61	34.7	[81]
Acid Resins	Amberlyst-15	3:1		110	0.5	97	31	54	13	[68]
	Amberlyst-15	6:1		105	4	98.6	n.r.	n.r.	25	[69]
	Amberlyst-35	3:1	1:1	105	4.25	100	0	0	100	
	Amberlyst-70	6:1		105	4	100		<47	>47	[70]
Sílica	Sílica –Propyl-SO_3H	3:1		105	3	100	0	51	49	[66]
	Sílica H_2SO_4	6:1		110	5	>99	30	55	15	[76]
	Sílica H_3PO_4					>85	15	45	40	
	Sílica H_3PO_4	9:1		120	1	90			26.1	[83]
	Sílica $(NH_4)_2PO_4$								13.8	
	Sílica-Alumina	6:1		100	8	98		39	3	[84]
	Sílica MoO_3	10:1		100	8	100	17	33	50	[85]
Organically functionalized mesoporous materials	Yttrium/SBA-3	8:1		100	3	97	19	25	56	[80]
	Molybdophosphoric/SBA-15	6:1		110	3	100	14	67	19	[86]
	Pr-SBA-15	9:1		125	4	80	15	85		[87]
	Pr-SO_3H/SBA-15	6:1		80	8	100		64.6	19.6	
	SO_3H /SBA-15	6:1		80	8	100		61.9	27	[81]
	MCM-48		5:1	100	0.83	100	40	47.3	12.7	
Zeolite	HUZY	3:1		110	0.5	14	79	14	0	[68]
	H - β		4:1	60						
	HZSM-5				0.83		0	40.6	59.4	
	H - β		5:1	100	0.83	100	0	34.3	65.7	[81]
	H - Y				0.33		0	0	99.8	
	HZSM-5	3:1		110	0.5	30	83	10	0	[68]

Table 6 (continued) – Summary of the catalysts used in the acetylation of Glycerin, obtained from literature.

Section	Catalyst	HAc:Glyc	Ac_2O:Glyc	T(^oC)	t(h)	%Conversion	% SMAG	% SDAG	% S TAG	Reference
Metal Oxide	MoO_3/TiO_2-ZrO_2	6:1		100	3	100	52	40.5	7.5	[1]
	ZrO_2					86.3	57.9	36.7	5.4	
	TiO2-ZrO_2					91.5	54.7	39.4	5.9	
	WO_3/TiO_2-ZrO_2					99	53.2	40	6.8	
	CeO_2-ZrO_2			120	1	68.1		22.7	2.1	[82]
	CeO_2-Al_2O_3				1	59.4		11.6	0.3	
	SO_4^{2-}/CeO_2-ZrO_2				1	100		57.7	16.5	
	SO_4^{2-}/CeO_2-Al_2O_3				1	79.9		35.5	5.6	
	SO_4^{2-}/ZrO_2-TiO_2	4:1		130		96			93	
	Sulphated Zirconia	3:1		130	0.5	>90	15	37	48	[74]
Modified Clay	K10	4:1	4:1	120	2	100	36	52	6	[71]
				60	0.3	100	0	0	100	
	K10	3:1		110	0.5	96	44	49	5	[68]
	Methanosulfonicacid/ Mt	3:1		120	4	94	11.7	37.2	51.1	[72]
	P-Toluenesulfonic/ Mt				1	94	30	37.2	30.9	
	PDSA/ Mt				1	96	15.9	27.1	57	
	Al/ Mt	3:1		120	1	60	68.3	16.7	15	
	KSF	11:1		107	2.7	99.7	12.9	57.7	29.4	[83]
	H3PO4/ KSF	10:1		115	7	99.8	10.4	49.1	40.5	
Mesoporous Carbonaceous Material	AC/ H_3PO_4	8:1		120	3	47			23	[73]
	AC/ H_2SO_4	8:1		120	3	91	38	28	34	
	AC/ H_3PO_4		5:1	100	0.83	100	0	0	100	[81]
	Starbon-400-SO_3H	3:1		130	0.5	>99	8	15	77	[74]
	AC	16:1		120	3	15	42	54	3	[73]
	Biochar	5:1		120	4	88.5	62.4	30.5	1.8	[88]

Table 6 (continued) – Summary of the catalysts used in the acetylation of Glycerin, obtained from literature.

Section	Catalyst	HAc:Glyc (mol)	Ac_2O:Glyc (mol)	T (^oC)	t (h)	% Conversion	% S MAG	% S DAG	% S TAG	Reference
Sugar Catalyst	Glycerin/ H_2SO_4	10:1		115	4	100	0	60.2	39.8	[59]
	Sucrose/ H_2SO_4	9:1		105	4	>99	n.r.	n.r.	9	[89]
Heteropolyacids	Tungstophosphoric acid Immobilized in Niobic acid	5:1		120	4	98	24	56	20	[77]
	12-Molybdophosphoric Immobilized in HUSY	n.r.		n.r.	3	68	37	59	2	[90][90]
	12-Tungstophosphoric immobilized in silica matrix	16:1		120	4	74	33	62	3	
	12-Tungstophosphoric immobilized in ac. carbon				3	86	25	63	11	[75]
	Silicotungstic acid	6:1		105	4	>97		75	>10	[70]
	Tungstophosphoric acid				4	>95		70	>7	
Ionic Liquids	$[HO_3S\text{-}(CH_2)_3\text{-}NEt_3]Cl\text{-}[FeCl_3]_{0,75}$	5:1			4	98.7			98.8	[91]
	$[HO_3S\text{-}(CH_2)_3\text{-}NEt_3]Cl$	5:1			4	80.9			84	
Magnetic Solids	Fe-Sn-Ti(SO_4^{2-})		5:1	80	0.5	100	0	1	99	[92]
Polymers	Sulfonated Polyethersulfone	8:1		120	3	100	11	54	35	[93]
	12-Tungstophosphoric / PDVC	8:1		100	3	99.9	0.5	26.5	73	[31]
Homogeneous	H_2SO_4	3:1		130	0.5	85	43	32	25	[74]
	HCl	8:1		120	5	49	n.r.	n.r.	n.r.	[73]
	H_3PO_4	8:1		120	5	57	n.r.	n.r.	n.r.	
	P--Toluenesulfonic acid	3:1		105	3	100		55	38.7	[66]

n.r. – not reported

3 Experimental procedure

3.1 Preparation of the Catalysts samples

The acetylation of glycerin was performed using acid treated and activated Mt and sugar-based catalysts. Amberlyst-15 was also used as a reference for the following analysis.

3.1.1 *K10, K30 & KSF*

Given the significant relevance of clays in the catalysis world, three different Mt were chosen, namely acid treated Mt K10, K30 and KSF, with different characteristics (Table 5) and their performance in the Acetylation reaction tested in similar conditions with refined (> 99.5 %) and crude Glycerin (provided by Sovena a local biodiesel factory [20]).

3.1.2 *K10*

The main treatments applied on the K10 were with the strong mineral acids, such as hydrochloric, sulfuric and phosphoric, as they were assumed to yield better results. For comparison, Mt K10 was also treated with weaker and organic acids, including citric, oxalic, tartaric, acetic, lactic and propionic acids. The Pka values of the used acids in the K10 tuning can be observed in the following Table 7.

Table 7 – Pka values of the organics and inorganics acids [94].

Acids	**Pka**		
Sulfuric	-3	2	
Hydrochloric	-7		
Phosphoric	2.1	7.2	12.3
Citric	3.14	4.77	6.39
Acetic	4.75		
Oxalic	1.46	4.40	
Tartaric	3.04	4.36	
Propionic	4.87		

For the procedure, 20 g of K10 were dispersed in 200 mL of 1 M of solution of each acid. The mixture was stirred for 30 minutes at boiling temperature, filtered with deionized water, dried at 60°C overnight and, finally, calcined at 275 °C for 2 hours, with a heating rate of 5 ºC/min.

It is known that when Mt K10 is exposed to hydrochloric acid, the acid attacks alumina structures and extracts aluminum, forming aluminum chloride ($AlCl_3$), destroying the structure, depending on the exposure time span, temperature and the acid's concentration. In these experiments, it was observed that when using the citric and lactic acids, the solution exhibits a strong yellow color, indicating the possible existence of aluminum citrate and aluminum lactate (Figure 11) [95].

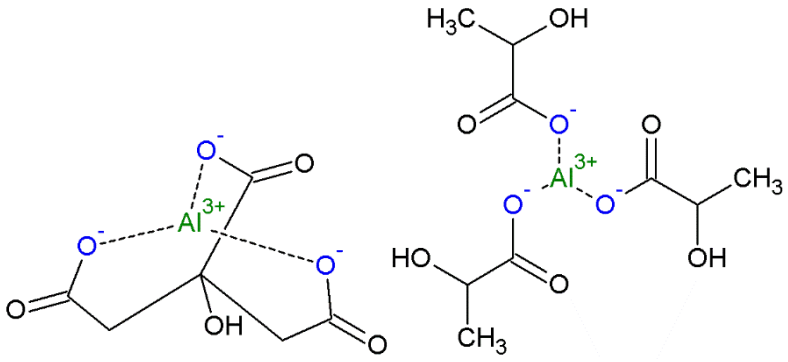

Figure 11 - Aluminum Citrate (on the left) and Aluminum Lactate (on the right).

3.1.3 *Sugar Catalysts*

A mixture of glycerin and concentrated sulfuric acid, with a ratio of 1:4, respectively, was placed in a 1 L glass cup and gently heated from ambient temperature up to 100 ºC, with agitation, to promote *in situ* carbonization and sulfonation. The resultant carbon was cooled to ambient temperature and filtered with deionized water, under vacuum, and dried at 60 ºC overnight. The same procedure was applied for D-(+)-Glucose monohydrate, instead of glycerin.

3.2 Reactor Set-Up

The acetylation reactions were carried out with a three necked round flask equipped with a condenser, a temperature controller with a set point of 125 °C and a magnetic stirrer. The device was placed in a heating nest and the stirring was fixed at 1500 rpm for all experiments to minimize external diffusion problems (Figure 12).

Figure 12 – Experimental *set-up* of the acetylation reaction.

The reaction procedure was performed as follows:

The catalyst and acetic acid were added into the round flask;

The mixture was heated to the reaction temperature (about 20 min);

The Glycerin was injected;

In order to investigate the influence of time on the reaction, some intermediate samples were taken out and analyzed by gas chromatography with a fused Silica non polar capillary column and a Flame Ionization Detector (FID).

The experimental conditions of the reactions performed are in Table 8.

Table 8 – Experimental conditions for acetylation reaction. *W HAc /W Gly* refer to the molar ratio between acetic acid and glycerin.

Catalyst	m_cat (g)	wt% catalyst	*W HAc/WGly*	t (hours)
No catalyst	---	---	9.6	5
Amberlyst15 wet	2.02	10.1	9.6	5
Gly_SO4		9.8	9.4	5
KSF		10.1	9.6	4
K30		10.1	9.6	4.6
K10		10.1	9.6	5
K10 hydrochloric (1M)		10.0	9.6	5
		10.0	6	5
K10 sulfuric (1M)		10.1	9.6	5
K10 sulfuric (2M)		10.0	9.6	4.5
K10 phosphoric (1M)		10.1	9.6	5
K10 citric (1M)		10.1	9.7	5
K10 citric (2M)		10.1	9.6	4.1
		10.0	6	4.5
K10 oxalic (1M)		10.1	9.6	5
K10 tartaric (1M)		10.1	9.6	5
K10 lactic (1M)		10.1	9.6	5
K10 acétic (1M)		10.1	9.6	5
K10 propiónic (1M)		10.1	9.6	5
KSF-crude glycerin		10.1	9.6	5
K30- crude glycerin		10.1	9.6	3
K10- crude glycerin		10.0	9.6	5
Glucose_ crude glycerin		10.1	9.6	2.5
Glucose_SO4	2.02	10.1	9.6	4.8
	1.45	7.5	9.6	2.5
	1.01	5	9.6	2.5
Glycerin_SO4- crude glycerin	2.02	10.1	9.6	2.5

3.3 Characterization Methods/Techniques

3.3.1 X-ray Powder Diffraction (XRD)

X-ray Powder Diffraction is a versatile, non-destructive technique that reveals detailed information about the chemical composition and crystallographic structure of materials, employing a powdered or polycrystalline material, which consists in several randomly oriented particles. Some particles are, therefore, properly oriented and every set of crystallographic planes will be available for diffraction, analyzing the quality of crystallite lattices in the sample. A crystal lattice is a regular 3D distribution of atoms in space, which is arranged/orientated so that it forms a series of parallel planes in a number of different orientations, separated one from another by its own specific *d*-spacing (the spacing between atomic planes in the crystalline phase) as seen in Figure.

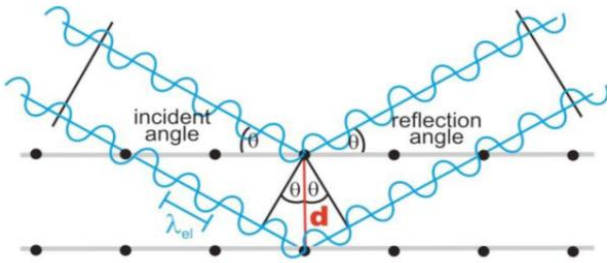

Figure 13 - Bragg Law schematic, with constructive interference.

When a monochromatic X-ray beam with wavelength *λ* is projected onto a crystalline material at an angle θ (angle between the incident ray and the scattering planes), diffraction occurs only when distance traveled by the rays reflected form successive planes differs by a complete number *n* of wavelengths, according to Bragg's law Equation 1 [96][97]**.**

$$n\lambda = 2d \sin\theta \qquad \text{Equation 1}$$

The diffraction analysis was performed with a *Bruker D8 Advance Powder Diffractometer*, using a Bragg Brentano geometry, under Cu Kα radiation (λ: 0.15406 nm) and a secondary monochromator in the angler of $5 - 70\,°\,(2\theta)$. The scan was conducted with an increment of 0,034º/step and an acquisition time of 2 seconds per step, at 40 mA and 40 kV[98].

Plotting the angular positions and intensities of the resultant diffracted peaks of radiation produces a pattern, which is characteristic of the sample.

3.3.2 Fourier Transform Infrared Spectroscopy (FTIR)

Infra-Red Spectroscopy is a useful technique, based on the phenomenon of infrared absorption by molecular vibrations. When irradiating a molecule with electromagnetic waves within infrared frequency range, one particular frequency may match the vibrational frequency of the molecule, causing excitation of the molecular vibration. Consequently, the vibrational energy levels of sample molecules transfer from ground state to excited state.

The frequency of the absorption peak is determined by the vibrational energy gap, *ΔE (Planck's Equation)*; the number of absorption peaks is related to the number of vibrational freedom of the molecule, and the intensity of the absorption peaks to the change of dipole moment and the possibility of the transition of energy levels. Therefore, by analyzing the Infra-Red spectrum, one can readily obtain abundant structure information of a molecule [99][100][101].

There are a few ways a bond can vibrate, according to its degrees of freedom, as displayed in Figure 14. The frequency of a given stretching bonds depends on the mass of the atoms, its geometry and the stifness of the bond [99][100].

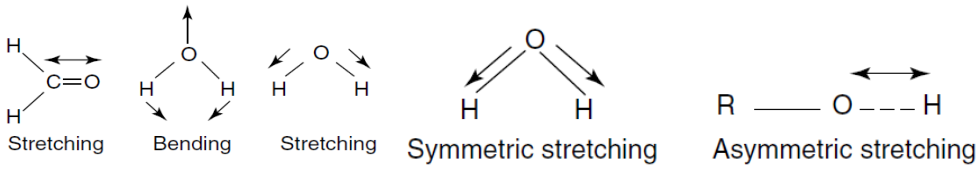

Figure 14 – Stretching and Bending vibrations[99]

Fourier transform infrared spectroscopy (FTIR) is the most widely used vibrational spectroscopic technique, in which the Fourier transform method is used to obtain an infrared spectrum in a range of wavenumbers simultaneously and has a high signal-to-noise ratio, compared to the old method, the dispersive method [100].

In these days, IR-measurements are performed in ATR (Attenuated Total Reflection), since this technique is simpler to manage, compared to the conventional transmission mode (which uses KBr pellets and liquid cells) and can analyze all type of samples, whether they are solid, liquid, powder, paste or fiber, placing them on a ATR crystal [102].

The Infrared spectra were obtained in transmission mode with a spectrometer, using *ZnSe* crystal for ATR sampling, with a range of 4000–600 cm^{-1} and a resolution of 4 cm^{-1}. The resulting infrared spectrums were treated using the *Kubelka-Munk* method [103]

3.3.3 Catalytic Isomerization of 1-Butene

The product distribution of the catalytic 1-Butene isomerization is widely used to evaluate the acidity of heterogeneous catalysts, since the molecule reacts readily in the presence of catalytic materials containing a high concentration of protons. The product distribution is divided into several groups, with double-bond isomerization (cis-2-butene and trans-2-butene) and skeletal isomerization products (isobutene) being the most important ones, as can be seen in Figure 15 [104].

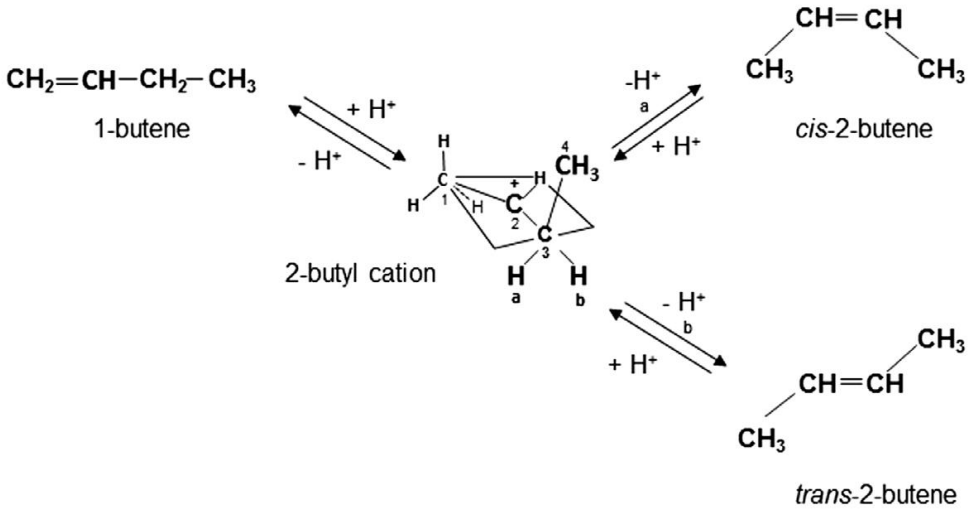

Figure 15 – Mechanism of acid catalyzed isomerization of 1-butene [105].

A high cis/trans ratio is observed for the basic-catalyzed isomerization since the cis-1-methyl-allyl anion intermediate is more stable than the trans-isomer, contrasting with the acid-catalytic isomerization, which presents a ratio close to or less than 1 [106].

The experiments were carried out in a tubular glass flow reactor, with a catalyst sample of around 500 mg, using 1-butene (5 wt%) mixed with compressed air. All the catalysts were tested for more than 80 min on stream. The existing product gases were sent to the AutoSystem gas chromatograph equipment from Perklin Elmer and analyzed by the integrator (Shimadzu, C-R6A Chromatopac).

The process diagram of this activity is presented in *Appendix A2*.

3.3.4 Scanning Electronic Microscopy (SEM)

The Scanning Electron Microscopy is an instrument that produces a largely magnified image by using electrons, e^-, instead of light to form an image. In SEM, the electron gun produces a beam ofe^-, the primary beams, allowing the formation of an e^- probe. These e^- are accelerated by a specific voltage towards an anode, following a vertical path through the microscope, which is held within a vacuum [107].

The beam travels through electromagnetic fields and lenses, focusing the beam down towards the sample (Figure 16). Once the beam hits the sample, a number of interactions occur that result in the generation of several signal types and, consequently, the emission of e^- and photons from the sample.

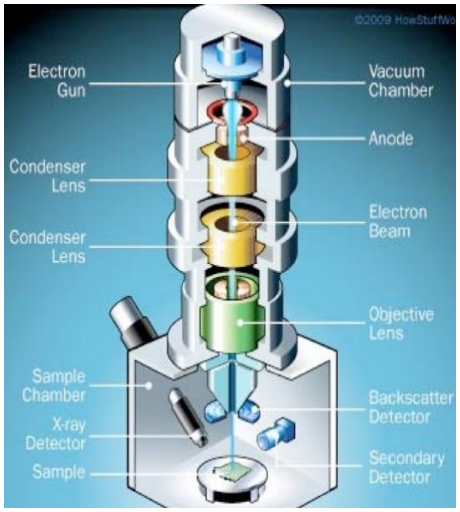

Figure 16 – Principal design of a scanning electron microscopy (SEM) available at[108].

The main images produced in the SEM are elemental X-rays maps, backscattered electrons (BSE) and secondary electrons (SE). The products emitted from the sample surface are collected by the detector and their signals, which are proportional to the product yield, modulate the brightness of the corresponding pixels in the screen.

SE are usually the result of an inelastic collision in which the transferred energy of the primary beam is transferred to an e^- that is emitted (with energy less than 50 eV) from the atom. The e^- produced throughout the interaction region can only escape from the uppermost portion due to their low energy, providing information on the surface topography.

BSE are the result of elastic collisions with atoms of the sample. They result in emitted e^- that have nearly the same energy as the primary beam. As such, BSE can escape from deeper regions in the sample and so the image maps a deeper region. However, they cannot be used for elemental identification [109][96].

Lastly, X-Rays are indirectly produced when an electron is displaced through a collision with a primary beam electron and is replaced by another e^-. The resultant loss of energy takes the form of an X-ray and can escape from even deeper regions in the sample than the BSE [110].

Because SEM operates in vacuum conditions and uses e^- to form an image, the sample must have special preparations prior to the SEM's analysis. All non-metals need to be made conductive by covering the sample with a thin layer of conductive material. Otherwise, these tend to charge when scanned by the e^- beam leading to scanning faults and other image artifacts. Additionally, coating the sample increases the signal and surface resolution [111].

This is done by using a device called a "sputter coater", where the sample is placed in a small chamber that was at a vacuum (10^{-3} – 10^{-5} bar) and gold/palladium atoms fall and settle onto the surface of the sample producing a thin 20 nm Au/Pd coating[107].

The SEM analysis was carried at the RNME pole of Instituto Superior Técnico (IST), in Lisbon, using a JEOL SEM, model 7001F, a tungsten Field Emission Gun (FEG) SEM with Schottky emission, resolution of 1.2 nm at 15kV, equipped with secondary and backscattered electron detectors, and with an Energy Dispersive Spectroscopy (EDS) light elements detector [112].

3.3.5 Energy Dispersive Spectroscopy (EDS)

EDS systems are mounted in the electron microscope and take advantage of the X-Rays produced during the interaction of the primary beam with the sample to analyze the sample's composition. A semi-quantitative material elemental analysis of the surface layers of the catalysts used is provided by the SEM, built by matching the peak energies and intensities with a database of periodic table elements [113][97].

3.3.6 Gas Chromatography (GC)

Gas Chromatography (GC) equipped with flame ionization detector with model Varian CP 3800 was used to determine the main products, namely, MAG, DAG and TAG in the sample collected. The principle of GC is to study the different in retention time of vaporized component in sample though a capillary column. Fused Silica capillary column constituted by Methyl 5 % Phenyl Silicone was used with a 0.1 u of film thickness, 0.32 mm of internal diameter and a length of 15 meters.

Samples were prepared by mixing some drops of product with Isopropyl Alcohol (IPA) (GC grade) as internal standard. About 2 µL of the sample was then injected into the column and the data acquisition was manually triggered and printed out, as can be seen in Figure 17.

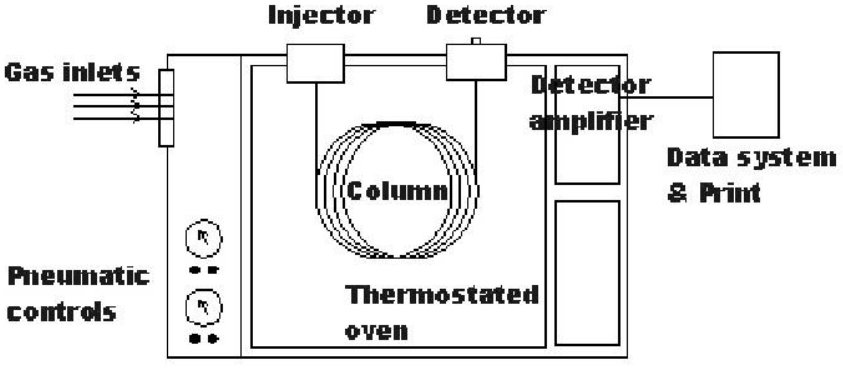

Figure 17 – Schematic Diagram of GC [114].

Table 9 – Gas Chromatography specifications

Specification	GC
Column	Non Polar Fused Silica
Carrier Gas	He
Initial Temperature	100 ºC
Ramp	10 ºC/min to 140 ºC
Injection Temperature	280 ºC with split ratio 10
FID	300 ºC
H_2 (Pressure, Flow)	2.8 bar; 30 mL/min
Air (Pressure, Flow)	4 bar; 300 mL/min
He (Pressure, Flow)	2.8 bar; 25+5 mL/min

Table 9 shows the summary of GC specification.

For a given set of conditions, in this case expressed above in Table 9, the retention time of any compound is always constant and can, therefore, be used to make a quantitative analysis, as the area under a GC peak is proportional to the amount of moles of the eluted compound. As such, the molar percentage composition of a mixture can be approximated by comparing relative peak areas, using the help of the *Galaxie* software, incorporated with the used GC, in order to obtain the relative areas of the acquired peaks. This was the method applied to obtain the relative composition of MAG, DAG and TAG present in the sample [115].

To obtain Glycerin's conversion (Equation 2), it was necessary to calculate the *Glycerin Entrance*, which is equal to the sum of the peak areas relatively to itself and the other acetins, e.g. the sum of the peak area of Glycerin that did not react along with the following peak areas.

$$\%\ Conversion = \frac{\sum \left\{ {Area_i}/{Molecular\ Weight_i} \right\}}{Glycerin\ Entrance} \times 100\ \% \qquad \text{Equation 2}$$

Through Equation 3, the selectivity of each acetin, *i*, was calculated.

$$\%\ Selectivity_i = \frac{\left\{ {Area_i}/{Molecular\ Weight_i} \right\}}{Glycerin\ Entrance - \left\{ {Area_{Glycerin}}/{Molecular\ Weight_{Glycerin}} \right\}} \times 100\ \% \qquad \text{Equation 3}$$

4 Results and Discussion

4.1 Characterization of Glycerin

4.1.1 Crude Glycerin

In these experiments there was the necessity in testing the performance of the catalysts with unrefined glycerin. The composition of the crude glycerin given by a local biodiesel production facility has the following composition, Table 10.

Table 10 – Composition of crude glycerin provided by a local Biodiesel factory.

Compound	Characteristics Maximum
Water (% m/m)	Max. 10
Glycerin (% m/m)	Max. 82
Methanol (% m/m)	Max. 0.1
Matter Organic Non Glycerol – MONG (% m/m)	Max. 1.5
Ash (% m/m) – of which 80 % are from NaCl	Max. 7

4.2 Characterization of Catalysts

4.2.1 Crystalline phases by XRD

4.2.1.1 – Commercial Mt Catalysts

When any Mt is treated with acid, several transformations can occur, such as dissolution of impurities (e.g. carbonates and feldspars); partial or total destruction of the most defective phyllosilicate phases, this being the most relevant transformation; substitution of interlayer cations (e.g. Mg^{2+}, Ca^{2+}, Na^{2+}, K^{+}) with H_3O^{+}. Accordingly, when H^{+} attacks on the edge surface or on the regular plane surface during activation, the protoned surface is dissolved, leading to a partial destructed edge surface [116].

Although all the catalysts are based on acid treated Mt, there are significant differences between Mt K10, Mt K30 and Mt KSF, as can be seen in Figure 18. The Mt KSF appears to be the most attacked catalyst, since in general, the diffraction lines are the ones with the lowest intensity, except at 2θ ~ 20°, line corresponding to Mt structure.

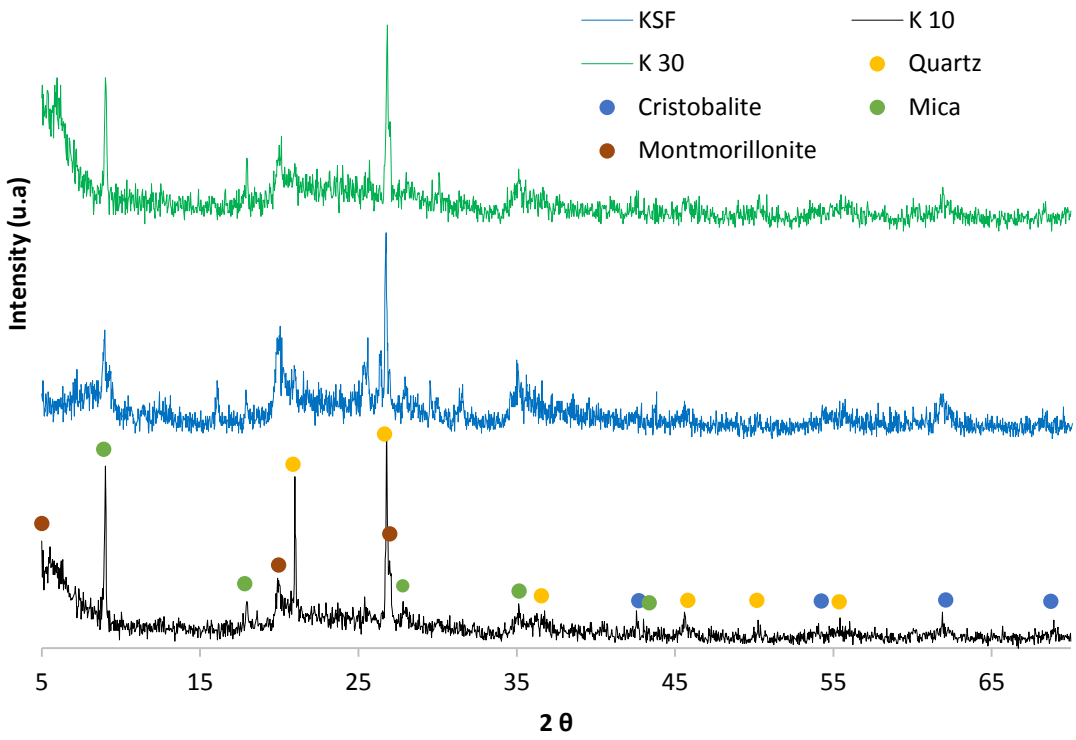

Figure 18 – XRD patterns of Mt K10, K 30 and KSF.

In a typical natural Mt, there is a line around 2θ=6º corresponding to the basal spacing d (001) of laminar clay, characteristic of Monoclinic structures. In the case of the Mt K10 and K30 a wide hump reflection 2θ around 5-6º (d ~ 15 $\dot{A}$) is observed, corresponding to the remaining Mt structure clay, reflecting a disordered stacking in the layers with a basal space around. This reflection is practically amorphous for the KSF catalyst, as can be seen in Figure 18 [117].

Also, there is a sharp and intense reflection at 2θ = 9º (d = 9.8 $\dot{A}$) which is more pronounced for the catalyst K 10, suggesting the presence of a clay-mineral of the mica group (for example, phengite or muscovite), which is typical of collapsed 2:1 phyllosilicates [118][53][119]. The existence of the hexagonal and trigonal crystal structure of quartz can also be identified by the intense diffraction lines at 2θ = 21º and 2θ = 26.7º, respectively [120][121][122].

4.2.1.2 – Acid treated Mt K10

It's noted that K10 with additional acid treated samples keep the same lattice structures as the K10 when calcined at 275 ºC, although the intensity of the diffraction lines is generally only slightly reduced. Therefore, no serious changes were observed in the samples compared to K10. In the case of the basal spacing of K10, it can be observed that the acid that deformed this hump the most was acetic acid (1M), as can be seen in Figure 19. Accordingly to the intensity of the diffraction lines, the calcined K10 with phosphoric acid (1M) was the sample that showed less destroyed lines in comparison with K10.

As a consequence of the calcination step, the catalysts under the action of acetic, citric and lactic acid display an intensification of their quartz related diffraction lines, owing to the dissolution of

Silica in the K10 tetrahedron sheet, leading to SiO_2 recrystallization (Table 11) [122][123][124]69]. However, due to the relatively low temperature of calcination – 275 ºC, this unstable recrystallization eventually collapsed.

Table 11 – XRD values of the catalysts treated with acetic, lactic and citric acids.

Catalyst	Intensity line of Quartz (2θ= 26.76 º)	
	Before Calcination	After Calcination
K10	89	
K10 Acetic Acid (1M)	125	45.5
K10 Citric Acid (1M)	129.5	66.5
K10 Lactic Acid (1M)	127	61.5

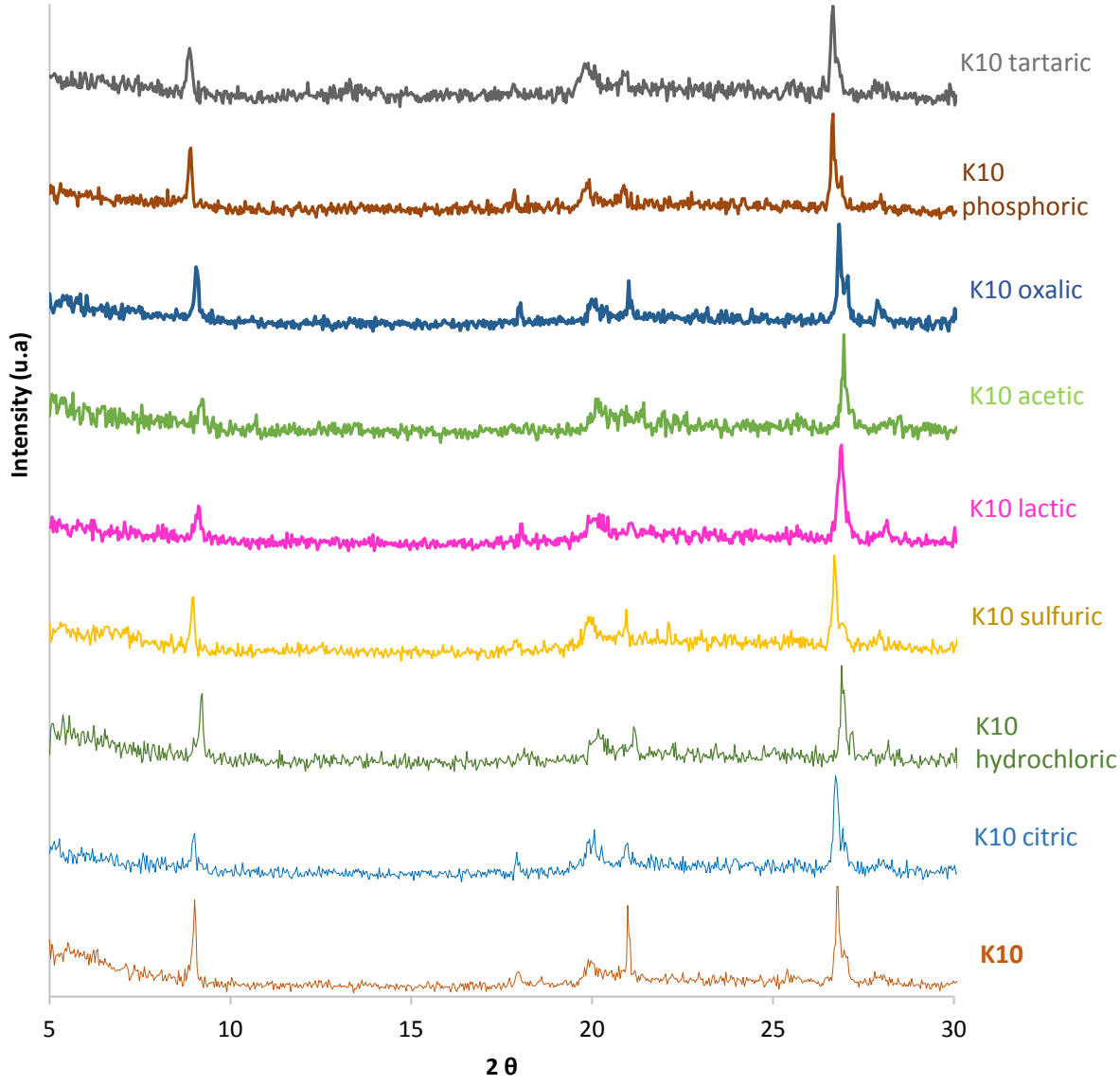

Figure 19 – XRD patterns of Mt K10 treated with different acids.

The X-ray results from the post-reaction are observed in *Appendix 4*, where it can be seen that in general, the crystallographic structure of the catalysts has only slightly decrease in some of

them. Therefore, it can indicate that the acid treatment did not significantly destroy the structure neither it was after the use in the glycerin's acetylation.

4.2.1.3 – Sugar Catalysts

The X-ray diffraction pattern of the sugar catalyst prepared with Glycerin showed weak humps at 2θ values between 15 º and 20 º, as can be seen in Figure 20, consequence of the amorphous nature of the randomly-oriented aromatic carbon sheets carbon [126].

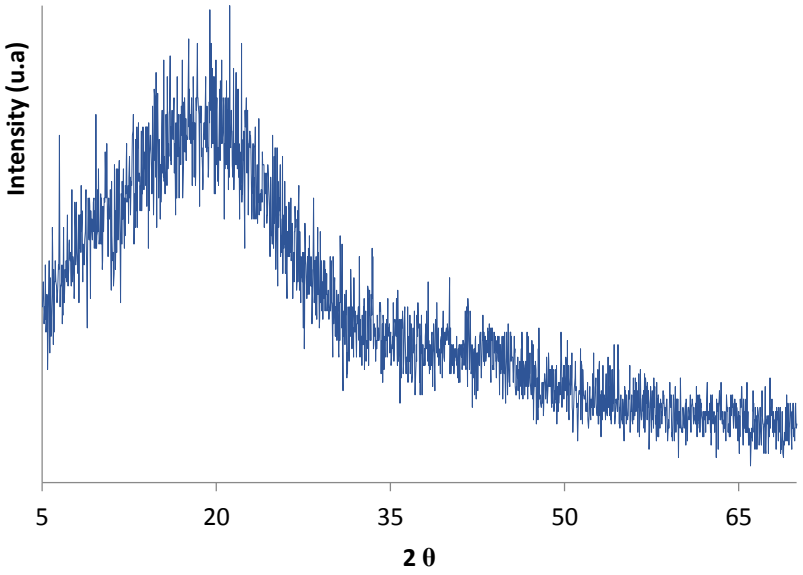

Figure 20 – XRD patterns of the sugar catalyst made with Glycerin.

4.2.2 FTIR

4.2.2.1 – Commercial Mt Catalysts

With the help of IR spectra in the range of 4000 – 600 cm^{-1}, it is possible to analyze the assignments of the vibration modes of acid treated Mt, distinguishing several aspects between the three acid treated clays: *Mt K10, Mt K30* and *Mt KSF*.

As can be seen in Figure 21, the spectrum suggests that *KSF* contains the weakest intensity at 1035 cm^{-1}, which corresponds to *Si–O–Si* stretching vibrations of the tetrahedral layer. This is due to the strong acid attack that has led to the accentuated leaching of this sheet. However, the presence of this peak indicates that the layered structure of the original clay is not fully destroyed, e.g., the clay is relatively stable. The bands around 798, 761, 674, 629 and 1100 cm^{-1} indicate the presence of *free* silica, as quartz (admixtures) or cristobalite, also confirmed by X-Ray, which shows increasing intensity of these bands with the increasing acidity of the catalyst, revealing that *Mt KSF* has a higher content of these impurities than *Mt K10* and *Mt K30* [125][41] [127].

The signal around 910 cm^{-1} represents *Al–OH–Al* bending in the octahedral layers sheet

[128], and is observed in the three catalysts, though in *Mt KSF* this band is more intense, implying that in this case the acid treatment did not remove as much aluminum in these sheets as the other two.

At around 3620 cm^{-1} absorption on Figure 22, the *O–H* stretching of structural inner hydroxyl groups bonded with Al^{3+} cations, between the tetrahedral and the octahedral sheets, is observed [53][129][130]. This is possibly due to the decomposition stage, where octahedral Al ions are preferentially released from the clay structure of Mt, causing the formation of additional Al–OH (and Si–OH) vibration bands.[128] At the 1624 cm^{-1} band the presence of bending water molecules, due to hydration in the interlayer, can also be noted [130][131][132][133].

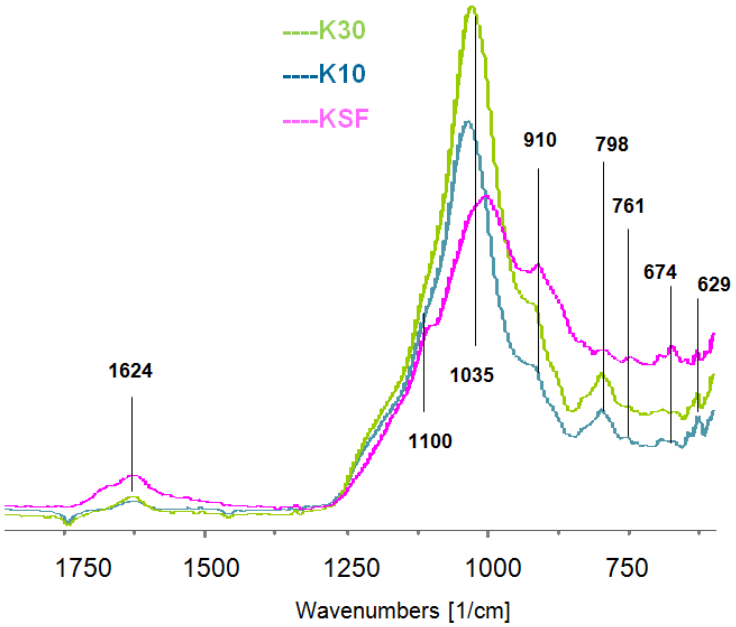

Figure 21 – FTIR of catalysts Mt KSF, Mt K10 and Mt K30 in the range of 2000 – 600 cm^{-1}.

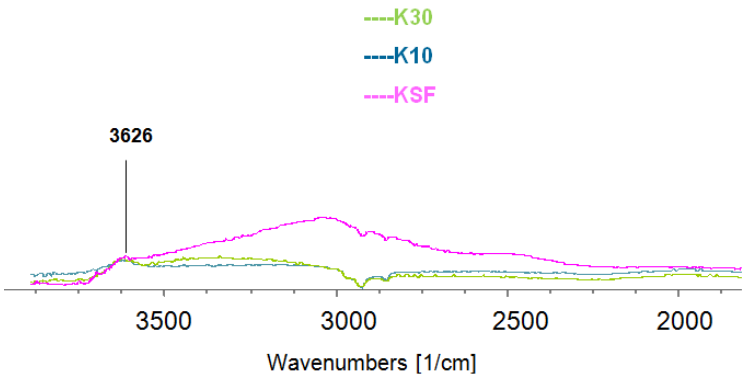

Figure 22 – FTIR of catalysts Mt KSF, Mt K10 and Mt K30 in the range of 4000 – 2000 cm^{-1}.

4.2.2.2 – Acid treated Mt K10

When Mt K10 is treated with citric (1M) and hydrochloric (1M) acids, as can be observed in the Infrared Spectrum on Figure 23, it is clear that the intensity of the band at 1035 cm^{-1} decreases when citric acid 1M is used, implying that the tetrahedral structure is affected by the acid trough a leaching process.

As for the K10 treated with hydrochloric acid (1M), it is shown that in this specific band (1035 cm^{-1}) the intensity increases, possibly due to the exposed sheet tetrahedral (result of the leaching of the octahedral sheet, more affected at lower acid concentration, than tetrahedral and exchangeable cations) [132][117][125][122][41]. A test of reproducibility should have been done to the catalyst K10 with hydrochloric acid (1M) in order to confirm these statements.

One interesting way to analyze whether citric acid is better at removing aluminum than hydrochloric acid is to study the stability of the formed complex with Aluminum. If one were more stable than the other, then its yield would be higher.

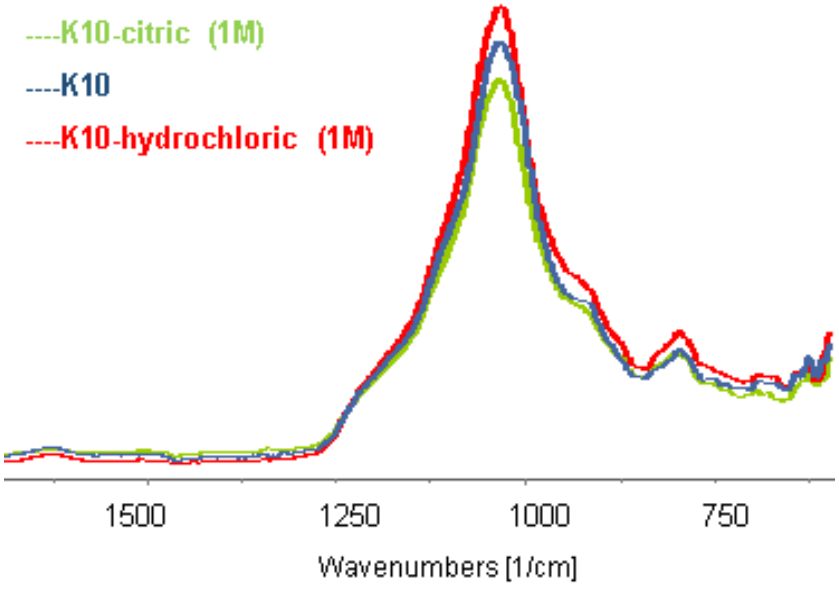

Figure 23 – FTIR spectrum of the catalysts Mt K10, Mt K10 with citric acid (1M) and Mt K10 with hydrochloric acid (1M).

As observed on Figure 24, in general, Mt K10 is affected by the acidity, tending to decrease its intensity bands, the most aggressive case being when *Mt K10* is treated with H_2SO_4 (1M), leading to a lesser intensity in all characteristic bands of Mt K10, and resulting in the catalyst with the most (partial) destroyed structure.

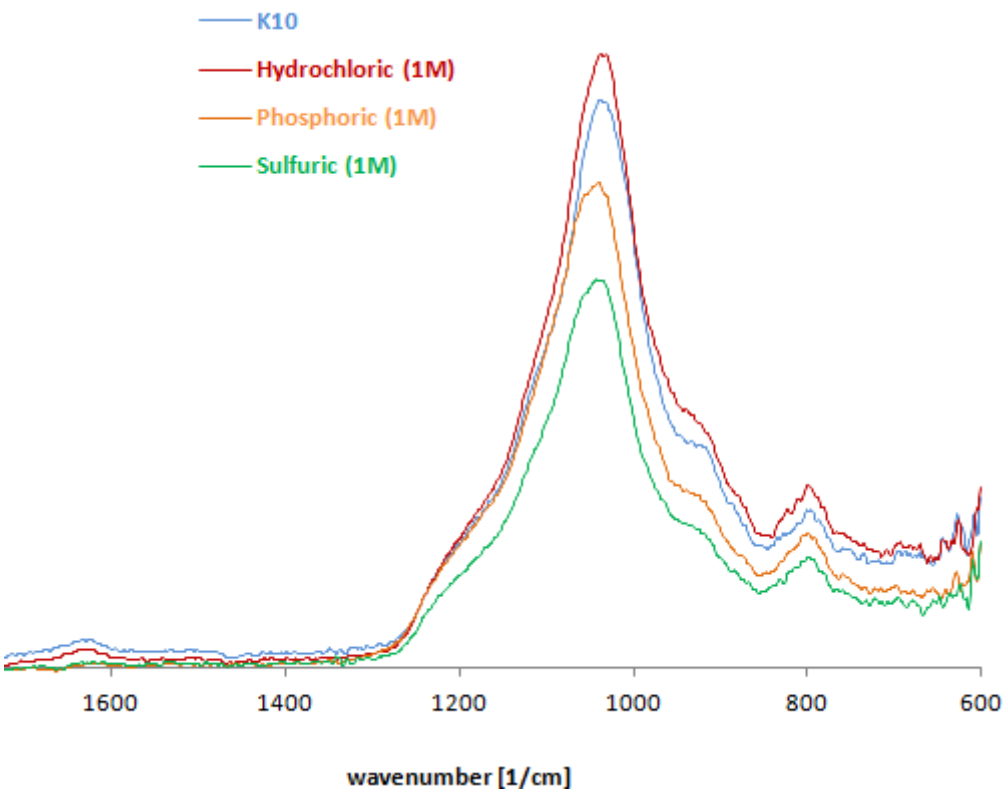

Figure 24 – FTIR spectrum of the catalysts raw K10, k10 with Hydrochloric acid (1M), phosphoric acid (1M) and sulfuric acid (1M).

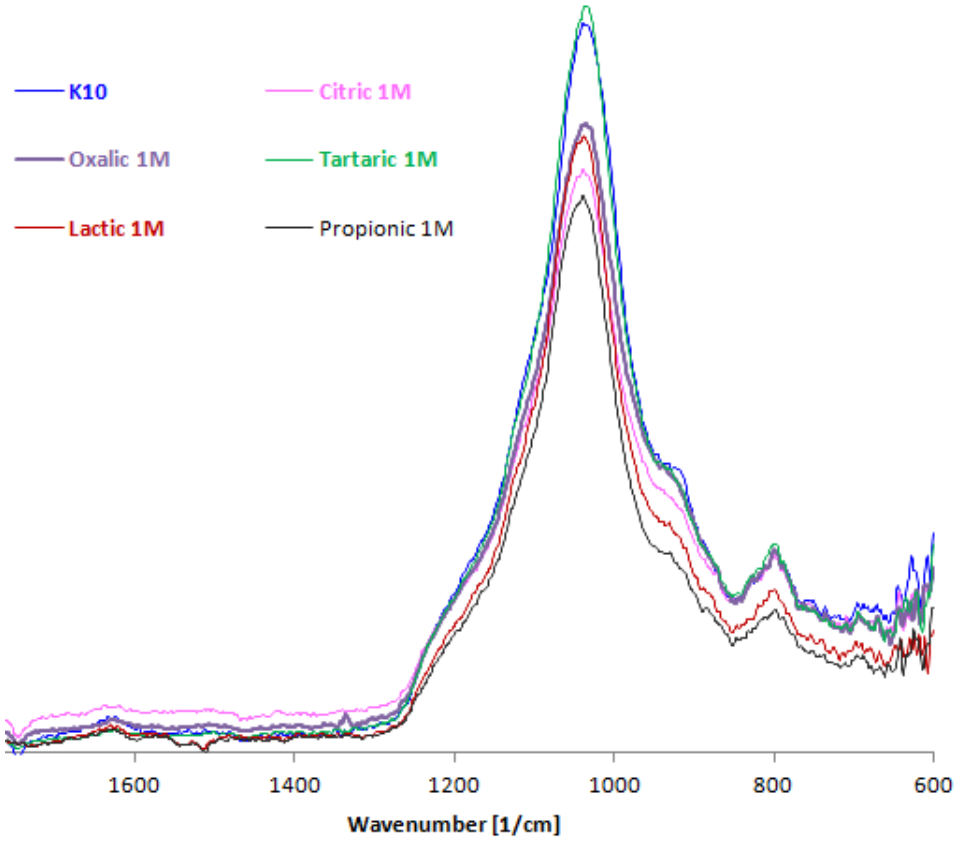

Figure 25 – FTIR spectrum of the catalysts K10, K10 with citric acid (1M), oxalic acid (1M), tartaric acid (1M), propionic acid (1M) and lactic acid (1M).

When using different organic acids on K10 (Figure 25) the tartaric acid (1M) has little to no effect, when comparing to the Mt K10 spectrum, despite the lesser intensity observed in the characteristic bands of impurities such as cristobalite.

The post-reaction Infrared spectrum has some changes, when compared to the infrared prior to the reaction, as can be seen in Figure 26. The main differences are the emergence of the band around 1720 to 1740 cm^{-1}, corresponding to the C=O bond, and the band around 1220 to 1240cm^{-1} due to C– O stretch bond, characteristic of carboxylic acids, in this case, acetic acid and the acetins produced in this reaction [134].

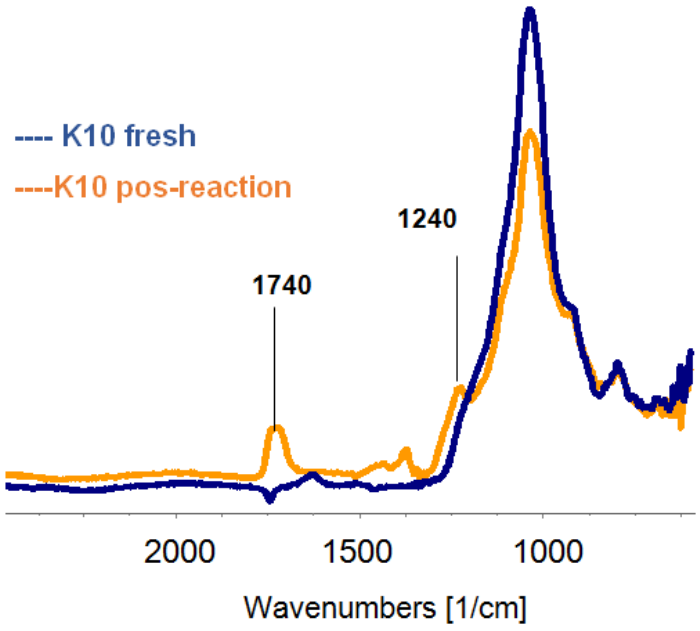

Figure 26 – FTIR spectrum of the catalyst K10 fresh and K10 post-reaction.

4.2.2.3 – Sugar Catalysts

Concerning the catalysts Glycerin_SO_4 and Glucose_SO_4, there is evidence of predominant bands around 1690 and 1025 cm^{-1}, typical of SO_3H structures, as can be seen in Figure 27 and Figure 28 [135][126]. Like Mt K10 catalysts with different acids used in acetylation reaction, catalysts glycerin and glucose also report the characteristic band of acetic acid at 1740 cm^{-1}.

About the structure of these catalysts after a single reaction, it is possible to observe that Glycerin_SO_4 is more stable and resistant that Glucose_SO_4, since this last one shows a significant decrease in intensity at its bands.

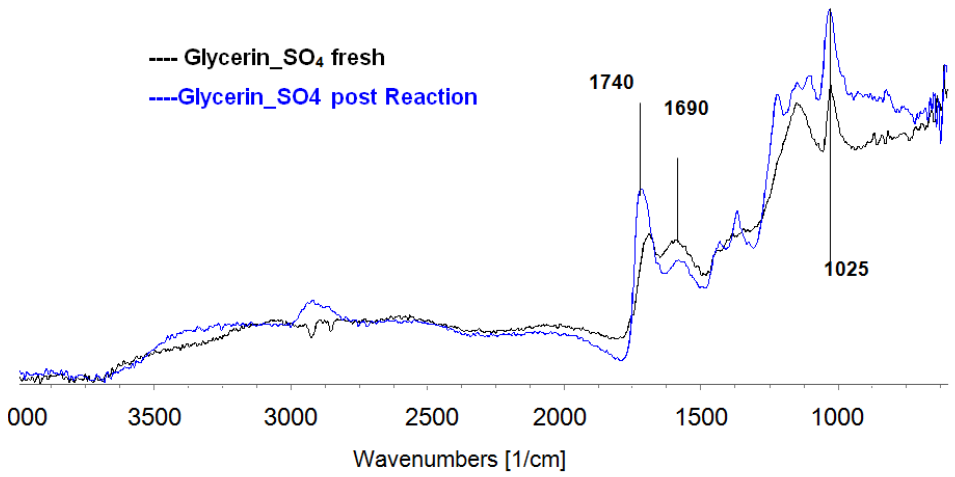

Figure 27 – FTIR spectrum of the catalyst Glycerin_SO_4 fresh (red) and post-reaction (black).

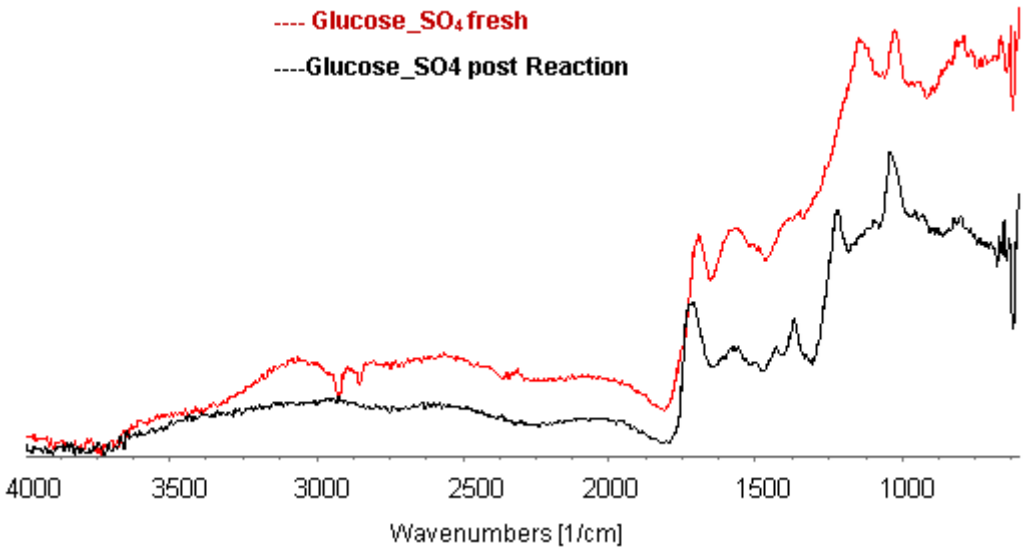

Figure 28 – FTIR spectrum of the catalyst Glucose/SO_4 fresh (red) and post-reaction (black).

4.2.3 SEM-EDS

The morphology of the fresh and post reaction catalysts was assessed by Scanning Electron Microscopy using a FEG equipment.

As such, up to five different particles from each photograph were chosen and analyzed in terms of chemical composition. For every figure analyzed the species O, Na, Mg, Al, K, Ca, Fe, were present, although in some cases the atomic weight was below the detection limit and, consequently, were not possible to quantify. Additionally, due to the sulfuric acid treatment of KSF and the sugar catalysts, they will be the only ones containing sulfur.

4.2.3.1 – Commercial Mt Catalysts

By analyzing the SEM pictures, significant differences in terms of morphology and composition can be noted for the three commercial Mt Catalysts. The Mt KSF shows bigger and more irregular grains in comparison with Mt K10 and Mt K30 as can be seen in Table 12, whereas Mt K10 has generally the lowest grain sizes, Table 14 .

In terms of chemical composition, due to the fact that only a few number of points were analyzed, conclusions can hardly be drawn over their Si/Al ratio. However, one can see that Mt K30 displays the highest Si/Al ratio, in contrast with Mt KSF, the lowest. These ratios can be corroborated with the available data as shown in appendix A3.

As said in section 4.2.2.1, FTIR analysis indicated KSF for being the catalyst with the highest intensity in the band around 910 cm^{-1} representing *Al–OH–Al* bending. From the EDS analysis, this can be corroborated by the fact that has the lowest Si/Al ratio.

Table 12 – The quantitative elemental composition of KSF and corresponding figure with a magnitude x400.

KSF (x 400 ; 10 µm)

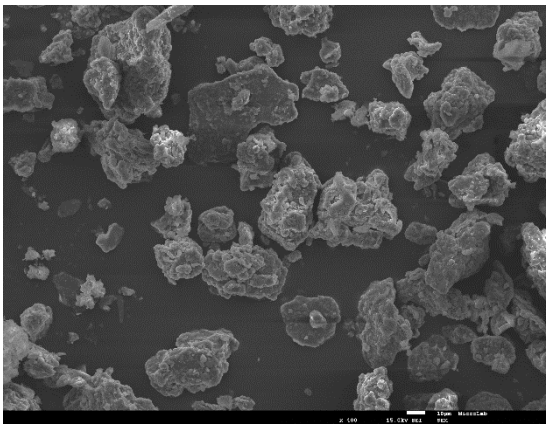

Element	Atom 1%	Atom 2%	Atom 3%	Atom 4%
O	67.31	69.98	62.86	56.48
Mg	1.45	1.53	1.31	1.16
Al	5.89	5.38	7.33	12.42
Si	14.95	13.82	18.12	26.63
S	7.20	5.97	4.8	0.34
K	7.20	0.74	1.21	5.34
Ca	0.66	0.56	0.99	----
Fe	0.46	2.02	3.4	1.62
Total (%)	100			
Si/Al				
2.4 ± 0.2				

Table 13 – The quantitative elemental composition ofK30 and corresponding figure with a magnitude x400.

K30 (x 400 ; 10 µm)

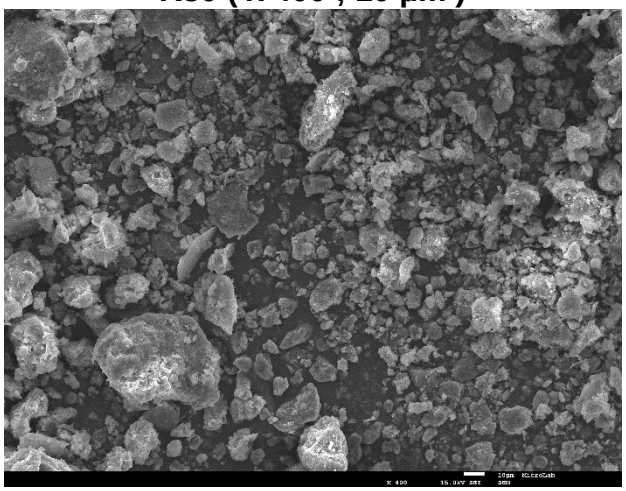

Element	Atom %
O	65.95
Mg	1.07
Al	6.10
Si	25.25
K	0.41
Ca	0.28
Fe	0.93
Total (%)	100
Si/Al	
4.1	

Table 14–The quantitative elemental composition of K10 and corresponding figure with a magnitude X400.

K10 (x 400 ; 10 µm)

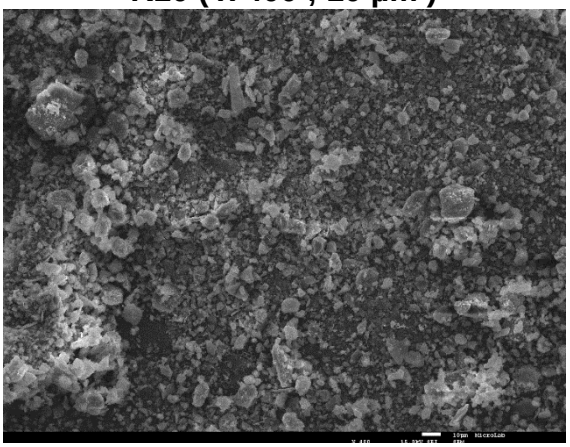

Element	Atom % 1	Atom % 2
O	55.32	67.01
Mg	0.99	0.54
Al	7.58	7.7
Si	34.14	21.39
K	0.93	---
Ca	0.29	2.21
Fe	0.76	1.15
Total (%)	100	100
Si/Al		
3.7		

4.2.3.2 – Acid treated Mt K10

The following SEM pictures are related to the different acid treatment of Mt K10 with organic and inorganic acids. Considering the SEM picture of Mt K10 with citric acid (1M), in Table 15, the majority of the smaller grains of Mt K10 were heavily attacked by the citric acid (1M), leading to their agglomeration. This phenomenon is also noted in the remaining SEM pictures of the acid treated Mt K10 catalysts (Table 16 to Table 25), although in the case of the use of tartaric acid (Table 17) the agglomeration occurred to a lesser extent.

Table 15 – The quantitative elemental composition of K10 citric acid (1M) and corresponding figure.

K10 / Citric Acid (1M)
(x 400 ; 10 µm)

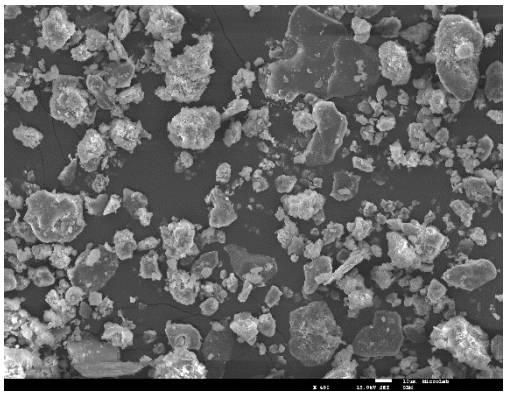

Element	Atom % 1	Atom % 2	Atom % 3	Atom % 4
O	66.82	47.32	64.96	59.43
Mg	0.70	0.51	0.61	0.80
Al	4.12	6.17	4.94	5.16
Si	27.85	15.19	27.79	33.49
K	0.51	5.02	0.85	---
C	---	23.84	---	---
Fe	---	1.97	0.85	1.13
Total (%)	100			
Si/Al				
5.3 ± 0.6				

Table 16 – The quantitative elemental composition of K10 citric acid (2M) and corresponding figure.

K10 / Citric Acid (2M)
(x 400 ; 10 µm)

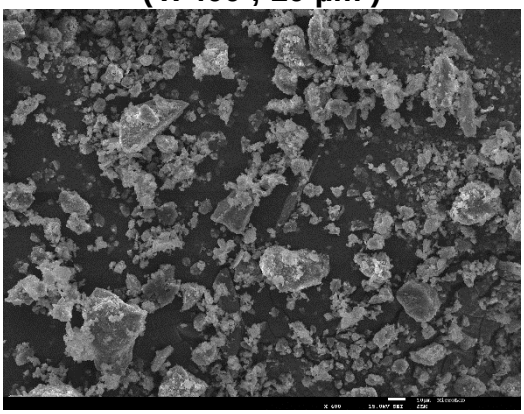

Element	Atom % 1	Atom % 2	Atom % 3
O	63.43	71.88	36.90
Mg	0.64	---	---
Al	5.91	4.02	6.73
Si	26.74	23.81	56.37
K	---	0.29	---
Na	2.79	---	---
Fe	0.50	---	---
Total (%)	100		
Si/Al			
6.37 ± 1.6			

Table 17 – The quantitative elemental composition of K10 tartaric acid (1M) and corresponding figure.

K10 / Tartaric Acid (1M)
(x 400 ; 10 µm)

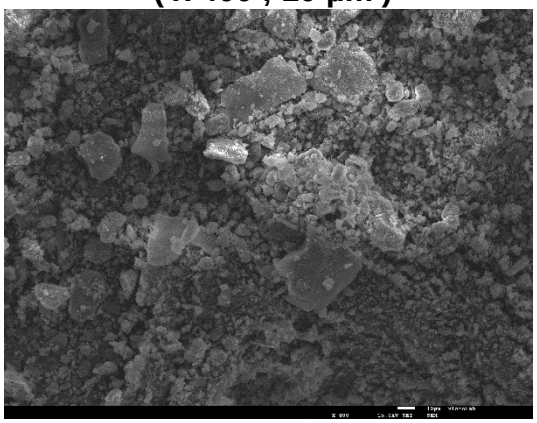

Element	Atom % 1	Atom % 2	Atom % 3	Atom % 4
O	67.45	71.50	59.66	63.75
Mg	0.6	0.62	0.49	0.76
Al	4.53	5.36	4.17	4.81
Si	26.06	20.93	33.92	29.26
K	0.6	1.01	0.95	0.50
Fe	0.75	0.58	0.81	0.92
Total (%)	100			
Si/Al				
6.0 ± 1.5				

Table 18 – The quantitative elemental composition of K10 oxalic acid (1M) and corresponding figure.

K10 / Oxalic Acid (1M)
(x400; 10 µm)

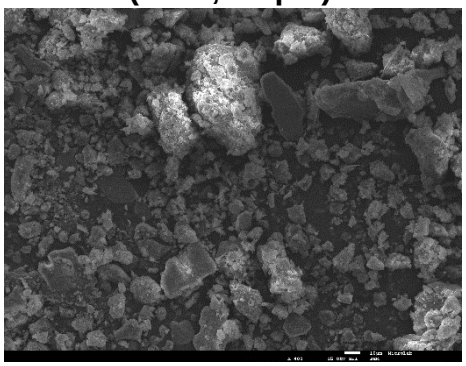

Element	Atom % 1	Atom % 2	Atom % 3	Atom % 4	At % 5
O	64.88	58.87	61.95	64.01	65.32
Mg	0.69	1.25	0.97	1.00	0.74
Al	4.91	5.9	6.81	4.51	4.96
Si	28.14	32.29	25.62	29.63	27.69
K	0.65	0.64	2.84		0.54
Fe	0.74	1.06	1.81	0.84	0.74
Total (%)	100				
Si/Al					
5.4 ± 0.9					

Table 19 – The quantitative elemental composition of K10 hydrochloric acid (1M) and corresponding figure.

K10 / Hydrochloric Acid (1M)
(x 400 ; 10 µm)

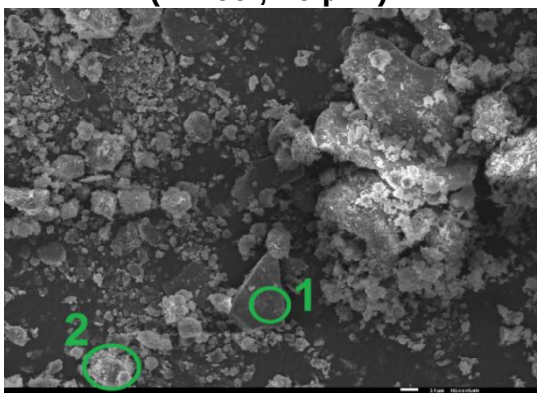

Element	Atom % 1	Atom % 2	Atom % 3	Atom % 4
O	59.01	63.65	66.20	65.66
Mg	0.91	0.78	0.57	0.61
Al	13.08	4.98	4.09	5.43
Si	20.64	29.61	27.84	26.36
K	5.45	---	0.41	1.27
Fe	0.91	0.98	0.88	0.67
Total (%)	100			
Si/Al				
5.9 ± 0.8				

Table 20 – The quantitative elemental composition of K10 sulfuric acid (1M) and corresponding figure.

K10 / Sulfuric Acid (1M)
(x 400 ; 10 µm)

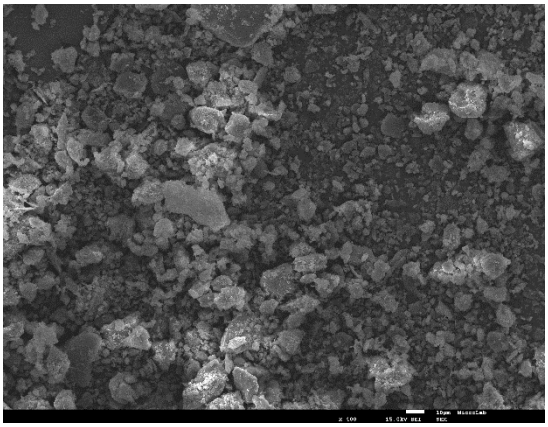

Element	Atom % 1	Atom % 2	Atom % 3	Atom % 4
O	64.12	65.89	62.80	66.69
Mg	---	0.65	0.59	---
Al	5.54	6.23	9.41	9.70
Si	25.17	26.48	23.63	21.58
K	2.95	---	2.72	0.53
Na	---	---	---	1.51
Fe	2.23	0.74	0.85	---
Total (%)	100			
Si/Al				
3.4 ± 1.0				

Table 21 – The quantitative elemental composition of K10 phosphoric acid (1M) and corresponding figure.

K10 / Phosphoric Acid (1M)
(x 400 ; 10 µm)

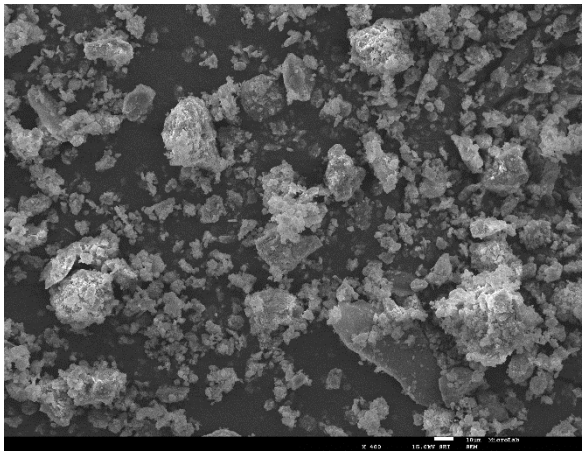

Element	Atom % 1	Atom % 2	Atom % 3	Atom % 4
O	41.35	60.55	62.02	65.68
Al	7.65	3.93	4.6	4.26
Si	13.12	34.17	31.31	27.89
Na	0.54	---	---	---
K	2.82	0.49	0.59	0.64
P	---	0.86	---	0.67
Fe	0.51	---	0.84	0.86
C	33.99	---	---	---
Total (%)	100			
Si/Al				
5.9 ± 2.6				

Table 22 – The quantitative elemental composition of K10 acetic acid (1M) and corresponding figure.

K10 / Acetic Acid (1M)
(x400 ; 100µm)

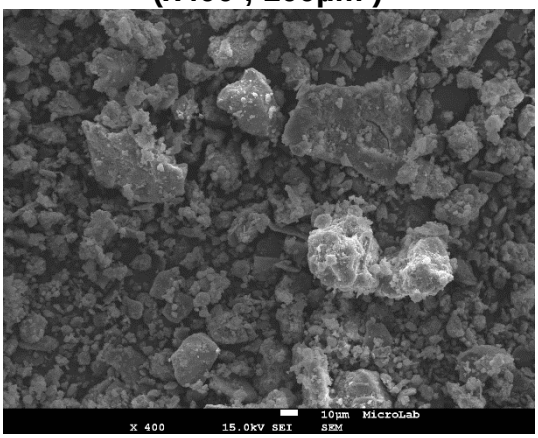

Element	Atom % 1	Atom % 2	Atom % 3	Atom % 4
O	63.41	56.11	67.47	63.51
Al	3.48	5.7	3.97	5.53
Si	33.11	34.93	27.83	30.96
Mg	---	0.67	0.72	---
K	---	0.83	---	---
P	---	---	---	---
Fe	---	1.75	---	---
Total (%)	100			
Si/Al				
7.1 ± 1.5				

Table 23 – The quantitative elemental composition of K10 sulfuric acid (1M) and corresponding figure.

K10 / Sulfuric Acid (2M)
(x400 ; 10 µm)

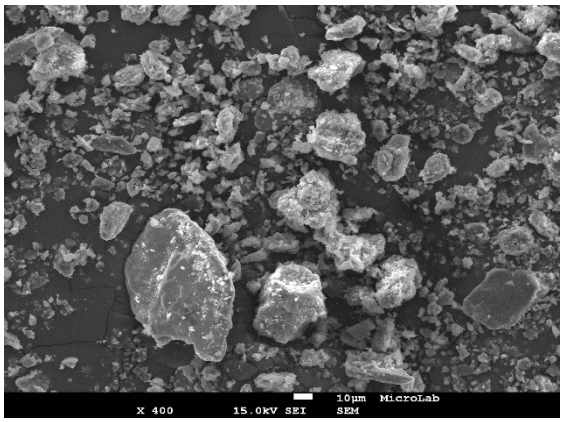

Element	Atom % 1	Atom % 2	Atom % 3	Atom % 4	At % 5
O	62.91	64.03	56.93	65.73	60.16
Al	8.97	3.64	3.07	4.35	12.10
Si	13.81	30.01	21.78	21.74	21.05
K	3.07	0.54	036	---	5.10
C	10.21	---	17.15	2.78	---
Fe	0.62	0.64	0.46	1.83	0.75
Mg	---	0.41	0.38	0.30	0.84
S	---	0.72	0.12	---	---
Ca	---	---	---	3.26	---
Total (%)	100				
Si/Al					
5.5 ± 1.3					

Table 24 – The quantitative elemental composition of K10 propionic acid (1M) and corresponding figure.

K10 / Propionic Acid (1M)
(x400 ; 10 µm)

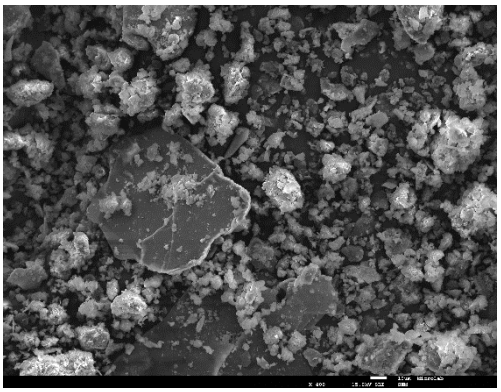

Element	Atom % 1	Atom % 2	Atom % 3	Atom % 4	At % 5
O	66.6	57.38	56.79	54.37	36.51
Al	12.41	3.74	4.48	3.37	7.03
Si	16.49	22.59	18.91	22.32	14.23
Na	0.77	---	---	---	---
K	374	0.32	0.54	0.39	3.62
C	---	14.77	17.97	18.64	37.49
Fe	---	0.68	0.72	0.56	0.73
Mg	---	0.52	0.59	0.34	0.40
Total (%)	100				
Si/Al					
4.7 ± 1.8					

Table 25 – The quantitative elemental composition of K10 lactic acid (1M) and corresponding figure.

K10 / Lactic Acid (1M)
(x400 ; 10 µm)

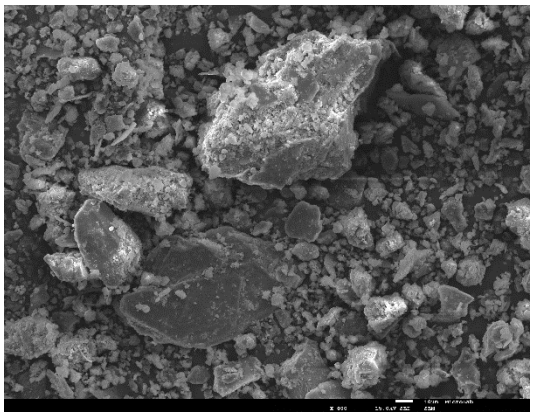

Element	Atom % 1	Atom % 2	Atom % 3	Atom % 4
O	65.10	65.00	56.49	59.80
Al	5.80	4.45	3.48	5.92
Si	26.51	26.44	21.18	28.59
Na	---	---	---	1.64
K	1.10		0.42	---
Mg	0.84	0.63	0.29	---
Fe	0.64	0.74	0.57	0.77
C	---	2.75	17.58	3.29
Total (%)	100			
Si/Al				
5.4 ± 0.7				

4.2.3.3 – Sugar Catalysts

The remaining SEM pictures analysis are of the sugar catalysts: Glucose_SO_4 (Table 26) and Glycerin_SO_4 (Table 27), both of which are shown below. It can be established that the sulfur's attack was more aggressive towards the grain sizes in the glycerin catalyst, when compared to the glucose.

Also, it is interesting to note the corroboration of the theory of the sugar catalysts' formation mechanism, where the sulfonic groups are attached to the corresponding structure, by the appearance of the sulfur element.

Table 26 – The quantitative elemental composition of Glucose/SO_4 and corresponding figure (mag. X400).

Glucose_SO_4 (x 400 ; 10 µm)

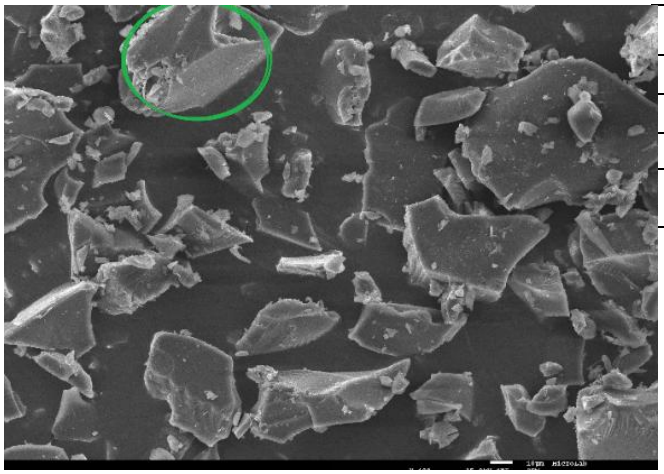

Element	Atom %
O	36.92
C	61.80
S	1.27
Total (%)	100

Table 27–Quantitative elemental composition of Glycerin/SO_4 and corresponding figure (mag. X400).

Glycerin_SO_4 (x 400 ; 10 µm)

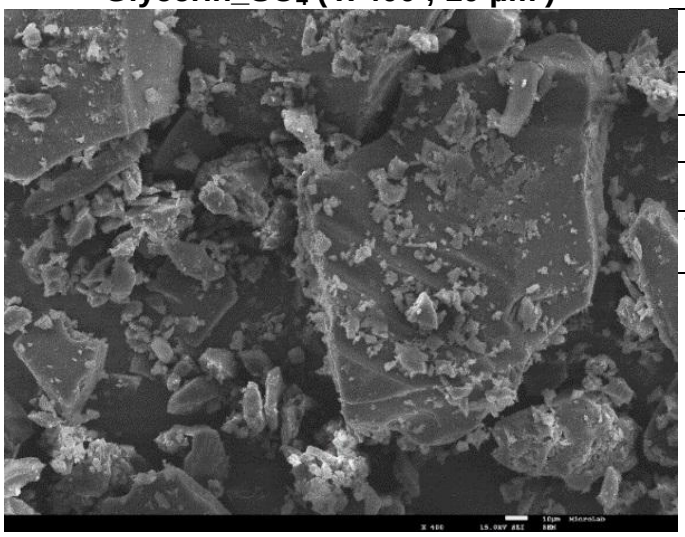

Element	Atom % 1	Atom % 2
O	27.8	27.79
C	69.03	70.06
S	3.17	1.61
Total (%)	100	

4.2.3.4 – SEM Post Reaction

The acetylating agent used in this work was acetic acid, known to be a weak organic acid, and during the 5 hours of the reactions, there may be damage to the structure of the catalyst, leading to a loss of aluminum during the glycerin's acetylation. In order to analyze whether or not the structure was highly damaged, the catalysts were dried overnight after being used in the reaction, and analyzed by SEM.

As can be seen in Table 28, there were no significant changes in the atomic ratio Si/Al, although in some catalysts, namely K10 treated with lactic acid (1M), more pronounced changes in the ratio can be observed, as supported in FTIR graphic in *Section 4.1.2*.

Table 28 – Summary of the atomic ratio Si/Al of the catalysts before and after used in the Acetylation reaction.

Catalyst	Si/Al Atomic ratio	
	Fresh	Post Reaction
K30	4.1	4.6 ± 1.6
K10	3.6	4.6 ± 1.5
KSF	2.3 ± 0.2	2.7 ± 1.4
K10 hydrochloric (1M)	5.9 ± 0.8	5.5 ± 1.0
K10 citric (1M)	5.3 ± 0.6	5.5 ± 0.4
K10 citric (2M)	6.3 ± 1.6	6.9 ± 1.9
K10 tartaric (1M)	6.0 ± 1.5	5.3 ± 1.7
K10 oxalic (1M)	5.4 ± 0.9	5.7 ± 1.1
K10 phosphoric (1M)	5.9 ± 2.6	6.7 ± 0.1
K10 sulfuric (1M)	3.4 ± 1.0	5.4 ± 0.4
K10 sulfuric (2M)	5.5 ± 1.3	n.a
K10 acetic (1M)	7.1 ± 1.5	7.2 ± 1.7
K10 lactic (1M)	5.4 ± 0.7	9.3 ± 2.9
K10 propionic (1M)	4.7 ± 1.8	n.a

n.a - not available

For the case of sugar catalysts, as can be seen in Table 29 and Table 30, the composition is still the same: carbon, oxygen and sulfur, which may confirm that sugar structure still intact. Also, the morphology practically stays the same.

However, it is possible to see that sulfur element in catalyst Glucose_SO4 has significantly decreased, corroborating the results obtained from FTIR in section 4.4.4.3, which show a decrease in intensity for the SO_3H frequency.

Therefore, the stability of the Glycerin_SO_4 catalyst can be verified since the post-reaction catalyst still contains sulfur attached to the matrix.

Table 29 – The quantitative elemental composition of Glucose_SO_4 post reaction

Glucose_SO_4 Post Reaction(x 400 ; 10 µm)

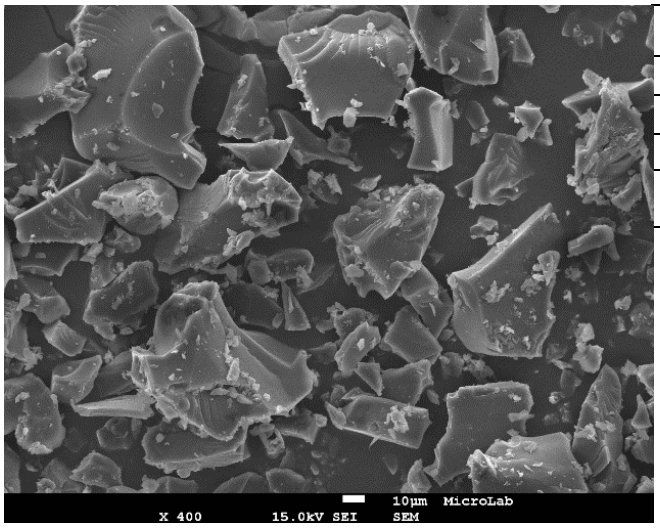

Element	Atom % 1	Atom % 2	Atom % 3
O	52.84	53	55.28
C	47.45	47.08	44.66
S	0	0	0.06
Total (%)	100	100	100

Table 30 – The quantitative elemental composition of Glycerin_SO_4 post reaction.

Glycerin_SO_4 Post Reaction(x 400 ; 10 µm)

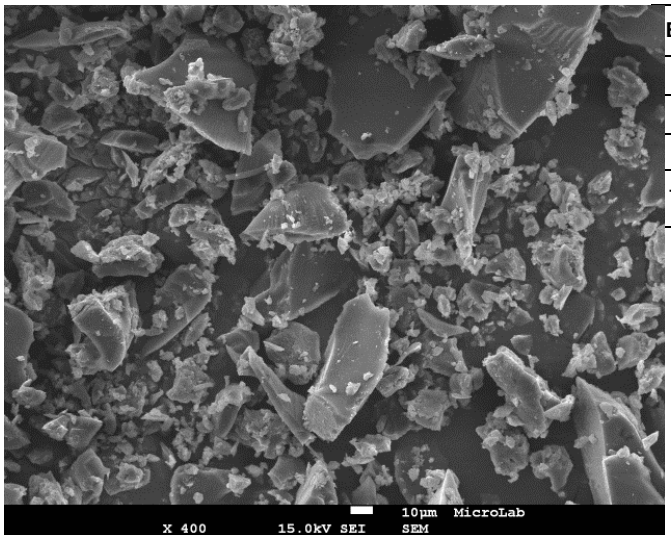

Element	Atom % 1	Atom % 2	Atom % 3	Atom % 4
O	60.34	58.13	69.58	64.53
C	38.14	40.76	26.25	32.48
S	1.52	1.12	4.17	2.99
Total (%)	100	100	100	100

4.2.4 Catalytic Isomerization

1-Butene isomerization is a test reaction that can be used for estimating the nature of active sites, whether they are acid or basic. This reaction yields mainly two groups of products: isobutene (from skeletal isomerization) and cis-trans isomerization of 2-butene. At very low quantity there are also gaseous sub-products from cracking, like methane, ethane, propane, propene and isobutane that quickly exit out of the furnace, as can be seen in Appendix A2.

Isomerization of 1-Butene is mainly controlled by acidity and limitations of pore size, as reported by Xu *et al* [136]. The roles of strength and density of active sites (protonic sites), though, are limited when compared with the role of the size and shape of the channels and cavities as well as the locations of cations and the distribution of Al or other T-atoms, determining the thermal and hydrothermal stabilities of the framework [137][138].

It was reported that the presence of monocations and dications (Mg^{2+}, Fe^{2+} and Na^{+}) in the catalyst structure is detrimental to isomerization reactions, since they contribute to channel blocking, limiting the diffusion of butene molecules [136]. Coke deposition also blocks channels and modifies the space around acid sites, although at temperatures below 200 ºC, coke generally involves condensation and rearrangement steps [139].

4.2.4.1 – Commercial Mt Catalysts

The catalytic performance of the acid treated K10 during the 1-Butene isomerization was determined at temperatures between 125-127 ºC and 139-140 ºC. As time goes by, the conversion of 1-butene decreases due to its deactivation, stabilizing at a constant rate reported below in Table 31.

Figure 29 displays the catalytic activity, expressed as 1-butene conversion for the K10, K30 and KSF, where both 1-butene conversion and the yield in Cis and Trans decrease in the order K30 > K10 > KSF. It is also observed that by increasing temperature, catalytic activity increases. Despite the fact that this analysis reports that K30 is the most acid catalyst, it cannot be ignore the properties of each catalyst, as can be seen in Table 5, where the most acid catalyst is KSF and the most porous is K30. This may indicate that isomerization of 1-butene not only depends of the existing acidity but also their porosity and superficial area.

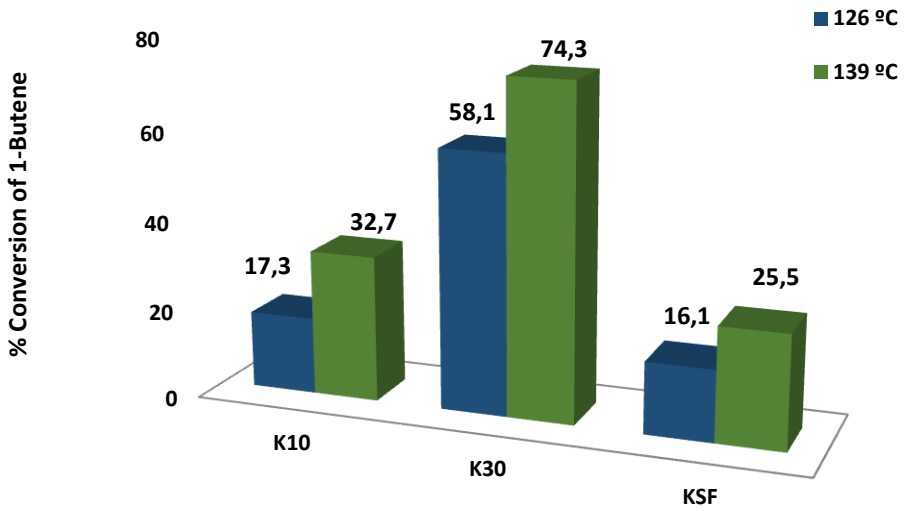

Figure 29 –1-Butene %C isomerization for commercial montmorillonites catalysts at 126 and 139 ºC.

4.2.4.2 – Acid treated Mt K10

When it comes to the strength of active sites, it has been proven that the formation of isobutene requires stronger *Brønsted* acid (BA) sites (Hr < -6.63) than those needed for Cis and Trans isomers (Hr > -4.04) [140][141] [142]. Additionally, BA sites were found to be important for the activity for skeletal isomerization of 1-butene, concerning the fact that Lewis acid (LA) sites alone cannot act as active centers for skeletal isomerization [143].

Table 31 – 1-Butene %C isomerization (conversion, selectivities and consumption rate) for acid treated K10 montmorillonite and raw clays (K10, K30 and KSF), at 127 ºC.

	Catalyst	Conversion (%)	r1-butene (µmol/(gcat·s))	Selectivity (%) Cis	Trans
	K30	58.1	42.4	49.8	50.0
	K10	17.3	12.6	56.6	42.9
	KSF	16.1	11.8	57.3	42.1
K10	Citric (2M)	6.9	5.0	56.7	42.0
	Hydrochloric (1M)	20.3	14.8	54.3	45.3
	Citric (1M)	27.1	20.4	55.1	44.5
	Tartaric (1M)	28.3	20.7	56.1	43.7
	Oxalic (1M)	30.2	22.1	57.1	42.6
	Phosphoric (1M)	33.2	24.2	53.1	46.7
	Lactic (1M)	47.4	34.6	52.7	47.2
	Acetic (1M)	49.4	36.1	53.0	46.9
	Propionic (1M)	53.7	40.1	53.0	46.9
	Sulfuric (1M)	56.9	41.5	47.6	52.3
	Sulfuric (2M)	63.6	46.5	45.5	54.4

This may reflect the fact that the catalysts reported here are mainly constituted by weak *Brønsted* acid sites, since the formation of Isobutene is practically null, as can be seen in Table 31. The number of BA sites is also directly associated with the amount of framework AL, and in general these outnumber the LA sites, as cited by [144].

From Table 32, it can be concluded that overall the cis-isomer was favored. This could be explained by a 1-butene adsorbed state that limited the free movement of the carbon atoms [145][146].

Table 32 – 1-Butene isomerization rate (127ºC and 139ºC) and cis/trans 2-butene selectivities ratio.

	Catalyst	$R_{Butene-1}$ (µmol.gcat^{-1}·s^{-1})		Cis/Trans	
		127 ºC	139 ºC	127 ºC	139 ºC
	K30	42.4	54.3	1.0	0.8
	K10	12.6	23.9	1.3	1.2
	KSF	11.8	18.6	1.4	1.3
K10	Citric (2M)	5.0	9.3	1.4	1.3
K10	Hydrochloric (1M)	14.8	24.0	1.2	1.1
K10	Citric (1M)	20.4	29.8	1.2	1.2
K10	Tartaric (1M)	20.7	28.8	1.3	1.2
K10	Oxalic (1M)	22.1	32.1	1.3	1.2
K10	Phosphoric (1M)	24.2	31.8	1.2	1.1
K10	Lactic (1M)	34.6	44.7	1.1	1.0
K10	Acetic (1M)	36.1	42.3	1.1	1.0
K10	Propionic (1M)	40.1	52.4	1.1	0.9
K10	Sulfuric (1M)	41.5	52.6	0.9	0.8
K10	Sulfuric (2M)	46.5	59.1	0.8	0.7

4.2.4.3 – Sugar Catalysts

In the case of sugar catalysts, the results were substantially different when it comes to the conversion of 1-Butene. As can be seen in Table 33, the conversion of 1-Butene is practically null, which may be correlated with the fact that, as literature refers, they are non-porous or almost nothing. [126] [59]. Therefore and as already said, the isomerization of 1-Butene not only depends the catalyst acidity, but also the size and shape of the channels and cavities. Also for these catalysts, the selectivity towards isobutene is higher than cis and trans butane, possibility indicating the presence of strong Brønsted acids.

Table 33 - 1-Butene %C isomerization (conversion, selectivities and consumption rate) for sugar catalysts at 127 ºC.

Catalyst	Conversion (%)	r1-but (µmol/(gcat·s))	Selectivity Cis (%)	Selectivity Trans (%)	Cis/Trans
Glycerin_SO_4	0.3	0.2	24.6	17.0	1.5
Glucose_SO_4	1.7	0.3	29.2	20.5	1.4

4.2.5 GC Analysis

Firstly, internal standards were prepared in order to identify the retention time of each product, resulting in the following times, seen in Table 34.

Table 34 – Summary of the retention time of the compounds.

Compounds	Retention time, min
Acetic Acid/Isopropanol	0.8 – 0.82
Glycerin	1 – 1.02
1-Monoacetin	1.28 – 1.30
2-Monoacetin	1.41 – 1.43
1- and 2-Diacetin	1.97 – 2.05
Triacetin	2.71 – 2.74

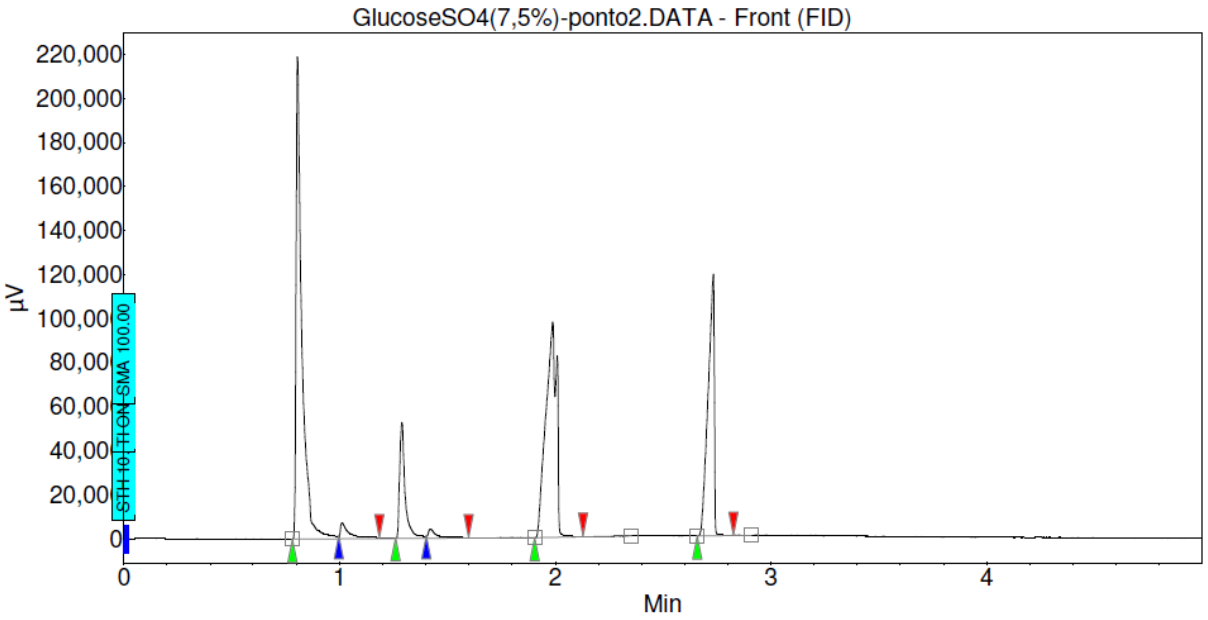

Figure 30 – GC patterns of a common result obtained at Glycerin Acetylation.

Although it is possible to visualize the 1- and 2-acetylated isomers in Figure 30, for both MAG and DAG, it wasn't possible to quantify the 1,2 and 1,3 DAG isomers.

The GC conditions were optimized to separate simultaneously the acetin species and glycerin

4.2.5.1 – Commercial Mt Catalysts

The main objective of these experiments was not only to reach maximum glycerin conversion but also maximum selectivity towards the most valuable acetylated product, TAG. In this section the performance of the three different acid treated Mt was evaluated: K10, K30 and KSF (all 10 wt% of glycerin). When crude glycerin was used, with purity inferior to 82 %, it was possible to see that, after 3 hours and with a molar ratio of HAc to Glycerin of 9.6:1, the conversion of glycerin tends to reach > 80 %, where the predominant acetin in the end is DAG, followed by MAG, as can be seen in Figure 33. At the end of reaction time the formation of TAG was not negligible, reaching the highest value when using KSF catalyst, although the difference between the catalysts was minimal (Figure 31) compared to the values when refined glycerin was used (Figure 32). The main difference is the presence of water in crude glycerin that deactivates the active sites, which are essencial to the formation of TAG

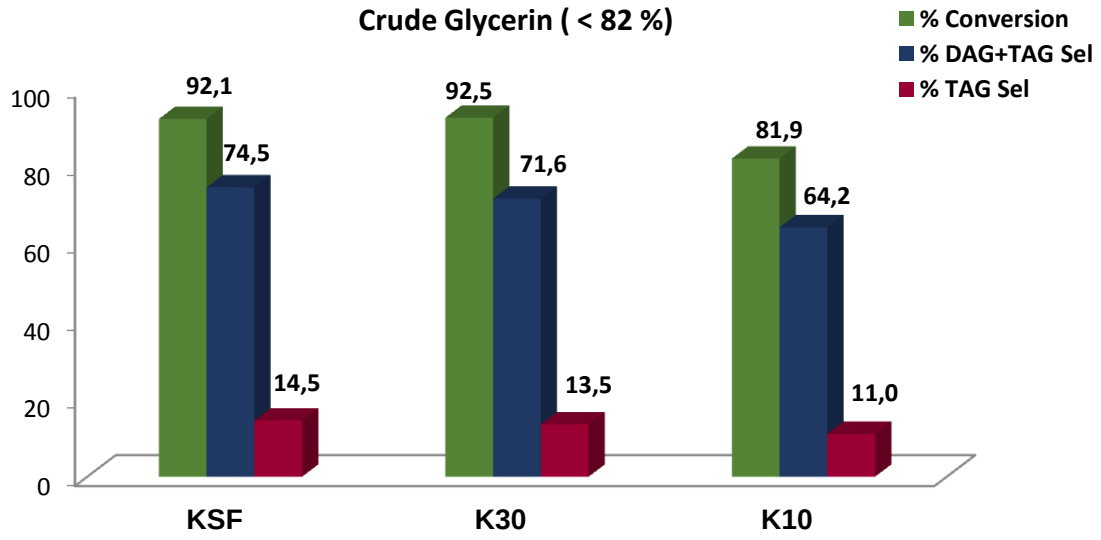

Figure 31 – Final values of conversion and selectivity of crude glycerin and TAG, respectively, after 3 hours of reaction, with a ratio of HAc to Glycerin of 9.6 : 1, using different catalyst (10 wt% of glycerin).

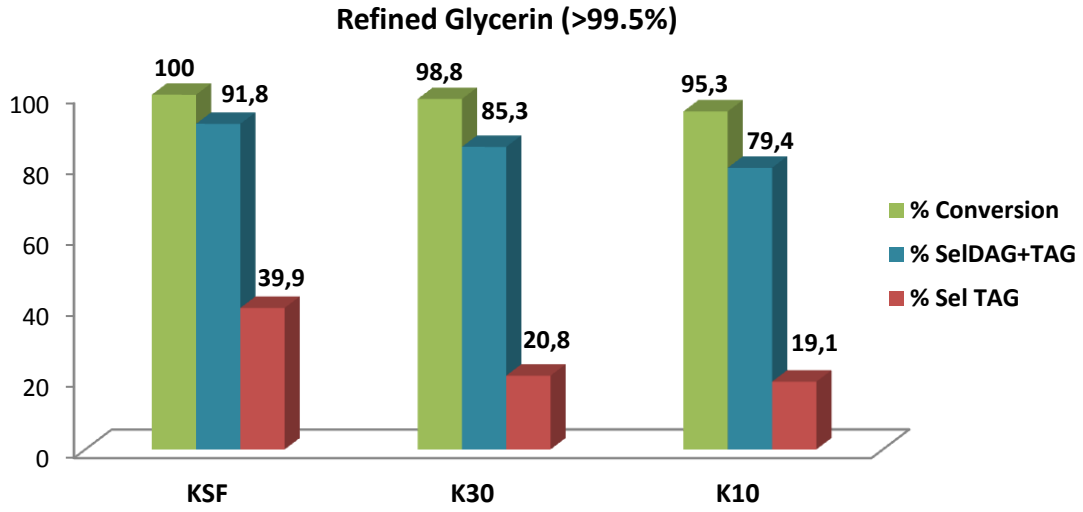

Figure 32 –Final values of conversion and selectivity of refined glycerin and TAG, respectively, after 3 hours of reaction, with a ratio of HAc to Glycerin of 9.6 : 1, using different catalyst (10 wt% of glycerin).

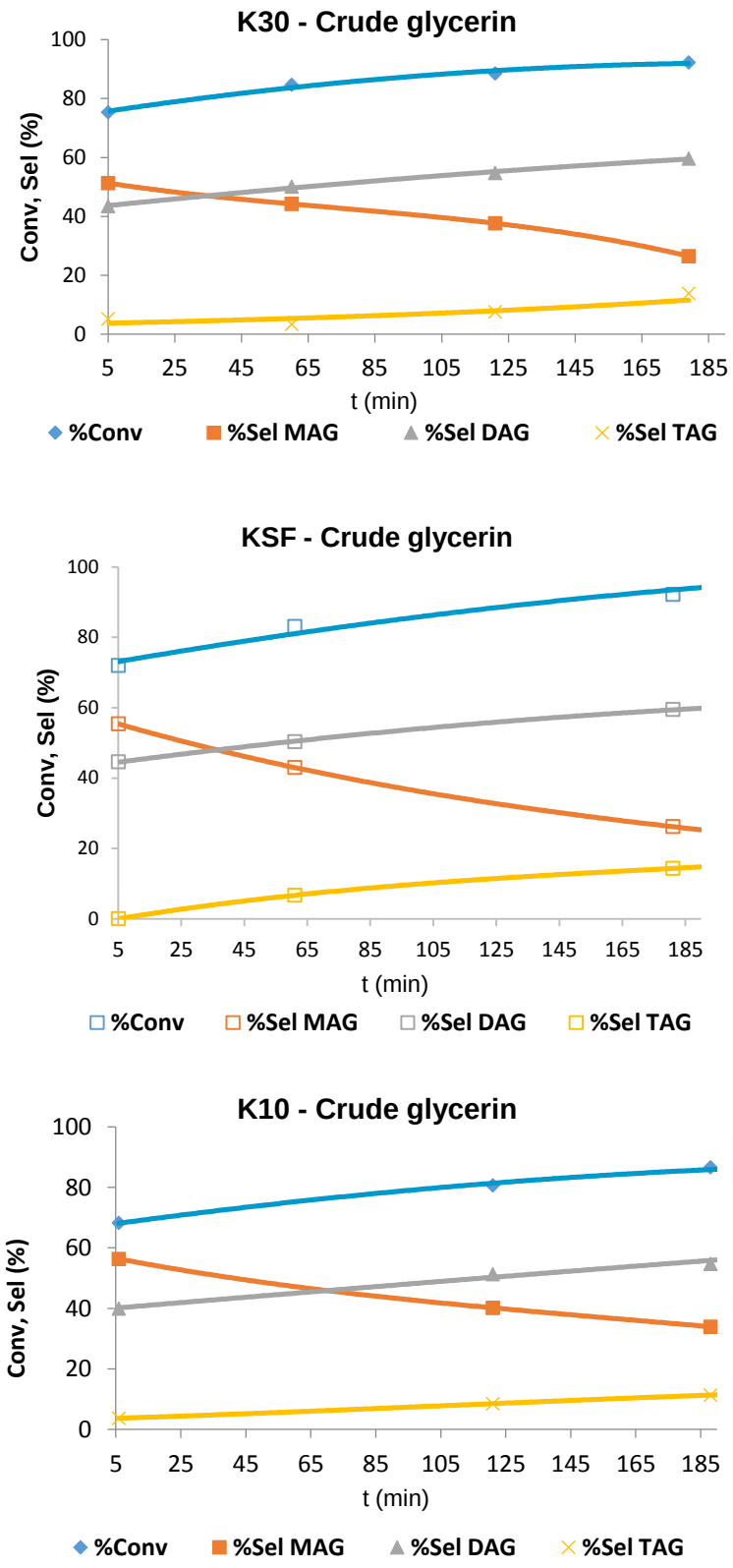

Figure 33 – Profile of glycerin acetylation with the catalysts K30, KSF and K10.

When refined glycerin with purity greater than 99.5 % was used, there was a slight increase in the conversion and towards TAG's selectivity. The predominant catalysts that showed excellent catalytic behavior in this reaction were the polymeric sulfonic Amberlyst (reference) and the KSF. The main characteristic that these two catalysts have in common is the existence of strong sulfonic groups [66] [87] [147] [148] [148][149].

Table 35 – Results of the K10, K30, KSF and Amberlyst15, after 3 hours of reaction with a ratio of HAc to Glycerin of 9.6:1 (catalyst: 10 wt % of Glycerin).

Catalyst	% Conversion	Selectivity (%)		
		MAG	DAG	TAG
None	97.0	19.2	63.9	15.9
Amberlyst 15	99.0	9.0	53.2	37.9
KSF	100	8.1	51.9	39.9
K30	98.8	14.7	64.5	20.8
K10	95.3	20.6	60.3	19.1

It is important to see that initially all three Mt catalysts have similar behavior as can be seen in Figure 34, whereas as time goes by, it seems that K10 and K30 deactivate and the reaction rate of formation of the TAG acetin decreases (Figure 35). This can be explained by the deactivation of the catalytic sites by the formation of water, produced as by-product in this reaction. As already said, the catalyst KSF is treated with sulfuric acid, and the sulfonic groups cause the water to be repelled, maintaining the catalytic sites available [66] [150]. As already has been proven by Jinyan Sun *et al* [92], the presence of water affects negatively the selectivity toward TAG, where in their experiments a certain percentage of water was added to the mixture, and they observed that although it didn't affect glycerin's conversion, it negatively affected TAG's selectivity, decreasing it from 99 % to 26 at the same conditions.

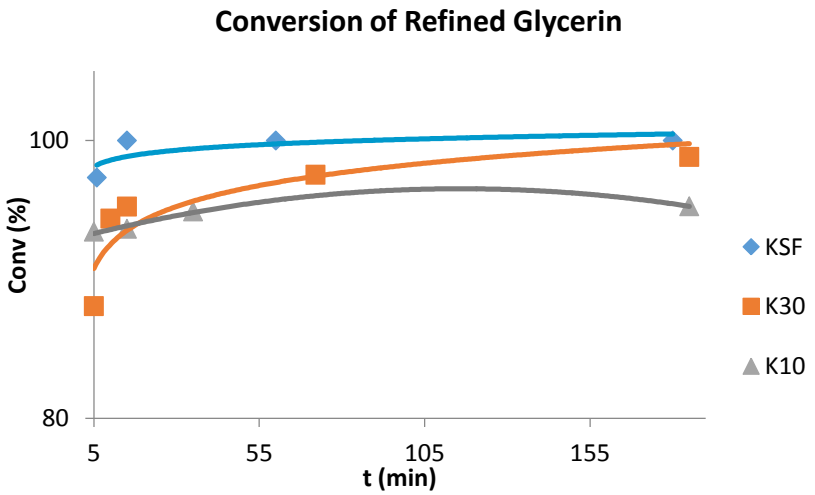

Figure 34 – Conversion of Glycerin after 3 hours of reaction, HAc: Glycerin of 9.6:1(catalyst: 10 wt% Glycerin), for the three different catalysts: KSF, K10 and K30.

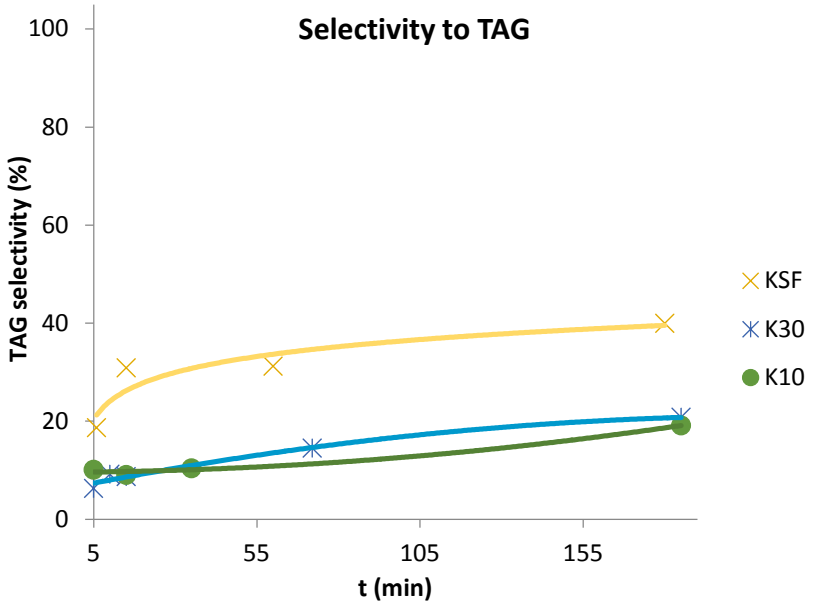

Figure 35 – Selectivity to TAG after 3 hours of reaction, HAc : Gly of 9.6:1 (catalyst: 10 wt% Glycerin), for the three different catalysts: KSF, K10 and K30.

4.2.5.2 – Acid treated Mt K10

In this section, the effect on the glycerin's acetylation using different acid tunings in the catalyst K10 is reported.

In the category of inorganic acids, it is interesting to notice that, although the hydrochloric acid is stronger than the sulfuric acid, this last one presented the best results towards TAG selectivity (Table 36). This is probably due to the fact that hydrochloric acid attaches to the tetrahedral sheet of Mt and removes aluminum from the structure, and consequently, affects negatively the acidity of the catalyst, reducing Lewis acidity, which is corroborated by the EDS analysis in *section 4.2.3*. On the other hand, the catalytic activity measured with the isomerization of 1-butene is higher when doped with 1M of sulfuric acid than 1M of hydrochloric acid, which may be connected to the porosity of the catalyst. Therefore, a BET analysis to ascertain the porosity is recommended.

In the category of organic acids, and taking into account the error in the determination of the specific percentage of the peak areas measured by the GC-FID, all acids slightly improved the conversion and selectivity toward TAG, except propionic and lactic acids, compared to the regular catalyst K10 (Table 36).

The citric acid stood out among the rest, reaching a TAG selectivity of 27.2 %, followed by oxalic acid with 25.6 %. This can be correlated with the SEM's analysis in which, in this category, these were the ones with the lower Si/Al ratio.

Table 36 – Summary of the results of glycerin acetylation during 5 hours, at 125 ºC with a ratio of 9.6:1, and a catalyst amount of 10 wt % of glycerin).

Catalyst	R_{butene} (127 ºC) (µmol.gcat^{-1}·s^{-})	Si/Al Fraction	Conversion (%)	Selectivity (%)		
				MAG	DAG	TAG
K10 sulfuric 2M	46.5	5.5 ± 1.3	97.4	8.9	51.0	40.0*
K30	42.5	4.1	98.4	14.8	60.7	24.5*
K10 sulfuric 1M	41.5	3.4 ± 1.0	100	8.5	57.9	33.6
K10 propionic 1M	40.1	4.7 ± 1.8	92.8	18.1	61.3	20.6
K10 acetic 1M	36.1	7.1 ± 1.5	97.9	16.2	58.4	25.4
K10 lactic 1M	34.6	5.4 ± 0.7	98.0	16.5	65.7	17.8
K10 phosphoric 1M	24.2	5.9 ± 2.6	96.2	15.4	62.0	22.6
K10 oxalic 1M	22.1	5.4 ± 0.9	97.4	13.7	60.8	25.6
K10 tartaric 1M	20.7	6.0 ± 1.5	98.0	15.3	62.3	22.4
K10 citric 1M	20.4	5.3 ± 0.6	99.0	11.3	61.4	27.2
K10 hydrochloric 1M	14.8	5.9 ± 0.8	96.7	15.6	59.2	25.3
K10	12.6	3.6	95.2	14.6	64.5	21.0
KSF	11.8	2.3 ± 0.2	99.3	8.1	51.1	40.7*
K10 citric 2M	5.0	6.3 ± 1.6	98.2	14.8	62.1	23.1**

* - corresponding to 4.5 hours

** - corresponding to 4 hours.

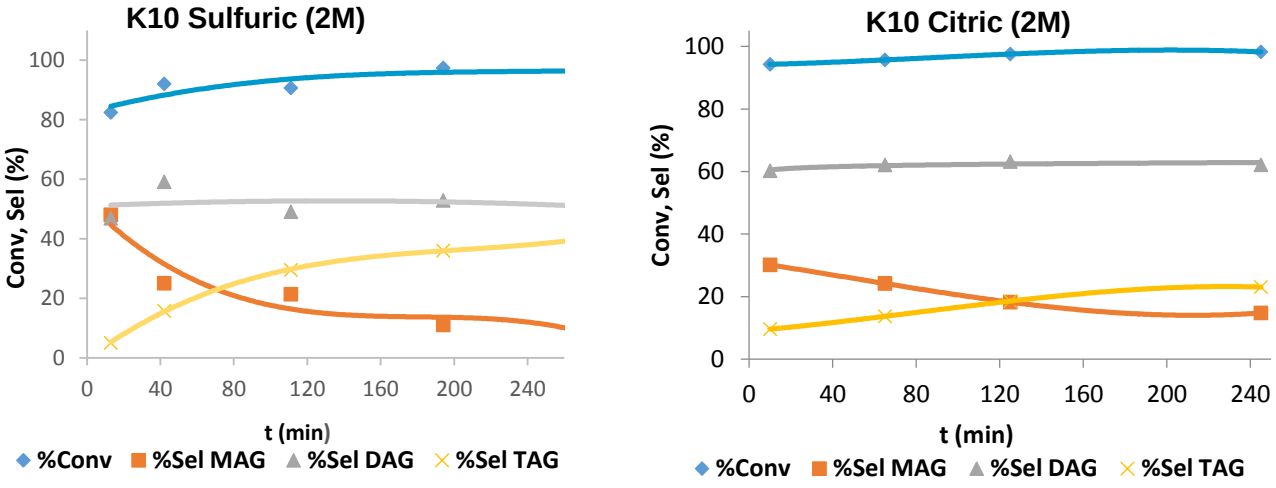

Figure 36 – Behavior of glycerin´s acetylation with K10 tuned with more concentrated acids.

It was relevant to analyze the behavior of the tuned catalyst, when more concentrated acid was introduced, treating K10 with 2M of sulfuric acid for inorganic acids and 2M of citric acid for organic acids. In the case of sulfuric acid, it accelerated the formation of TAG up to 40 % in just 4 hours (Figure 36), whereas for citric acid it did not influence the formation of TAG in 4 hours significantly, adding the fact that in catalytic Isomerization this catalyst had the worst performance, which may be due to the fact that there had been an excessive amount of aluminum removed, partially destroying the structure.

The GC performances of the other catalysts are observed in *Appendix 5*, where it can be seen

in general, the TAG selectivity of the glycerin acetylation has only slightly increase compared to the K10.

4.2.5.3 – Sugar Catalysts

Among the sugar catalysts made for this report the one with the best performance was the Glucose catalyst doped with concentrated Sulfuric acid, which led to a maximum of TAG selectivity of 46.1 % and a full conversion of glycerin, at the end of 2.5 hours, as can be seen in Figure 37.

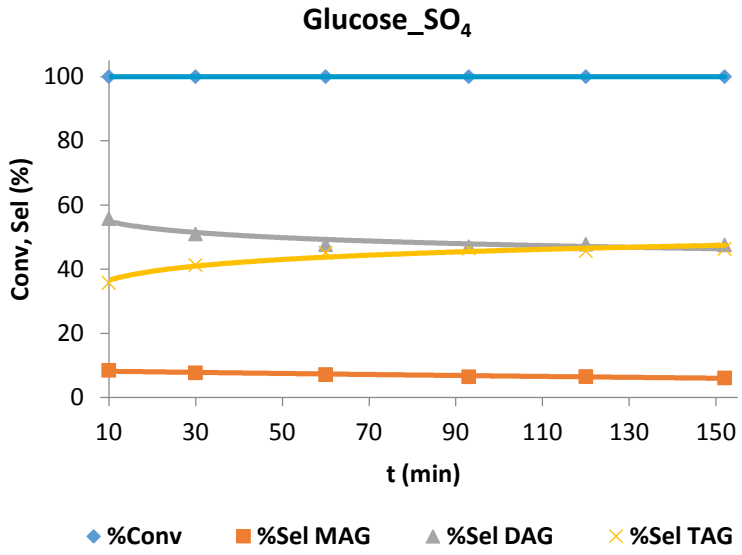

Figure 37 – Acetylation using catalyst Glucose_SO_4, with a catalyst amount of 10 wt% of glycerin and a molar ratio of HAc to Gly of 9.6:1, at 125 ºC during 2.5 hours.

When catalyst Glycerin_SO_4 was used, the behavior of the formation of TAG was slower than Glucose_SO_4 (Figure 38) as well as the needed time to reach full conversion of glycerin.

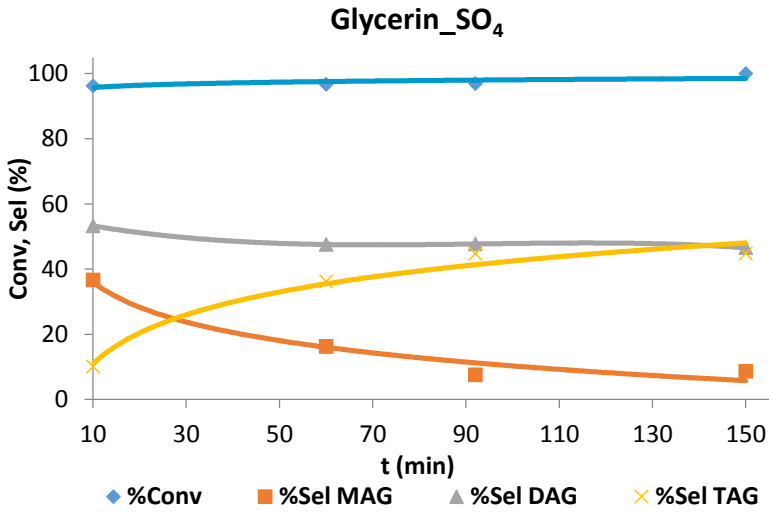

Figure 38 – Acetylation using catalyst Glycerin_SO_4, with a catalyst amount of 10 wt% of Glycerin and a molar ratio of HAc to Gly of 9.6:1, at 125 ºC during 2.5 hours.

Out of all experiments conducted in this thesis, the catalyst that has shown the highest

performance in terms of conversion of Glycerin and selectivity of TAG was the sugar catalyst made out of Glucose. Therefore, there was a need to investigate the influence of the amount of catalyst used in the reaction in order to optimize the reaction. As can be seen in Table 37, even if the amount of catalyst decreases to 5 wt% of Glycerin, the conversion of Glycerin practically total as TAG's selectivity maintains the same percentage.

Table 37 – Results obtained from the different amount of catalyst used for the sugar catalysts in 2.5 hours using refined glycerin.

Catalyst	Conversion (%)	Selectivity (%)		
		MAG	DAG	TAG
Glucose_SO_4 (10%)	100	6.5	47.0	46.5
Glucose_SO_4 (7.5%)	99.9	6.7	45.9	46.4
Glucose_SO_4 (5%)	99.3	6.9	46.4	46.7
Glycerin_ SO_4 (10%	100	8.6	46.5	44.8

New tests were made in order to analyze the behavior of glycerin acetylation of these sugar catalyst in the presence of crude glycerin (< 82% purity) in order to settle the potential industrial applicability of these solid acid catalyst. As can be seen in Figure 39, the selectivity of Tag has been negatively influenced, in comparison with the same procedure with refined glycerin. However conversions of glycerin was high and tend to increase towards 100 % as time goes by.

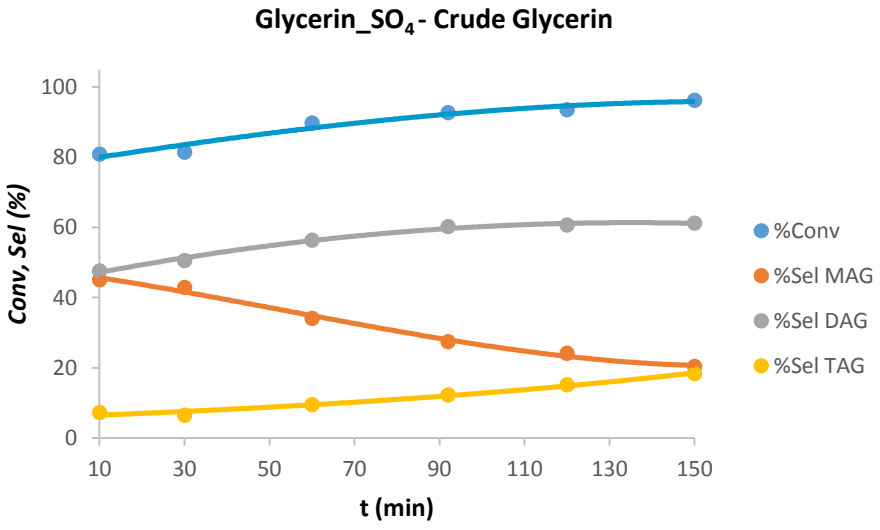

Figure 39 – Glycerin acetylation using catalyst Glycerin_SO_4, with a catalyst amount of 10 wt% of Glycerin and a molar ratio of HAc to crude Gly of 9.6:1, at 125 ºC during 2.5 hours.

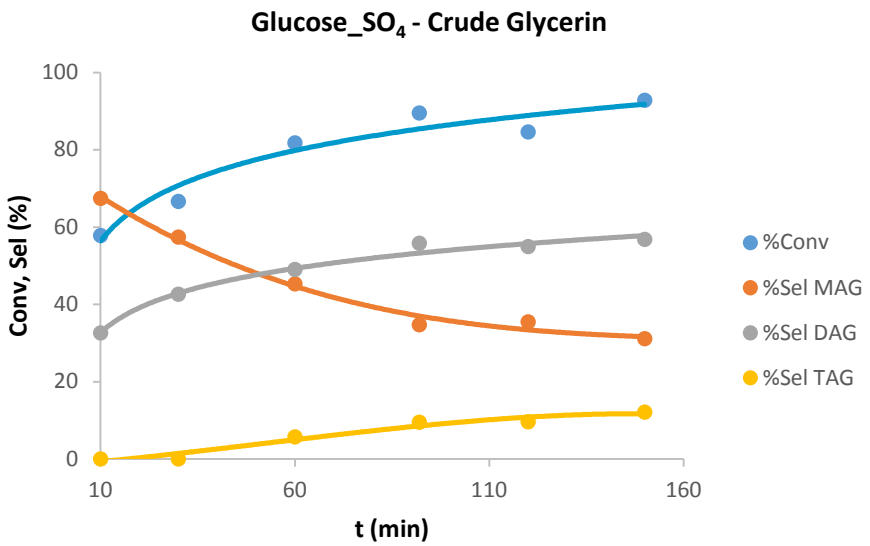

Figure 40 – Glycerin acetylation using catalyst Glucose_SO_4, with a catalyst amount of 10 wt% of Glycerin and a molar ratio of HAc to crude Gly of 9.6:1, at 125 ºC during 2.5 hours.

Interestingly, when the reaction was carried on with crude glycerin the catalyst Glycerin_SO_4 achieved higher results than Glucose_SO_4 in terms of TAG' selectivity. This may be explained by composition of crude glycerin deactivates the active sites of Glucose more quickly. Or it may be connected to the fact that the structure of Glycerin_SO_4 is stronger and more stable than the other sugar, since in EDS analysis post reaction, the sulfur groups are still attached to the structure.

Further investigation should be done in order to evaluate the cause behind this phenomenon.

Table 38 – Results obtained from the different amount of catalyst used for the sugar catalysts in 2.5 hours using crude glycerin.

Catalyst	Conversion (%)	Selectivity (%)		
		MAG	DAG	TAG
Glycerin_ SO_4 - Crude (10%)	96.2	20.4	61.2	18.4
Glucose_SO_4 - Crude (10%)	92.8	31.1	56.8	12.5

5 Economic Analysis

As the title of this thesis suggests, an economic analysis was made in order to evaluate the viability of the studied reactions and catalysts.

This section analyzes and estimates the capability of these experiments to be introduced in a company that produces BD and as Glycerin as a by-product. For the calculations it was assumed that:

- Glycerin has a purity inferior to 82 %;
- 5550 ton of Glycerin per year are converted;
- Period of working: 330 days per year;
- Catalyst duration: between 4 to 6 months;
- A dryer was already included in the factory;
- Molar ratio between Acetic Acid and Glycerin of 9.6 : 1;
- The reactors operate in batch, with 4 hours per cycle (3 of reaction and 1 of preparation);
- Nº of reactors: 4; Nº of cycles: 6;
- Filtered cake contains 15 % of liquid phase;

Firstly, there was a need to quantify the total production of TAG, therefore mass and heat balances were calculated for the process, according to Appendix 6.

5.1 Analysis and Design of the system's Equipment

5.1.1 Reactors

Two currents enter the reactor, the first corresponding to the Acetic acid with the catalyst, and the second to the Glycerin, straight from the factory, with a turbine agitator in order to keep the mixture homogenized. The reaction occurs at the reflux temperature of the Acetic acid with the help of a thermal blanket in order to maintain the reaction at reflux temperature (115 ºC), as the reaction is endothermic towards the formation of acetins. Both the mass and heat balance are summarized on Table 39. As for the design, the characteristics are shown in Table 40.

Table 39 – Mass balance and design for the reactor equipment.

Current	**1**	**2**	**3**
T (^{o}C)	25	25	115
Mass flow (ton/h)	4.39	0.79	5.09
Crude Glycerin		0.70	0
Acetic Acid	4.39		3.47
MAG			0.19
DAG			0.82
TAG			0.33
Water		0.09	0.32
Impurities		0.06	0.07
Heat Balance (kcal/h)	1.40×10^{8}	2.6×10^{8}	1.48×10^{8}
Q_R (kJ/h)*		3.23×10^{7}	

* ignoring the presence of impurities

Table 40 - Design of the reactor as well as its agitator and heating system.

Design	**Reactor**
Nº of reactors	3
Total flow (ton/cicle)	15.3
Volume (m^3)+safety	14.6
Diameter	1.8
Height	1.75
Agitator	
Type	Turbine
Re	1.05×10^{5}
Dt (m)	1.84
Da (m)	0.61
Po	5
N (rpm)	76
η (%)	70
P (kW)	2.21
Heating System	Jacket
U_{heat} (kj/s.m^2.^{o}C)	1.50
Saturated Steam (ºC)	160
Ti (ºC)	25
Tf (ºC)	115
P (kW)	371
Area (m^2)	3.6

5.1.2 Centrifuge

After 3 hours of reaction, the mixture is taken from the reactor and led to a centrifuge filter, which separates the catalyst from the liquid mixture.

Table 41 – Mass Balance and design for the equipment Filter Centrifuge.

Current	4 (Mix)		5 (Cake)		6 (Filtered)	
	ton/h	kg/h	kg/h	fraction	kg/h	fraction
Acetic Acid	3.47	3467.3	12.1		3455.2	0.68
MAG	0.19	191.9	0.1		191.8	0.04
DAG	0.82	820.6	0.1	0.15	820.5	0.16
TAG	0.33	332.1	0.1		332.0	0.06
Water	0.32	315.5	0.1		315.4	0.06
Catayst	0.07	70.1	70.1	0.85	0	0
Total	5.20	5197.3	82.5	1	5114.8	1
Diameter (m)					0.22	
Spin velocity (rpm)					1000	
W (rad/s)					104.7	
$v_{terminal}$ (m/s)					8.38×10^{-2}	
Re					0.193	

The mixture was introduced in a distillate column in order to separate all the water from the esters and acetic acid. After the distillate column the mixture containing the esters is introduced in a reactor with the addition of acetic anhydride in order to convert them all in TAG. Although this experiment was not conducted in this thesis, the idea is based on existing factories, as well as patents/articles, where a molar ratio of anhydride acetic to glycerin of 1:1 is usually used [69] [151].

5.1.3 Distillation Columns

The resultant reaction products enter a distillation column in order to separate and purify TAG up to 99.0 %. The remaining compounds, acetic acid and water, are introduced in a new extraction column and, with the help of a co-solvent named Isobutyl Acetate (IBA), are separated, with the acetic acid being reintroduced into the system continuously, at a purity of 99.5 %.

The following values related to the two distillation columns used for this operation were taken from the software Aspen Plus (Table 42 and Table 43)

Table 42 – Specifications of the first distillation column.

Characteristics	Feed Conditions Kg/h	Specifications	First Column
Temperature (ºC)	60	**Total Stages**	16
Pressure (bar)	1	**Pressure (bar)**	1
Flow rate	6137.27	**Reflux Ratio**	2
➢ **Acetic Acid**	4467.3	**Feed Location:**	4
➢ **Water**	325.46	**Qreboiler (Mcal/h)**	1778.9
➢ **Acetins**	1344.5	**Qcondenser (Mcal/h)**	-1418.3

Table 43 – Specifications of the second distillation column.

Characteristics	Feed Conditions Kg/h	Specifications	Second Column
Temperature (ºC)		**Total Stages**	10
Pressure (bar)	1	**Pressure (bar)**	1
Flow rate	7184.9	**Reflux Ratio**	1.5
➢ **TAG**	1507.4	**Feed Location:**	5
➢ **Acetic acid**	5677.5	**Qreboiler (Mcal/h)**	1571.9
		Qcondenser(Mcal/h)	-1321.8

Table 44 – Specifications of the third distillation column

Characteristics	Feed Conditions Kg/h	Specifications	Second Column
Temperature (ºC)		**Total Stages**	7
Pressure (bar)	1	**Pressure (bar)**	1
Flow rate	1534.0	**Reflux Ratio**	0.8
➢ **TAG**	1506.9	**Feed Location:**	4
➢ **Residues**	27.1	**Qreboiler (Mcal/h)**	184.2
		Qcondenser (Mcal/h)	-184.2

5.2 Economic Analysis

5.2.1 Equipment Estimation

Prior to the calculation of the overall investment costs, an estimation of the equipments' dimensions and prices was made and actualized (Figure 41) [152] [153]

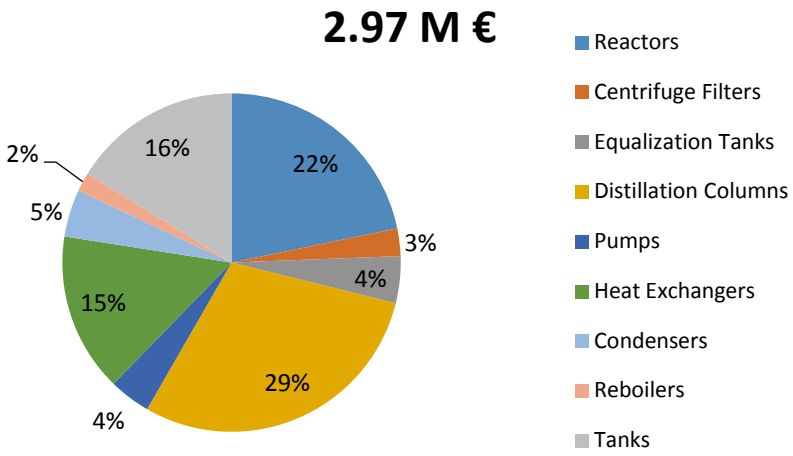

Figure 41 – Description of the total cost of equipment, actualized to 2015 in M€.

The investment is the necessary capital to invest, constituted by the sum of the fixed capital, the circulating capital and the interim interest.

Four methods were applied and the Base Equation Method was the chosen one as it presented the most disadvantageous scenario (Figure 42) [154] [155].

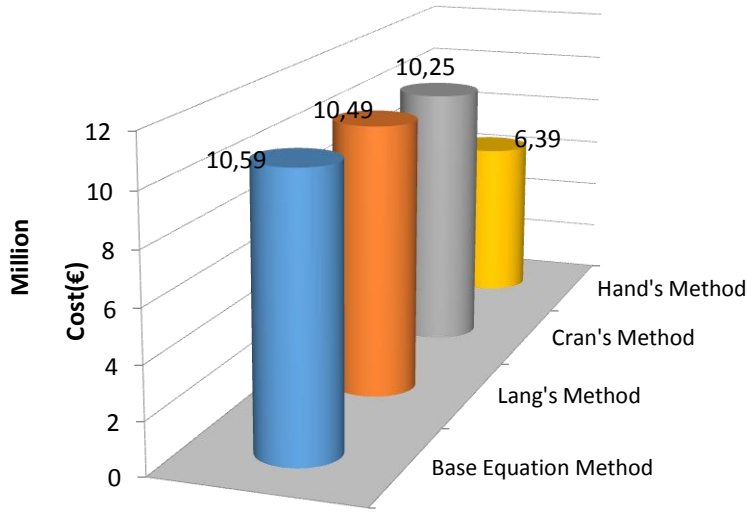

Figure 42 – Description of the results obtained for the four methods.

5.2.2 Circulating Capital

Circulating capital includes how stock, debtors and cash circulate continuously through the business, as raw materials are converted into good, ready to be sold [156].

Raw material prices were taken from *Comtrade* and *ICIS,* and are listed in the following Table 45. It was also taken into account the quantity needed per hour [157].

Table 45 – Description of the raw material prices.

Raw Material	Cost (€/ton)	Q (kg/h)	Cost (€ /year)
Crude Glycerin	0	700.8	0
Acetic acid (make up)	430	1098.2	1.5×10^4
Catalyst	200	70.1	200
Acetic anhydride	860	854.5	4.7×10^4
Total			6.2×10^4

The calculus of the circulating capital was done by three methods, whereas the following one was the chosen one for having the worst scenario corresponding to a value of 1.6×10^6 €.

On this method it was considered:

- Raw material stock: it is needed to avoid a disruption of supply, and its estimation is made based on a month's quantity;
- Credit presented to a client: it depends of the type of product, market and the costumer. It is moderated by taking into account one month of sales;
- Capital fund: it is a provision accrued, that may put in danger the continued of the activity, e.g., a fall in sales and it is equal to 5 to 10 % of the prior parcels;

5.2.3 Investment Plan

In order to calculate this parcel, it was taken into account:

- It was chosen an financial plan with the duration of 12 months;
- The use of ground is subject to a rent;
- The following numbers were obtained:

Table 46 – Numbers obtained and used for the calculus [158].

Euribor rate (%)	-0.129
Equity share (%)	70
Interim Interest (€)	4.2×10^4
Debt capital (€)	3.5×10^6
Equity (€)	8.3×10^6

- The debt capital and the interim payments are obtained by the following Equation 4 and Equation 5,

$$y = \frac{I_t^*(1-a)}{1 + a\,\frac{j \cdot n}{12} \Big/ \left(1 - \frac{j \cdot n}{12}\right)} \qquad \text{Equation 4}$$

$$J_{INT} = y\,\frac{j \cdot n}{12} \Big/ \left(1 - \frac{j \cdot n}{12}\right) \qquad \text{Equation 5}$$

- Considering a production with total capacity (100 %) by the 3rd year, the total cost of production is estimated to be 24.3 M € (Figure 43).

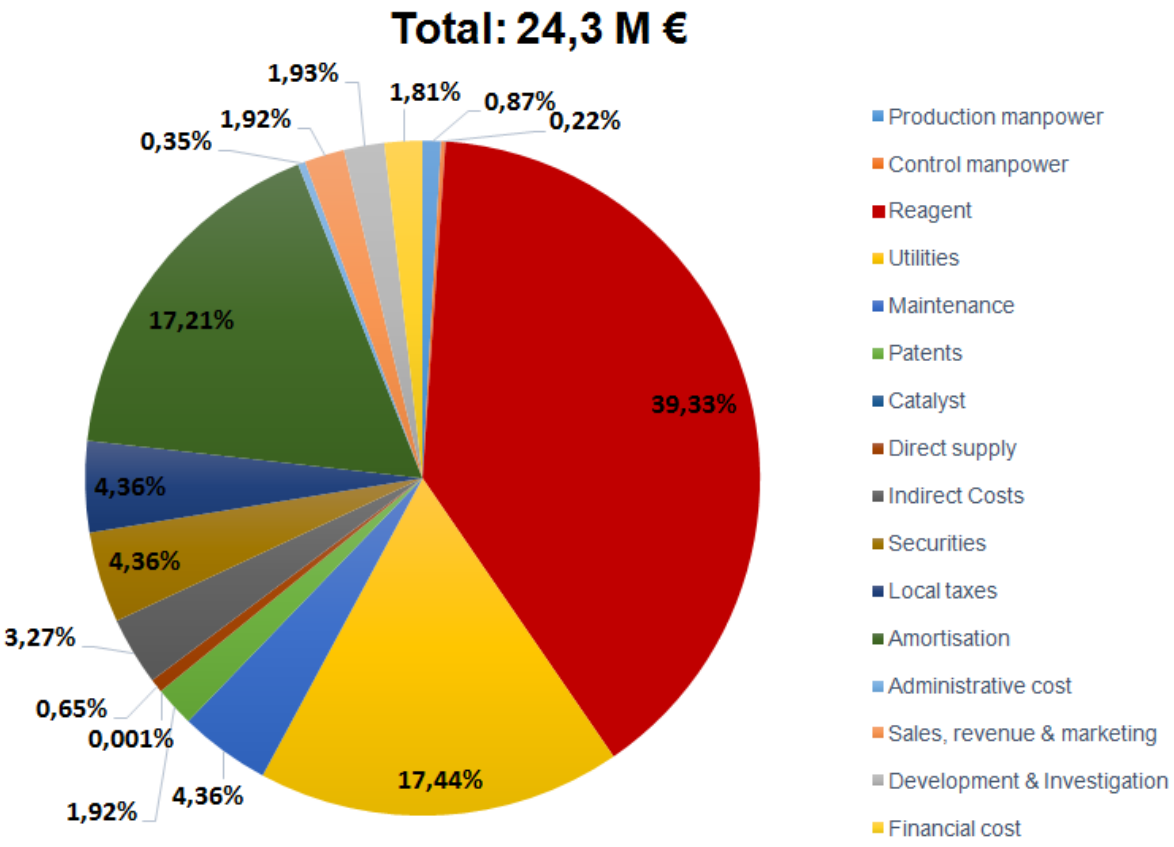

Figure 43 – Total costs of production of different sections considered for the analysis of the Investment.

5.2.4 Net Present Value (NPV)

The main goal of the project will be its own profitability, assuring that the investor will receive more equity than its own investment. However, due to inflation it will be needed to adjust the cash flows of each year after year 0, considering in this case that between 2018 and 2019 there is a period of preparation before the start of the activity. Assuming a typical value of the discount rate (*r = 7.5 %)* in the chemical industry, the obtained values are presented on Table 47.

$$NPV = \sum_{k=0}^{n} \frac{CF_k}{(1+r)^k}$$ Equation 6

Table 47 – Description of the cash flows during investment period and total NPV (M€).

Year	Years goes by	Cash Flow (M€)	Actualized Cash Flow (M€)
2018 - 2019	0	-8.51	-8.51
2020	1	1.69	1.58
2021	2	2.22	1.92
2022	3	3.24	2.61
2023	4	3.25	2.43
2024	5	3.26	2.27
2025	6	3.27	2.12
2026	7	3.28	1.98
2027	8	3.29	1.84
2028	9	3.30	1.72
2029	10	3.31	1.61
		NPV	11.6

5.2.5 Internal Rate of Return (IRR)

The IRR will be the actualization factor that assures a NPV equal to 0. Appealing to the tool *Goal Seek* from *Excel*®, it was possible to obtain an IRR equal to 29.07 %.

5.2.6 Payback Period (PP)

Payback Period consists in the needed time for recovering the investment by the cumulative cash flow of exploration (Equation 7). For the present work, at the 4th year, the investment is paid off.

$$PRC = \frac{\sum_{K=0}^{N} \frac{I_K}{(1+i)^K}}{\frac{\sum_{K=1}^{N} \frac{CF_K}{(1+i)^K}}{n}}$$

Equation 7

Table 48 – Description of the cash flows over the years in order to obtain the year of payback.

Year	Years goes by	Cash Flow (M€)	Actualized Cash Flow (M€)	Cumulative
2018 - 2019	0	-8.51	-8.51	-8.51
2020	1	1.69	1.58	-6.93
2021	2	2.22	1.92	-5.01
2022	3	3.24	2.61	-2.40
2023	4	3.25	2.43	0.03
2024	5	3.26	2.27	2.30
2025	6	3.27	2.12	4.42
2026	7	3.28	1.98	6.40
2027	8	3.29	1.84	8.24
2028	9	3.30	1.72	9.97
2029	10	3.31	1.61	11.57
		NPV	11.6	

6 Conclusion and Perspectives

The conversion of glycerin from biodiesel process into oxygenate fuel additives was studied. The acetylation using acetic acid was carried out using acid heterogeneous catalysts.

Commercial K10, K30 and KSF montmorillonite catalysts were used in the pure, and crude, glycerin acetylation with acetic acid. Crude glycerin promoted a decay of the catalytic performances. Being the water and sodium chloride contents the major responsible for such result. The KSF catalyst was the most active showing the highest selectivity towards TAG (39.9 %) underlining the role of the catalyst acidity since it was the commercial material with the lowest surface area and porosity. The K10 and K30 had analogous behaviors regardless their acidity and morphologic differences, with 19.1 and 20.8 % of TAG's selectivity, respectively. It seems that a combined or synergy effect between acidity and morphology control the acetylation performances of the tested catalysts.

In order to improve the performances, the K10 clay was treated with inorganic and organic acids. Acid leaching of Al from montmorillonite, among other elements, can improve the acidity and morphologic characteristics. Partial destruction of the montmorillonite structure was observed since Si/Al ratio increased indicating the extraction of a certain quantity of aluminum from the structure. Also, FTIR analysis reflects a little less intensity in the spectrum in both tetrahedral and octahedral sheets. From the organic acids, the ones that exhibit best performance in formatting TAG where citric and oxalic acids (1M) with a selectivity of 27.2 and 25.6 % respectively, where in the inorganic acids it was sulfuric acid (1M) with 33.6 % of selectivity in TAG. In terms of glycerin's conversion, all catalysts converted more than 95 %, except with propionic acid and hydrochloric acids (1M). Comparing with Si/Al, the three were the ones with the less difference in Si/Al ratio from original K10. However the sulfuric acid (2 M) was the one with the highest achievement in TAG, matching the performance of Amberlyst and KSF.

A second approach was made preparing acid activated carbon catalysts from glycerin and glucose (sugar catalysts). Their performances were excellent, rapidly converting glycerin towards DAG and TAG. The FTIR spectra of the post reaction catalysts showed that Glycerin_SO4 was more stable than the analogous from glucose. Both carbon catalysts exhibited very low activity in the conversion of 1-butene ascribable to their compact morphology as shown by SEM micrographs.

The economic analysis shows the worst scenario on the viability of this work. It can be concluded that using the crude glycerin provides the return of investment in only five years making it a sound investment to be furtherly analyzed.

For future references, the study of the porosity as well as the density of acid sites is proposed, in order to conclude the effect of the acidity in the used catalyst. For lack of time the study of the stability of the catalysts was not study, although the references acclaim that they are indeed stable.

The addition of anhydride acetic in the moment that there is no glycerin to convert in acetins should be studied and quantitative determinate in order to enhance the economic study made in this work.

7 References

[1] P. S. Reddy, P. Sudarsanam, G. Raju, and B. M. Reddy, “Synthesis of bio-additives: Acetylation of glycerol over zirconia-based solid acid catalysts,” *Catal. Commun.*, vol. 11, no. 15, pp. 1224–1228, 2010.

[2] S. Xiu and A. Shahbazi, “Bio-oil production and upgrading research: A review,” *Renew. Sustain. Energy Rev.*, vol. 16, no. 7, pp. 4406–4414, 2012.

[3] “Biofuels.” [Online]. Available: https://ec.europa.eu/energy/en/topics/renewable-energy/biofuels. [Accessed: 24-Feb-2017].

[4] M. Pagliaro and M. Rossi, *The Future of Glycerol*, 2nd ed. RSC Publishing, 2010.

[5] M. Aldhaidhawi, R. Chiriac, and V. Badescu, “Ignition delay, combustion and emission characteristics of Diesel engine fueled with rapeseed biodiesel – A literature review,” *Renew. Sustain. Energy Rev.*, vol. 73, pp. 178–186, 2017.

[6] P. G. Falkowski and J. Raven, “Aquatic Photosynthesis,” *Blackwell*, p. Oxford p.375, 1997.

[7] B. Vikash, KumarPatel;, and T. Ashish, *Biofuels Production*. Wiley, 2014.

[8] A. Jahandideh *et al.*, “Life cycle analysis of a large-scale limonene production facility utilizing filamentous N2-fixing cyanobacteria,” 2017.

[9] F. Arenas and F. Vaz-Pinto, “Marine Algae as Carbon Sinks and Allies to Combat Global Warming,” *Mar. Algae Biodiversity, Taxon. Environ. Assestment, Biotechnol.*, no. September, pp. 178–194, 2015.

[10] O. A. Outlook, “OECD-FAO Agricultural Outlook 2011 - 2020,” 2011.

[11] “Glycerin Market Report,” 2012.

[12] R. Ciriminna, C. Della Pina, M. Rossi, and M. Pagliaro, “Understanding the glycerol market,” *Eur. J. Lipid Sci. Technol.*, vol. 116, no. 10, pp. 1432–1439, 2014.

[13] Global Market Insights, “Glycerol Market size worth $3.04 bn by 2022,” 2016.

[14] B. J. Kerr, W. A. Dozier, K. Bregendahl, and M. State, “Nutritional value of crude glycerin for nonruminants,” *Proc. 23rd Annu. Carolina Swine Nutr. Conf.*, pp. 6–18, 2007.

[15] P. U. Okoye and B. H. Hameed, “Review on recent progress in catalytic carboxylation and acetylation of glycerol as a byproduct of biodiesel production,” *Renew. Sustain. Energy Rev.*, vol. 53, pp. 558–574, 2016.

[16] ICIS, “Crude Glycerine suppliers eye higher China prices,” 2016. .

[17] W. Zineng, “Market Watch - Greenea,” *Third Text*, vol. 25, no. 4, pp. 459–466, 2017.

[18] C. H. Zhou, J. N. Beltramini, Y. X. Fan, and G. Q. Lu, “Chemoselective catalytic conversion of glycerol as a biorenewable source to valuable commodity chemicals,” *Chem. Soc. Rev.*, vol. 37, no. 3, pp. 527–549, 2008.

[19] ICIS, “Asia crude glycerine market in stand-off; some sellers keep offers,” 2016. .

[20] “Sovena.” [Online]. Available: http://www.sovenagroup.com/en/. [Accessed: 29-May-2017].

[21] M. Pagliaro, *The Renewable Platform Chemical*, 1 st. Elsevier, 2017.

[22] B. Katryniok, S. Paul, V. Belliere-Baca, P. Rey, and F. Dumeignil, “Glycerol dehydration to acrolein in the context of new uses of glycerol,” *Green Chem.*, vol. 12, no. 12, pp. 2079–2098, 2010.

[23] Global Market Insights, “Glycerol Market Size by Application,” 2016. .

[24] Dante Siano, “Process for the production of alpha, gamma-dichlorohydrin from glycerin and hydrochloric acid,” WO 2006111810 A3, 2005.

[25] BioMCN, “Driven by nature.” [Online]. Available: http://www.biomcn.eu/. [Accessed: 02-Apr-2017].

[26] J. A. Kenar, “Glycerol as a platform chemical: Sweet opportunities on the horizon?,” *Lipid Technol.*, vol. 19, no. 11, pp. 249–253, 2007.

[27] J. J. Bozell and G. R. Petersen, “Technology development for the production of biobased products from biorefinery carbohydrates—the US Department of Energy’s ‘Top 10’ revisited,”

Green Chem., vol. 12, no. 4, p. 539, 2010.

[28] A. Behr, J. Eilting, K. Irawadi, J. Leschinski, and F. Lindner, “Improved utilisation of renewable resources: New important derivatives of glycerol,” *Green Chem.*, vol. 10, no. 1, pp. 13–30, 2008.

[29] J. Spooner-Wyman and D. Appleby, “Evaluation of Di-Butoxy Glycerol (DBG) for Use As a Diesel Fuel Blend Component,” p. 16, 2003.

[30] B. Nebel, M. Mittelbach, and G. Uray, “Determination of the Composition of Acetylglycerol Mixtures by H NMR Followed by GC Investigation Determination of the Composition of Acetylglycerol Mixtures by 1 H NMR Followed by GC Investigation,” vol. 80, no. 22, pp. 8712–8716, 2008.

[31] M. A. Betiha, H. M. A. Hassan, E. A. El-Sharkawy, A. M. Al-Sabagh, M. F. Menoufy, and H. E. M. Abdelmoniem, “A new approach to polymer-supported phosphotungstic acid: Application for glycerol acetylation using robust sustainable acidic heterogeneous-homogenous catalyst,” *Appl. Catal. B Environ.*, vol. 182, pp. 15–25, 2016.

[32] G. P. Touey and J. E. Kiefer, “Bonding Plasticizers for Cigarette filter of Cellulose Acetate Fibers,” 246362, 1968.

[33] C. V. Lacerda and M. J. S. Carvalho, “Synthesis of Triacetin and Evaluation on Motor,” *J. Brazilian Chem.*, vol. 26, 2015.

[34] I. Dincer, C. O. Colpan, O. Kizilkan, and M. A. Ezan, *Progress in Clean Energy, Volume 1: Analysis and Modeling*. Springer, 2015.

[35] P. U. Okoye and B. H. Hameed, “Review on recent progress in catalytic carboxylation and acetylation of glycerol as a byproduct of biodiesel production,” *Renewable and Sustainable Energy Reviews*. 2016.

[36] K. HIGHSMITH, Thomas, J. SANDERSON, Andrew, and F. CANNIZZO, Louis, “POLYMERIZATION OF POLY(GLYCIDYL NITRATE) FROM HIGH PURITY GLYCIDYL NITRATE SYNTHESIZED FROM GLYCEROL,” WO2001029111, 2001.

[37] H. . Murray, “Applied clay mineralogy today and tomorrow,” *Clay Miner.*, vol. 34, pp. 39–49, 1999.

[38] M. Ghadiri, W. Chrzanowski, and R. Rohanizadeh, “Biomedical applications of cationic clay minerals,” *RSC Adv.*, vol. 5, no. 37, pp. 29467–29481, 2015.

[39] B. S. Kumar, A. Dhakshinamoorthy, and K. Pitchumani, “K10 montmorillonite clays as environmentally benign catalysts for organic reactions,” *Catal. Sci. Technol.*, vol. 4, no. 8, p. 2378, 2014.

[40] W. F. Bleam and R. Hoffmann, “Isomorphous Substitution in Phyllosilicates as an Electronegativity Perturbation: Its Effect on Bonding and Charge Distribution,” *Inorg. Chem.*, vol. 27, no. 18, pp. 3180–3186, 1988.

[41] B. Tyagi, C. D. Chudasama, and R. V. Jasra, “Determination of structural modification in acid activated montmorillonite clay by FT-IR spectroscopy,” *Spectrochim. Acta - Part A Mol. Biomol. Spectrosc.*, 2006.

[42] R. E. Grim and G. Kulbicki, “Montmorillonite: High temperature reactions and classification,” *Am. Mineral.*, vol. 46, pp. 1329–1369, 1961.

[43] H. H. Murray, *Applied Clay Mineralogy*, First Edit. Elsevier, 2007.

[44] U. Flessner *et al.*, “A study of the surface acidity of acid-treated montmorillonite clay catalysts,” *J. Mol. Catal. A Chem.*, 2001.

[45] “EP 1 730 101 B1 EUROPEAN PATENT SPECIFICATION,” 2006.

[46] T. Shinoda, M. Onaka, and Y. Izumi, “Proposed Models of Mesopore Structures in Sulfuric Acid-Treated Montmorillonites and K10,” *Chem. Lett.*, 1995.

[47] T. I, P. Komadel, and D. Muller, “Acid-treated Montmorillonites - a study by Si and Al MAS NMR,” *Clay Miner.*, vol. 29, pp. 11–19, 1994.

[48] V. Luca and D. J. MacLachlan, “Site occupancy in nontronite studied by acid dissolution and mössbauer spectroscopy,” *Clays Clay Miner.*, vol. 40, no. 1, pp. 1–7, 1992.

[49] M. L. Rozalén, F. J. Huertas, P. V. Brady, J. Cama, S. García-Palma, and J. Linares, “Experimental study of the effect of pH on the kinetics of montmorillonite dissolution at 25 ??C,” *Geochim. Cosmochim. Acta*, vol. 72, no. 17, pp. 4224–4253, 2008.

[50] M.J.Wilson, *Rock-forming Minerals: Clay Minerals. Sheet silicates. Chapter Smectite Clay Minerals. Volume 3C*, 2nd Editio. The Geological Society of London, 2013.

[51] R. E. Grim and N. Guven, “Bentonites: Geology, Mineralogy, Properties and Uses (Developments in sedimentology).”

[52] I. E. Wachs and L. E. Fitzpartrick, *Characterization of Catalytic Materials*. Butterworth-Heinemann, 1992.

[53] L. R. S. Kanda, M. L. Corazza, L. Zatta, and F. Wypych, “Kinetics evaluation of the ethyl esterification of long chain fatty acids using commercial montmorillonite K10 as catalyst,” *Fuel*, vol. 193, pp. 265–274, 2017.

[54] J. Vodnár, J. Farkas, and S. Békássy, “Catalytic decomposition of 1,4-diisopropylbenzene dihydroperoxide on montmorillonite-type catalysts,” *Appl. Catal. A Gen.*, vol. 208, no. 1–2, pp. 329–334, 2001.

[55] “Montmorillonites and other Mineral Adsorbents,” *Sigma Adrich*. [Online]. Available: http://www.sigmaaldrich.com/catalog/product/sial/69904?lang=pt&region=PT&cm_sp=Insite-_-prodRecCold_xorders-_-prodRecCold2-1. [Accessed: 28-Oct-2016].

[56] S. M. Yakout and G. Sharaf El-Deen, “Characterization of activated carbon prepared by phosphoric acid activation of olive stones,” *Arab. J. Chem.*, 2012.

[57] E. L. K. Mui, W. H. Cheung, M. Valix, and G. McKay, “Mesoporous activated carbon from waste tyre rubber for dye removal from effluents,” *Microporous Mesoporous Mater.*, vol. 130, no. 1–3, pp. 287–294, 2010.

[58] B. Acevedo, C. Barriocanal, I. Lupul, and G. Gryglewicz, “Properties and performance of mesoporous activated carbons from scrap tyres, bituminous wastes and coal,” *Fuel*, vol. 151, pp. 83–90, 2015.

[59] U. Chandrakala, R. B. N. Prasad, and B. L. A. Prabhavathi Devi, “Glycerol valorization as biofuel additives by employing a carbon-based solid acid catalyst derived from glycerol,” *Ind. Eng. Chem. Res.*, vol. 53, no. 42, pp. 16164–16169, 2014.

[60] M. Vijay, R. B. N. Prasad, and B. L. A. P. Devi, “Bioglycerol-based Sulphonic Acid Functionalized Carbon: An Efficient and Recyclable, Solid Acid Catalyst for the Regioselective Azidolysis of Epoxides in Aqueous Acetonitrile,” *J. Oleo Sci.*, vol. 62, no. 10, pp. 849–855, 2013.

[61] I. M. Lokman, U. Rashid, Z. Zainal, R. Yunus, and Y. H. Taufiq-Yap, “Microwave-assisted biodiesel production by esterification of palm fatty acid distillate,” *J. Oleo Sci.*, vol. 63, no. 9, pp. 849–855, 2014.

[62] W. H. Chen *et al.*, “A solid-state NMR, FT-IR and TPD study on acid properties of sulfated and metal-promoted zirconia: Influence of promoter and sulfation treatment,” *Catal. Today*, vol. 116, no. 2 SPEC. ISS., pp. 111–120, 2006.

[63] Y. Fu and Y. Huang, “Hydrolysis of cellulose to glucose by solid acid catalysts,” *Green Chem.*, vol. 15, pp. 1095–1111, 2013.

[64] V. Nagabhatla, “Carbonized glycerol nano tubes as efficient catalysts for biofuel Production,” *RSC Adv.*, vol. 6, no. April, pp. 1–6, 2016.

[65] S. Horikoshi and N. Serpone, *Microwaves in Catalysis: Methodology and Applications*, 1st Editio. 2015.

[66] M. L. Testa, V. La Parola, L. F. Liotta, and A. M. Venezia, “Screening of different solid acid catalysts for glycerol acetylation,” *J. Mol. Catal. A Chem.*, vol. 367, pp. 69–76, 2013.

[67] S. S. Kale *et al.*, “Understanding the role of Keggin type heteropolyacid catalysts for glycerol acetylation using toluene as an entrainer,” *"Applied Catal. A, Gen.*, 2016.

[68] V. L. C. Gonçalves, B. P. Pinto, J. C. Silva, and C. J. A. Mota, “Acetylation of glycerol catalyzed by different solid acids,” *Catal. Today*, vol. 133–135, no. 1–4, pp. 673–677, 2008.

[69] X. Liao, Y. Zhu, S. G. Wang, and Y. Li, “Producing triacetylglycerol with glycerol by two steps: Esterification and acetylation,” *Fuel Process. Technol.*, vol. 90, no. 7–8, pp. 988–993, 2009.

[70] S. Kale, U. Armbruster, S. Umbarkar, M. Dongare, and A. Martin, “Esterification of glycerol with acetic acid for improved production of triacetin using toluene as an entrainer,” *10th Green Chem. Conf.*, pp. 70–71, 2013.

[71] L. N. Silva, V. L. C. Gonçalves, and C. J. A. Mota, “Catalytic acetylation of glycerol with acetic anhydride,” *Catal. Commun.*, vol. 11, no. 12, pp. 1036–1039, 2010.

[72] N. J. Venkatesha, Y. S. Bhat, and B. S. J. Prakash, “Volume accessibility of acid sites in modified montmorillonite and triacetin selectivity in acetylation of glycerol,” 2016.

[73] M. S. Khayoon and B. H. Hameed, “Acetylation of glycerol to biofuel additives over sulfated activated carbon catalyst,” *Bioresour. Technol.*, vol. 102, no. 19, pp. 9229–9235, 2011.

[74] R. Luque, V. Budarin, J. H. Clark, and D. J. Macquarrie, “Glycerol transformations on polysaccharide derived mesoporous materials,” *Appl. Catal. B Environ.*, vol. 82, no. 3–4, pp. 157–162, 2008.

[75] P. Ferreira, I. M. Fonseca, A. M. Ramos, J. Vital, and J. E. Castanheiro, “Acetylation of glycerol over heteropolyacids supported on activated carbon,” *Catal. Commun.*, vol. 12, no. 7, pp. 573–576, 2011.

[76] K. B. Ghoreishi, N. Asim, M. A. Yarmo, and M. W. Samsudin, “Mesoporous phosphated and sulphated silica as solid acid catalysts for glycerol acetylation,” *Chem. Pap.*, vol. 68, no. 9, pp. 1194–1204, 2014.

[77] M. Balaraju, P. Nikhitha, K. Jagadeeswaraiah, K. Srilatha, P. S. Sai Prasad, and N. Lingaiah, “Acetylation of glycerol to synthesize bioadditives over niobic acid supported tungstophosphoric acid catalysts,” *Fuel Process. Technol.*, vol. 91, no. 2, pp. 249–253, 2010.

[78] P. Ferreira, I. M. Fonseca, A. M. Ramos, J. Vital, and J. E. Castanheiro, “Glycerol acetylation over dodecatungstophosphoric acid immobilized into a silica matrix as catalyst,” *Appl. Catal. B Environ.*, vol. 91, no. 1–2, pp. 416–422, 2009.

[79] J. a. Melero, G. D. Stucky, R. van Grieken, and G. Morales, “Direct syntheses of ordered SBA-15 mesoporous materials containing arenesulfonic acid groups,” *J. Mater. Chem.*, vol. 12, no. 6, pp. 1664–1670, 2002.

[80] M. S. Khayoon, S. Triwahyono, B. H. Hameed, and A. A. Jalil, “Improved production of fuel oxygenates via glycerol acetylation with acetic acid,” *Chem. Eng. J.*, vol. 243, pp. 473–484, 2014.

[81] L. J. Konwar *et al.*, “Shape selectivity and acidity effects in glycerol acetylation with acetic anhydride: Selective synthesis of triacetin over Y-zeolite and sulfonated mesoporous carbons,” *J. Catal.*, vol. 329, pp. 237–247, 2015.

[82] P. S. Reddy, P. Sudarsanam, G. Raju, and B. M. Reddy, “Selective acetylation of glycerol over CeO 2-M and SO 4 2-/CeO 2-M (M=ZrO 2 and Al 2O 3) catalysts for synthesis of bioadditives,” *J. Ind. Eng. Chem.*, vol. 18, no. 2, pp. 648–654, 2012.

[83] A. P. S. Dias *et al.*, “Glycerine Valorisation by Acetylation Over Phosphated Silica Catalysts,” 2013.

[84] I. Kim, J. Kim, and D. Lee, “A comparative study on catalytic properties of solid acid catalysts for glycerol acetylation at low temperatures,” *Appl. Catal. B Environ.*, vol. 148–149, pp. 295–303, 2014.

[85] J. E. A. Chem, T. V Kotbagi, S. L. Pandhare, M. K. Dongare, and S. B. Umbarkar, “In situ Formed Supported Silicomolybdic Heteropolyanions : Efficient Solid Catalyst for Acetylation of Glycerol,” vol. 2, no. 5, 2015.

[86] M. S. Khayoon and B. H. Hameed, “Synthesis of hybrid SBA-15 functionalized with molybdophosphoric acid as efficient catalyst for glycerol esterification to fuel additives,” *Appl. Catal. A Gen.*, vol. 433–434, pp. 152–161, 2012.

[87] J. A. Melero, R. van Grieken, G. Morales, and M. Paniagua, “Acidic mesoporous silica for the acetylation of glycerol: Synthesis of bioadditives to petrol fuel,” *Energy and Fuels*, vol. 21, no. 3, pp. 1782–1791, 2007.

[88] J. M. Rafi, “Esterification of glycerol over a solid acid biochar catalyst derived from waste biomass,” *RSC Adv.*, p. 7, 2015.

[89] J. A. Sánchez, D. L. Hernández, J. A. Moreno, F. Mondragón, and J. J. Fernández, “Alternative carbon based acid catalyst for selective esterification of glycerol to acetylglycerols,” *Appl. Catal. A Gen.*, vol. 405, no. 1–2, pp. 55–60, 2011.

[90] P. Ferreira, I. M. Fonseca, A. M. Ramos, J. Vital, and J. E. Castanheiro, “Esterification of glycerol with acetic acid over dodecamolybdophosphoric acid encaged in USY zeolite,” *Catal. Commun.*, vol. 10, no. 5, pp. 481–484, 2009.

[91] S. Liu *et al.*, “Synthesis of Glycerol Triacetate Using a Br??nsted-Lewis Acidic Ionic Liquid as the Catalyst,” *JAOCS, J. Am. Oil Chem. Soc.*, vol. 92, no. 9, pp. 1253–1258, 2015.

[92] J. Sun, X. Tong, L. Yu, and J. Wan, “An efficient and sustainable production of triacetin from the acetylation of glycerol using magnetic solid acid catalysts under mild conditions,” *Catal. Today*, vol. 264, pp. 115–122, 2016.

[93] Z. Q. Wang, Z. Zhang, W. J. Yu, L. D. Li, M. H. Zhang, and Z. B. Zhang, “A swelling-changeful catalyst for glycerol acetylation with controlled acid concentration,” *Fuel Process. Technol.*, vol. 142, pp. 228–234, 2016.

[94] “Pub Chem.” [Online]. Available: https://pubchem.ncbi.nlm.nih.gov/compound/oxalic_acid. [Accessed: 18-May-2017].

[95] T. L. Feng, P. L. Gurian, M. D. Healy, and A. R. Barron, “Aluminum citrate: isolation and structural characterization of a stable trinuclear complex,” *Inorg. Chem.*, vol. 29, no. 3, pp. 408–411, 1990.

[96] G. Cao, *Nanostructures and Nanomaterials - Synthesis, Properties and Applications*, vol. 2. 2004.

[97] C. Hammond, *The Basics of Crystallography and Diffraction*, 3rd Editio. Oxford University Press, 2009.

[98] “CQE Xray Diffraction Facility.” [Online]. Available: http://groups.ist.utl.pt/~cqe.daemon/members-contacts/scientific-topics/x-ray-diffraction-facility/bruker-d8-advance-powder-diffractometer/. [Accessed: 20-Mar-2017].

[99] B. Stuart, *Infrared Spectroscopy: Fundamentals and Applications*. Wiley, 2004.

[100] Y. Leng, *Materials Characterization - Introduction to Microscopic and Spectroscopic Methods*. JOhn Wiley & Sons, 2008.

[101] B. C. Smith, *Fundamentals of Fourier: Transform INfrared Spectroscopy*, Second Edi. Taylor & Francis Group, 2011.

[102] “Attenuated total reflectance.” [Online]. Available: https://en.wikipedia.org/wiki/Attenuated_total_reflectance. [Accessed: 30-Apr-2017].

[103] Harrick, “What is Kubelka-Munk ?” [Online]. Available: https://www.google.pt/url?sa=t&rct=j&q=&esrc=s&source=web&cd=3&ved=0ahUKEwjfuu3syZzUAhVEWhoKHVdtB_YQFgg5MAI&url=https%3A%2F%2Fwww.researchgate.net%2Ffile.PostFileLoader.html%3Fid%3D5847d638eeae3986a1765e11%26assetKey%3DAS%253A436591379390465%2540481102904158&usg=AFQjCNGheMb4_5k2iCAxUjgH1xHbLTZreA&sig2=oDnMWt3S0mfUsfZpwv-mQg&cad=rja. [Accessed: 30-Apr-2017].

[104] A. Moronta *et al.*, “Isomerization of 1-butene catalyzed by ion-exchanged, pillared and ion-exchanged/pillared clays,” *Appl. Catal. A Gen.*, vol. 334, no. 1–2, pp. 173–178, 2008.

[105] H. Hattori and Y. Ono, *Solid Acid Catalysis, From Fundamentals to Applications*. Pan Stanford, 2015.

[106] I. K. A.Béres, I. Hannus, “Acid-Base Testing of Catalysts using 1-Butene Isomerization as Test Reaction,” *Elsevier*, vol. 56, no. I, pp. 55–61, 1995.

[107] A. I. Kirkland *et al.*, *Science of Microscopy*. Springer, 2007.

[108] Károly Havancsák, “High-Resolution Scanning Electron Microscopy.” [Online]. Available: http://www.technoorg.hu/news-and-events/articles/high-resolution-scanning-electron-microscopy-1/. [Accessed: 17-Mar-2017].

[109] L. Reimer, *Scanning Electron Microscopy: Physics of Image Formation and Microanalysis*, 2nd Editio. New York: Springer, 1998.

[110] Ray F. Egerton, *Physical Principles of Electron Microscopy*. Alberta: Springer, 2005.

[111] O. Imaging and M. Jan, *Scanning Electron Microscopy*. Rijeka, Croatia: InTech, 2012.

[112] “MicroLab - Electron Microscopy Laboratory.” [Online]. Available: http://groups.ist.utl.pt/microlab/microfacilities.html. [Accessed: 17-Mar-2017].

[113] H. Wu, H. Xie, G. He, Y. Guan, and Y. Zhang, “Effects of the pH and anions on the adsorption of tetracycline on iron-montmorillonite,” *Appl. Clay Sci.*, vol. 119, no. October, pp. 161–169, 2016.

[114] “Gas Chromatography,” 2012. [Online]. Available: https://www.slideshare.net/ummiabah/gas-chromatography-gc. [Accessed: 21-May-2017].

[115] “Techniques: Gas Chromatography.” [Online]. Available: http://ochem.weebly.com/uploads/1/0/5/0/10503018/d-question4info.pdf. [Accessed: 19-May-

2017].

[116] I. C. Bourg, G. Sposito, and A. C. M. Bourg, “Modeling the acid-base surface chemistry of montmorillonite,” *J. Colloid Interface Sci.*, vol. 312, no. 2, pp. 297–310, 2007.

[117] P. Kumar, R. V Jasra, and T. S. G. Bhat, “Evolution of Porosity and Surface Acidity in Montmorillonite Clay on Acid Activation,” *Ind. Eng. Chem. Res.*, vol. 1900, pp. 1440–1448, 1995.

[118] G. Ertl and E. Hasselbrink, “Keynote article,” *J. Chem. Soc. Perkin Trans.*, vol. 2, pp. 925–944, 1994.

[119] V. Tabernero, C. Camejo, P. Terreros, M. D. Alba, and T. Cuenca, “Silicoaluminates as ‘support activator’ systems in olefin polymerization processes,” *Materials (Basel).*, vol. 3, no. 2, pp. 1015–1030, 2010.

[120] L. Alamos, “Baseline studies of the clay minerals society source clays: poder X-RAY diffraction analyses,” *Clays Clay Miner.*, vol. 49, no. 5, pp. 398–409, 2001.

[121] “RRuff Database.” [Online]. Available: http://rruff.info/montmorillonite/display=default/. [Accessed: 18-Feb-2017].

[122] P. Wu and C. Ming, “The relationship between acidic activation and microstructural changes in montmorillonite from Heping, China,” *Spectrochim. Acta - Part A Mol. Biomol. Spectrosc.*, vol. 63, no. 1, pp. 85–90, 2006.

[123] V. O. Pashkova, P. Sarv, and M. Derewiński, “Composite porous materials containing zeolitic domains prepared by controlled partial recrystallization of amorphous aluminosilicates,” *Stud. Surf. Sci. Catal.*, vol. 170, no. A, pp. 289–296, 2007.

[124] V. Krupskaya *et al.*, “Experimental Study of Montmorillonite Structure and Transformation of Its Properties under Treatment with Inorganic Acid Solutions,” *Minerals*, vol. 7, no. 4, p. 49, 2017.

[125] J. Temuujin, T. Jadambaa, G. Burmaa, S. Erdenechimeg, J. Amarsanaa, and K. J. D. MacKenzie, “Characterisation of acid activated montmorillonite clay from Tuulant (Mongolia),” *Ceram. Int.*, 2004.

[126] B. L. A. P. Devi, K. N. Gangadhar, P. S. S. Prasad, B. Jagannadh, and R. B. N. Prasad, “A glycerol-based carbon catalyst for the preparation of biodiesel,” *ChemSusChem*, vol. 2, no. 7, pp. 617–620, 2009.

[127] L. Zatta, E. J. Paiva, M. L. Corazza, F. Wypych, and L. P. Ramos, “The Use of Acid-Activated Montmorillonite as a Solid Catalyst for the Production of Fatty Acid Methyl Esters.”

[128] K. G. Bhattacharyya and S. Sen, “Adsorptive Accumulation of Cd (II), Co (II), Cu (II), Pb (II) and Ni (II) Ions from Water onto Kaolinite : Influence of Acid Activation,” no. Ii, pp. 47–69, 2009.

[129] J. Madejová, “FTIR techniques in clay mineral studies,” *Vib. Spectrosc.*, vol. 31, no. 1, pp. 1–10, 2003.

[130] M. A. Vicente-Rodríguez, M. Suarez, M. A. Bañares-Muñoz, and J. de Dios Lopez-Gonzalez, “Comparative FT-IR study of the removal of octahedral cations and structural modifications during acid treatment of several silicates,” *Spectrochim. Acta Part A Mol. Biomol. Spectrosc.*, vol. 52, no. 13, pp. 1685–1694, 1996.

[131] M. N. Timofeeva, V. N. Panchenko, V. V. Krupskaya, A. Gil, and M. A. Vicente, “Effect of nitric acid modification of montmorillonite clay on synthesis of solketal from glycerol and acetone,” *Catal. Commun.*, 2017.

[132] L. Bieseki, H. Treichel, A. S. Araujo, and S. B. C. Pergher, “Porous materials obtained by acid treatment processing followed by pillaring of montmorillonite clays,” *Appl. Clay Sci.*, 2013.

[133] G. E. Christidis, P. W. Scott, and a. C. Dunham, “Acid activation and bleaching capacity of bentonites from the islands of Milos and Chios, Aegean, Greece,” *Appl. Clay Sci.*, vol. 12, no. 4, pp. 329–347, 1997.

[134] “The Nature of Vibrational Spectroscopy.” [Online]. Available: https://www2.chemistry.msu.edu/faculty/reusch/virttxtjml/spectrpy/infrared/irspec1.htm. [Accessed: 18-Mar-2017].

[135] M.-H. Zong, Z.-Q. Duan, W.-Y. Lou, T. J. Smith, and H. Wu, “Preparation of a sugar catalyst and its use for highly efficient production of biodiesel,” *Green Chem.*, vol. 9, no. 5, p. 434, 2007.

[136] W.-Q. Xu, Y.-G. Yin, S. L. Suib, J. C. Edwards, and C.-L. OYoung, “n-Butene Skeletal

Isomerization to Isobutylene on Shape Selective Catalysts: Ferrierite/ZSM-35," *J. Phys. Chem.*, vol. 99, no. 23, pp. 9443–9451, 1995.

[137] C. H. Bartholomew and G. A. Fuentes, Eds., *Studies in Surface Science and Catalysis, volume 111*. Elsevier, 1997.

[138] H. K. Beyer, H. G. Karge, I. Kiricsi, and J. B. Nagy, Eds., *Studies in Surface Science and Catalysis, volume 94*. Elsevier, 1995.

[139] M. Guisnet and P. Magnoux, "Organic chemistry of coke formation," *Appl. Catal. A Gen.*, vol. 212, no. 1–2, pp. 83–96, 2001.

[140] P. Patrono and A. La Ginestra, "Conversion of I-butene over WO3 -TiO2 Catalysts," *Appl. Catal. A Gen.*, no. 107, pp. 249–266, 1994.

[141] M. Perissinotto, M. Lenarda, L. Storaro, and R. Ganzerla, "Solid acid catalysts from clays: Acid leached metakaolin as isopropanol dehydration and 1-butene isomerization catalyst," *J. Mol. Catal. A Chem.*, vol. 121, no. 1, pp. 103–109, 1997.

[142] "Hammett acidity function." [Online]. Available: https://en.wikipedia.org/wiki/Hammett_acidity_function. [Accessed: 30-May-2017].

[143] S. Ernst, Ed., *Advances in Nanoporous Materials, vol 1*, 1st ed. Elsevier, 2009.

[144] W. Haag, B. Gates, and H. Knoezinger, Eds., *Advances in Catalysis, Volume 44*, 1st ed. Elsevier, 2000.

[145] P. J. Lucchesi, D. L. Baeder, and J. P. LongWell, "Isomerization of Butene-1 to Butene-2 over Silica-Alumina Catalyst," vol. 81, pp. 3235–3237, 1959.

[146] H. C. Woo, K. H. Lee, and J. S. Lee, "Catalytic skeletal isomerization of n-butenes to isobutene over natural clinoptilolite zeolite," *Appl. Catal. A Gen.*, vol. 134, no. 1, pp. 147–158, 1996.

[147] I. Dosuna-Rodríguez and E. M. Gaigneaux, "Glycerol acetylation catalysed by ion exchange resins," *Catal. Today*, vol. 195, no. 1, pp. 14–21, 2012.

[148] J. C. J. Bart, N. Palmeri, and S. Cavallaro, *Biodiesel science and technology, from soil to oil*, 1 st. Woodhead, 2010.

[149] J. V. Livingston, *Trends in Water Pollution Research*. Nova Sience Publishers, Inc, 2005.

[150] A. Pandley and C. Larroche, *Biofuels, Alternative feedstocks and conversion processes*, 1 st. Elsevier, 2011.

[151] L. N. Bremus and H. G. Dieckelmann, "Process for the continuous production of triacetin," 4381407, 1983.

[152] "Matche," 2014. [Online]. Available: http://www.matche.com/equipcost/Default.html. [Accessed: 02-Apr-2017].

[153] "No Title." [Online]. Available: http://www.mhhe.com/engcs/chemical/peters/data/ce.html. [Accessed: 02-Apr-2017].

[154] Jens Balchen, *Structure in Process Control*. Springer Science, 1987.

[155] Richard Westney, *The Engineer's Cost Handbook: Tools for Managing Project costs*. CRC Press, 1997.

[156] "Financial Dictionary." [Online]. Available: http://www.investopedia.com/terms/c/circulating_capital.asp. [Accessed: 30-May-2017].

[157] "All That Stats," 2017. [Online]. Available: http://www.allthatstats.com/en/. [Accessed: 30-Apr-2017].

[158] "Euribor-rates." [Online]. Available: http://pt.euribor-rates.eu/taxas-euribor-actuais.asp. [Accessed: 20-May-2017].

Appendix

A1 – FTIR analysis of the catalysts fresh and post-reaction.

- FTIR analysis of K10 (Blue) & K10 Post-Reaction (Orange):

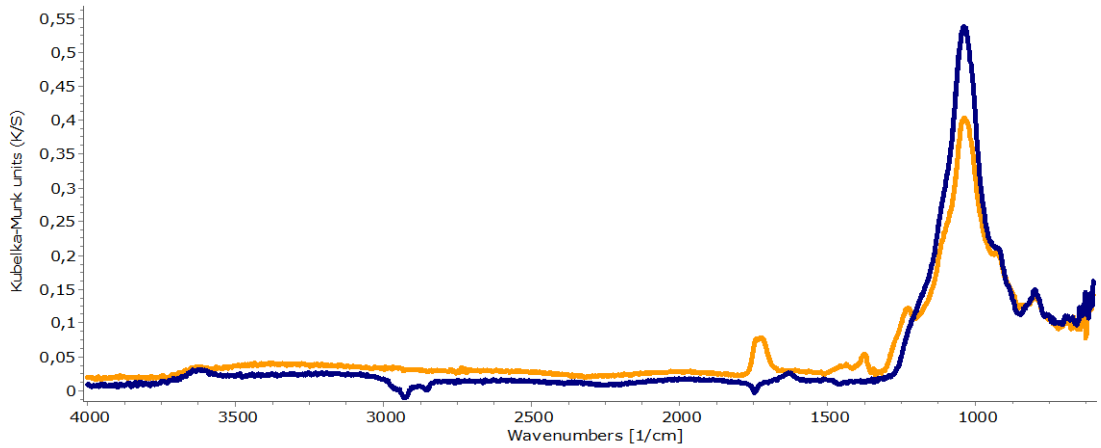

- FTIR analysis of K30 (Green) & K30 Post-Reaction (Orange):

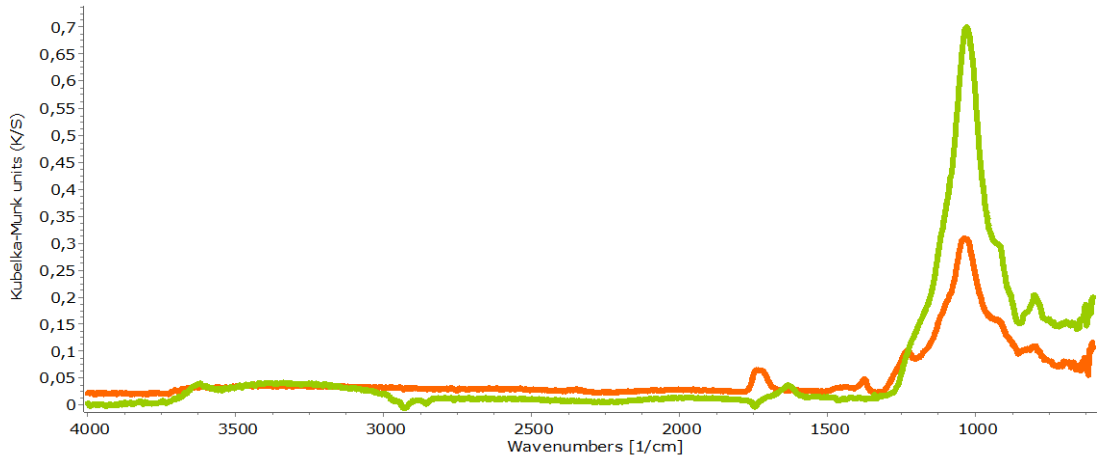

- FTIR analysis of KSF (Orange)& KSF Post-Reaction (blue):

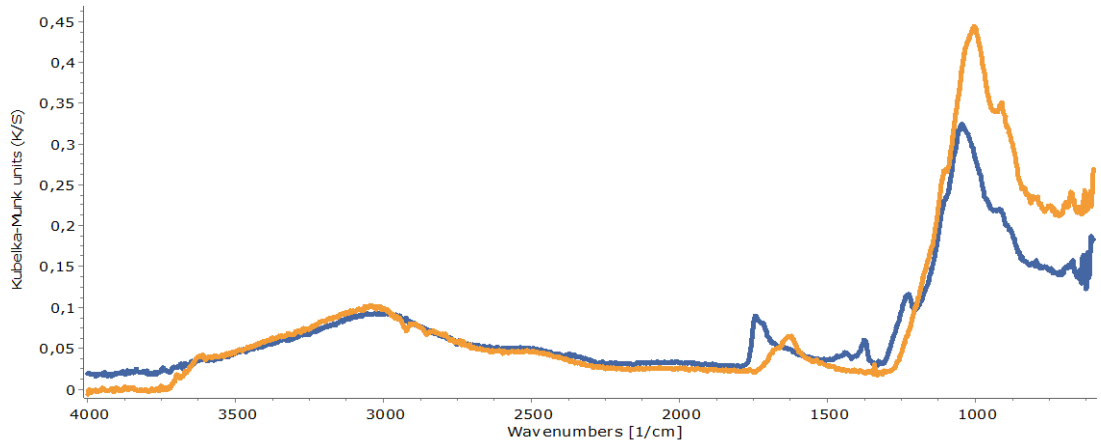

- FTIR analysis of K10/Citric (1M) fresh (brown) & K10/Citric (1M) Post-Reaction (Blue):

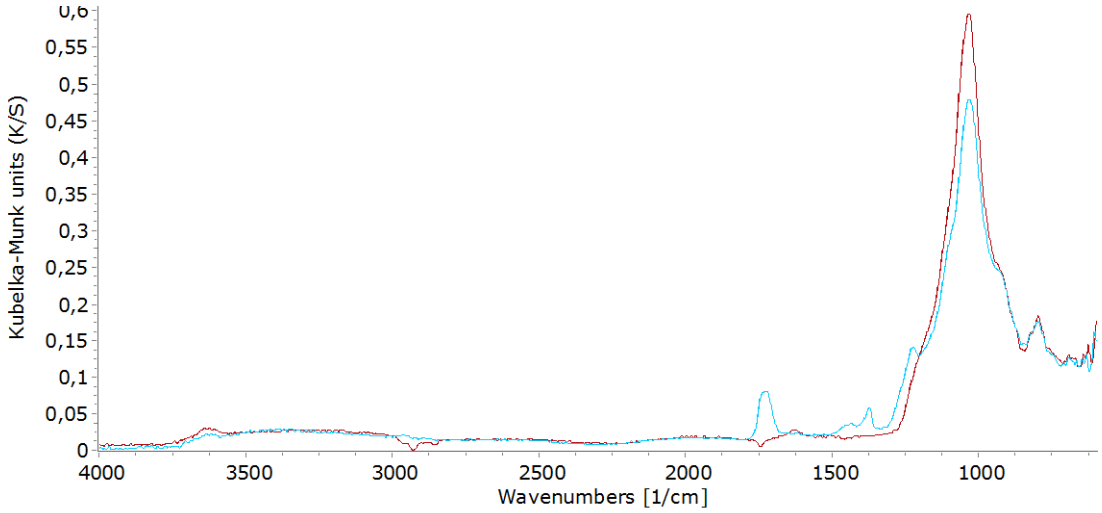

- FTIR analysis of K10 citric 2M (blue) & K10 citric 2M Post-Reaction (Orange):

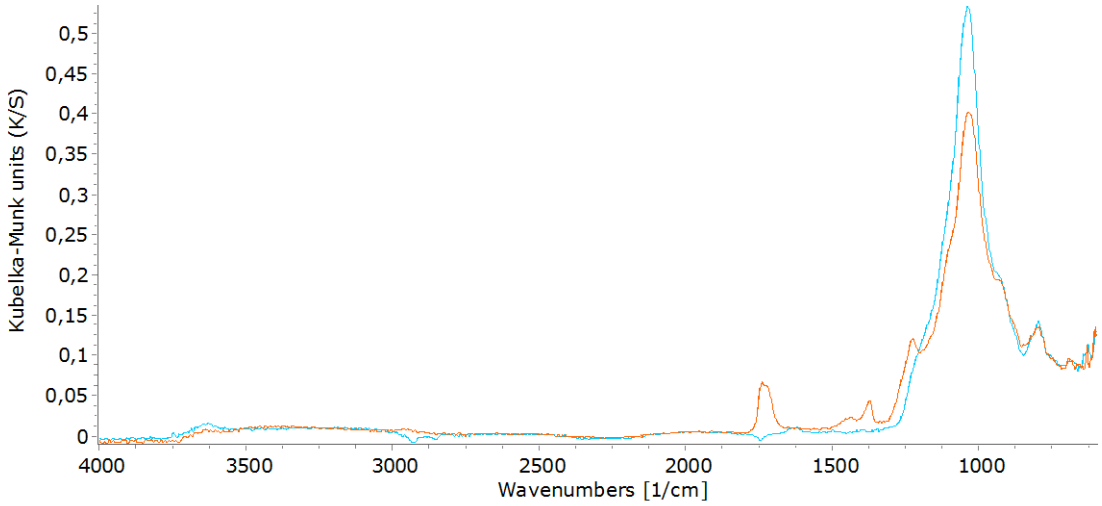

- FTIR analysis K10 phosphoric acid 1M (blue) & K10 phosphoric acid 1M Post-Reaction (green):

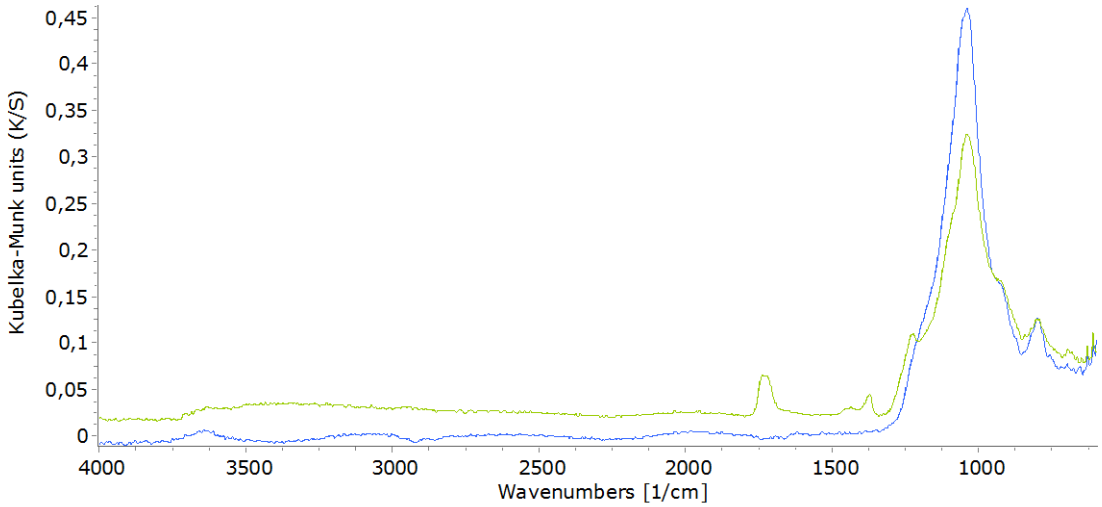

A2 – Process Diagram of Catalytic Isomerization

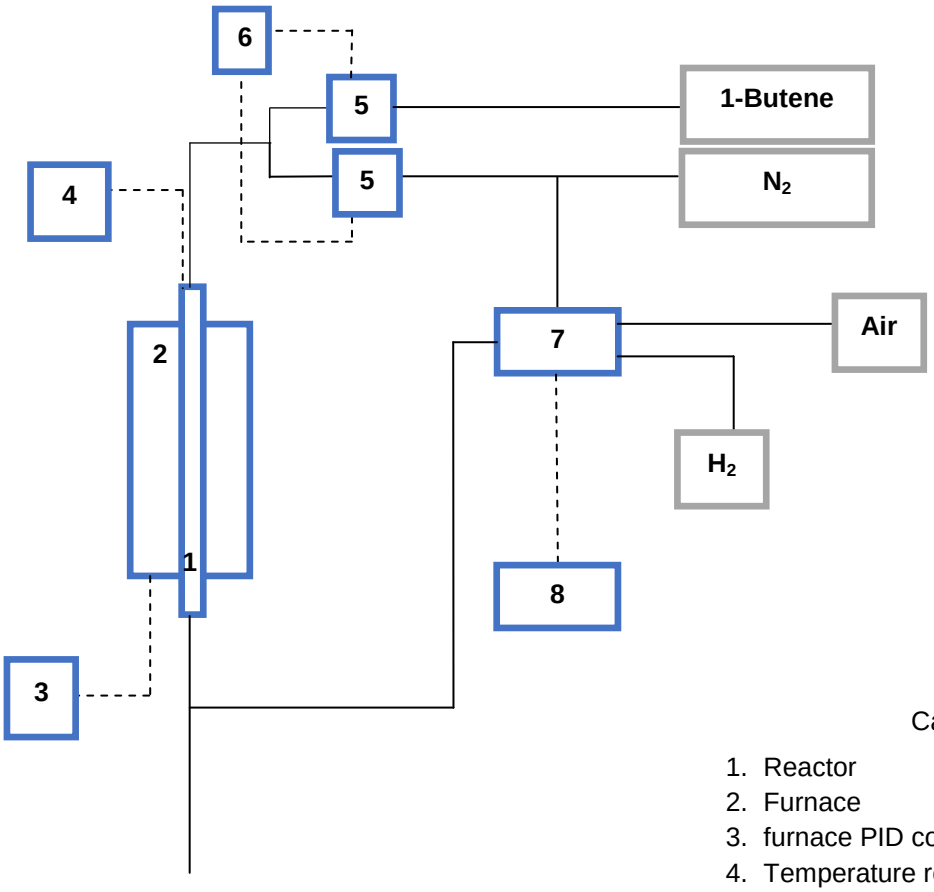

Caption:

1. Reactor
2. Furnace
3. furnace PID controller
4. Temperature reader
5. Massic flowmeters
6. Massic flowmeter controller
7. Chromatograph
8. Integrator

A3 – Chemical composition of the Commercial Catalysts

Chemical composition of the three Mt catalysts: K10 (Table 49), KSF (Table 50) and K30 (Table 51), taken from literature.

Table 49 – Chemical composition of catalyst Mt K10.

K10	Zatta, 2013	Molu, 2010	Virkutyte, 2012	Wei, 2006	Flessner, 2001	Marvi, 2011	ANL/NE, 2015
SiO2	0,44	0,69	0,69	0,4377	0,73	0,73	0,73
Al2O3	0,19	0,14	0,146	0,1857	0,14	0,14	0,14
CaO	0,01	0,015	0,015	0,0102	0,002	0,002	0,002
Na2O	0,01	0,015		0,0103	0,006	0,006	0,006
Fe2O3		0,045	0,029		0,027	0,027	0,027
H2O	0,36			0,3561			
K2O					0,019	0,019	0,019
MgO		0,02	0,02		0,011	0,011	0,011
Ignition loss		0,07			0,06		
Total	1,00	1,00	0,90	1,00	1,00	0,94	0,94

Table 50 – Chemical composition of catalyst Mt KSF

KSF	Molu, 2010	Habibi, 2007	Silva, 2011
SiO2	0,55	0,532	0,459
Al2O3	0,18	0,188	0,144
CaO	0,03	0,029	0
Na2O	0,05		0,0014
K2O	0,015		0,0028
Fe2O3	0,04	0,051	0,0318
MgO	0,03	0,028	0,0317
Sulphate	0,05	0,06	
Ignition loss	0,07	0,081	0,317
Total	1,02	0,97	0,99

Table 51 – Chemical composition of catalyst Mt K30.

K30	Flessner, 2001
SiO2	0,8
Al2O3	0,1
CaO	0,002
Na2O	0,003
K2O	0,005
Fe2O3	0,018
MgO	0,01
Ignition loss	0,06
Total	0,998

A4 – XRD patterns of the fresh and post reaction (PR) catalysts

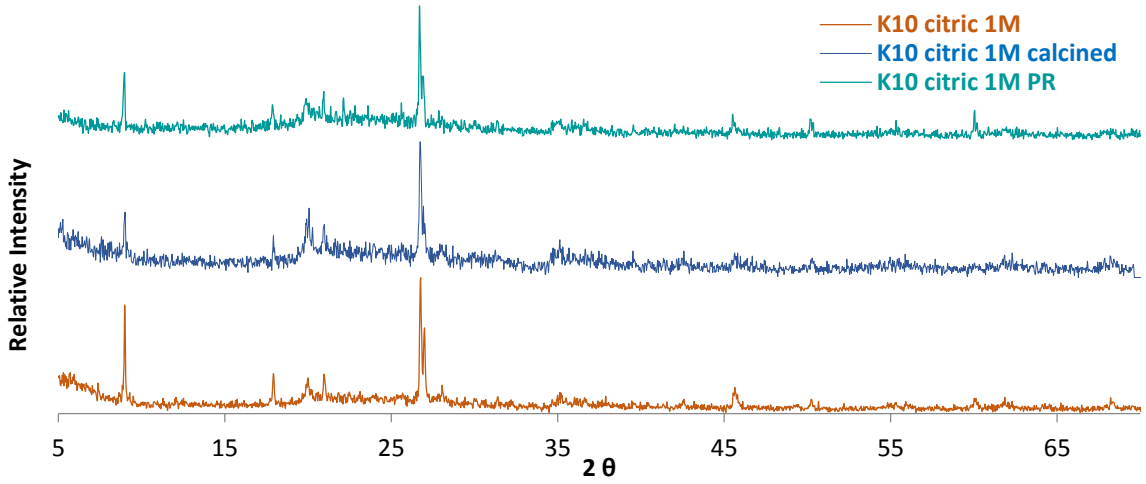

Figure 44 – XRD pattern of the catalyst K10 citric acid (1M) fresh and post reaction

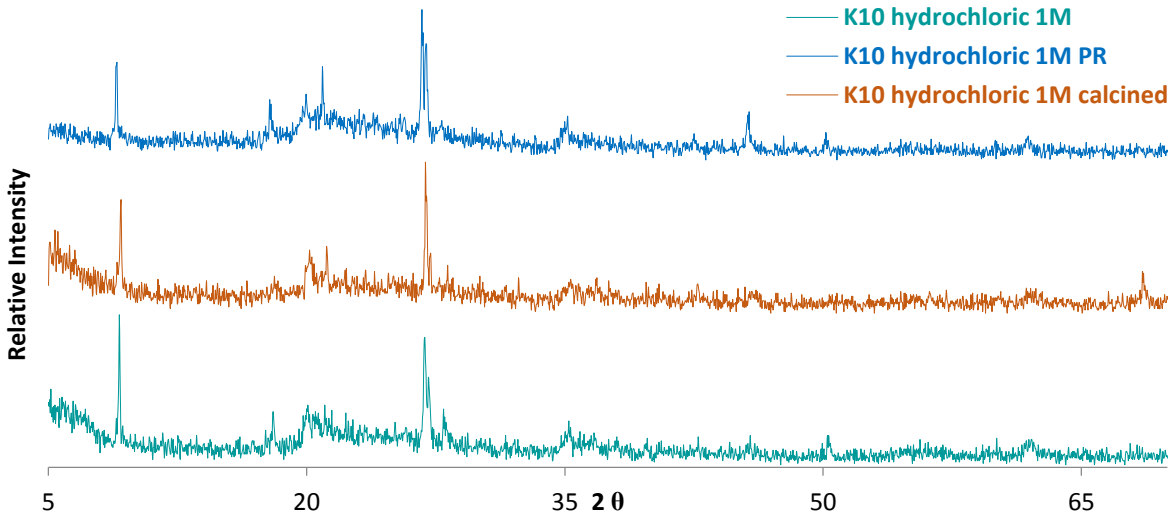

Figure 45 – XRD pattern of the catalyst K10 hydrochloric acid (1M) fresh and post reaction

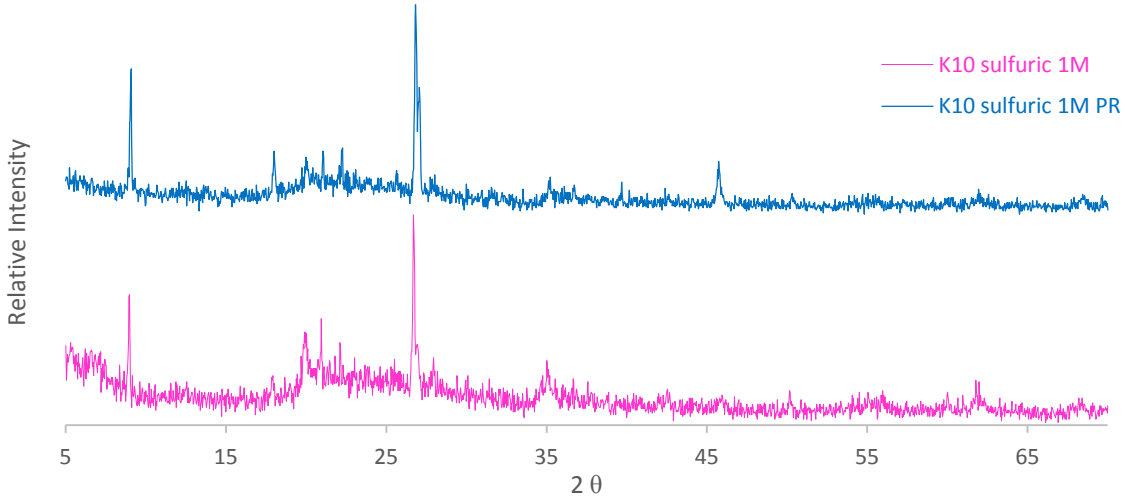

Figure 46 – XRD pattern of the catalyst K10 sulfuric acid (1M) fresh and post reaction

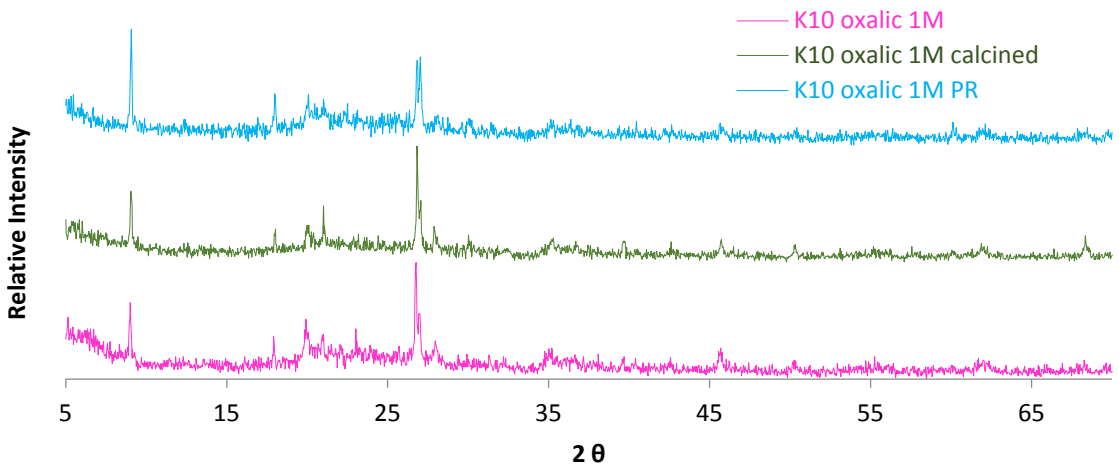

Figure 47 – XRD pattern of the catalyst K10 oxalic acid (1M) fresh and post reaction

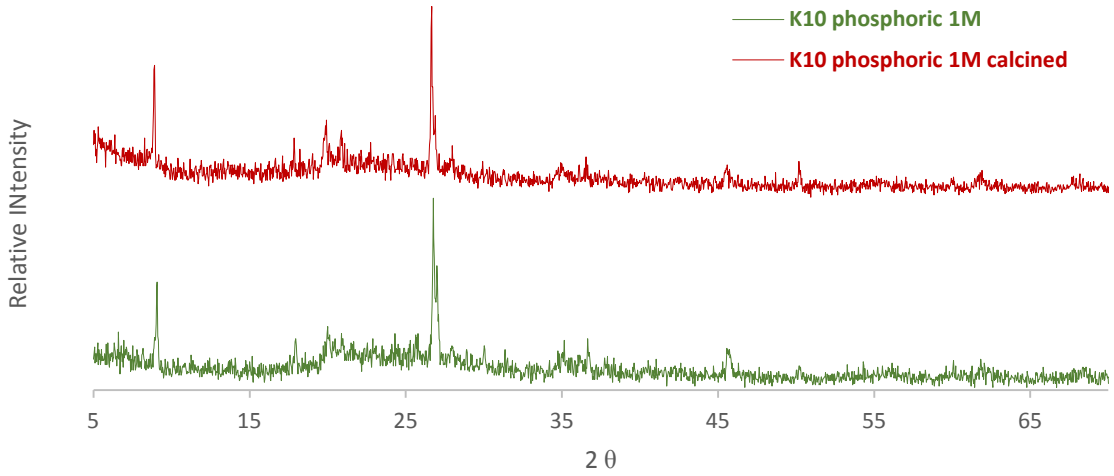

Figure 48 – XRD pattern of the catalyst K10 phosphoric acid (1M) fresh and post reaction

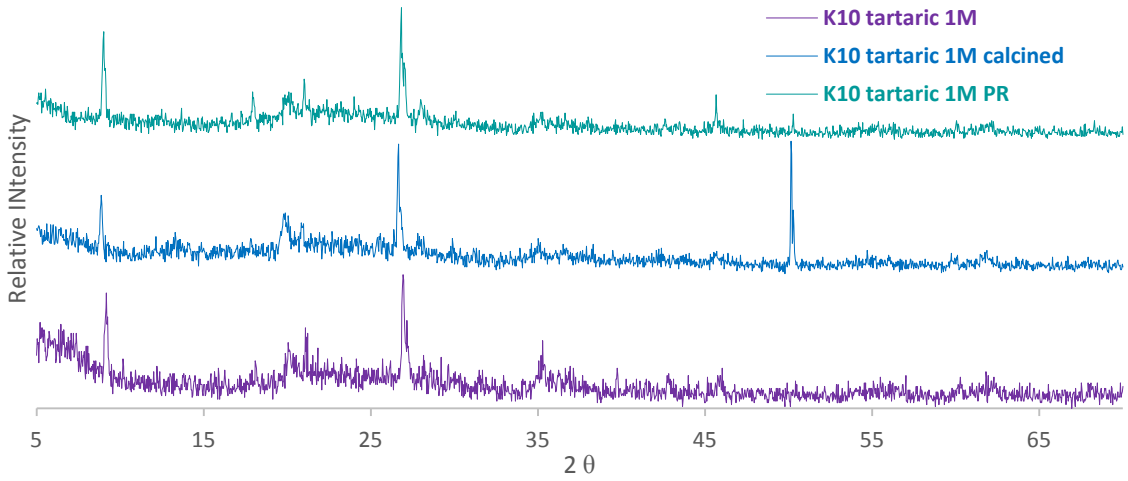

Figure 49 – XRD pattern of the catalyst K10 tartaric acid (1M) fresh and post reaction

A5 –Results of the studied catalysts in the Glycerin Acetylation.

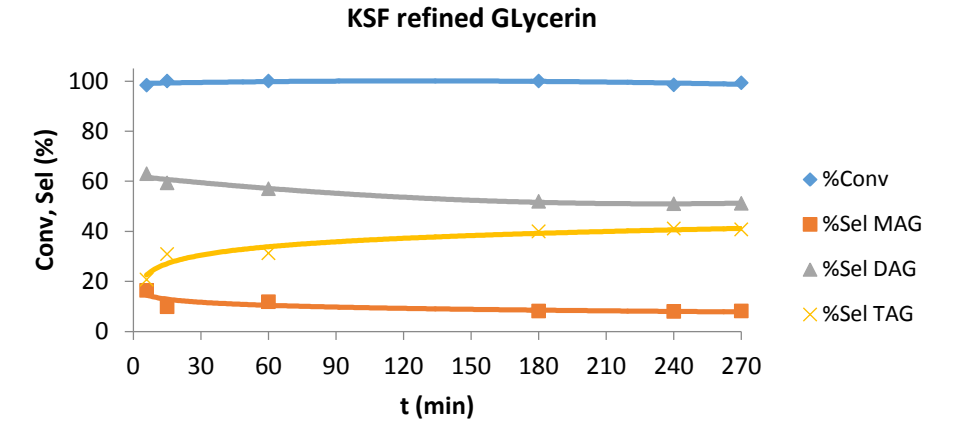

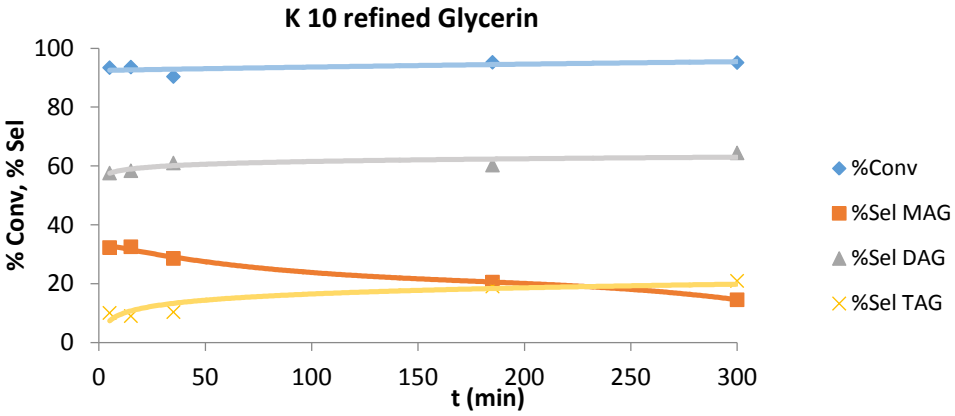

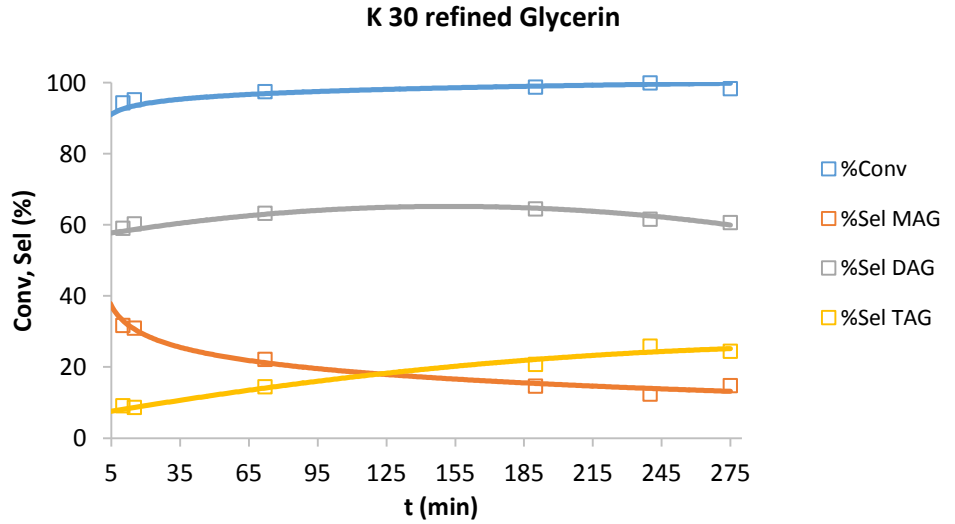

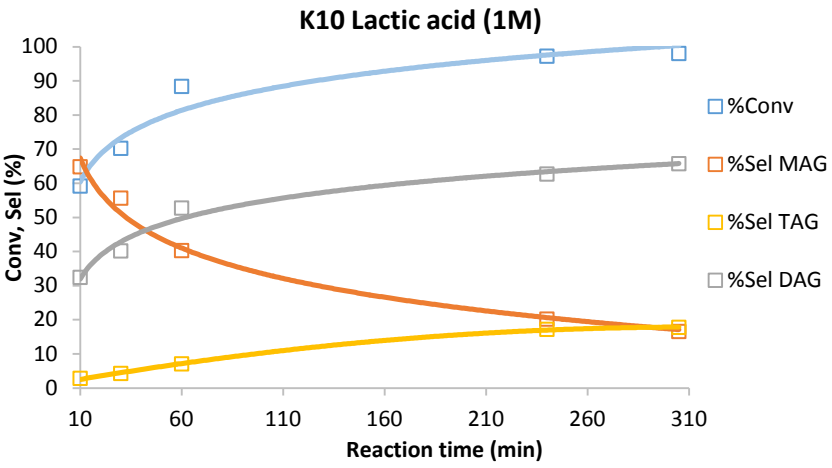
K10 Lactic acid (1M)
Conv, Sel (%)
Reaction time (min)
%Conv
%Sel MAG
%Sel TAG
%Sel DAG

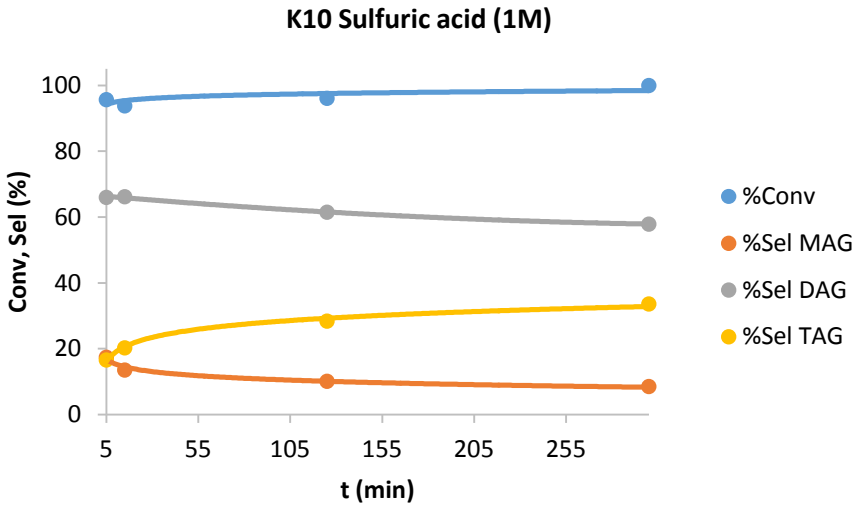
K10 Sulfuric acid (1M)
Conv, Sel (%)
t (min)
%Conv
%Sel MAG
%Sel DAG
%Sel TAG

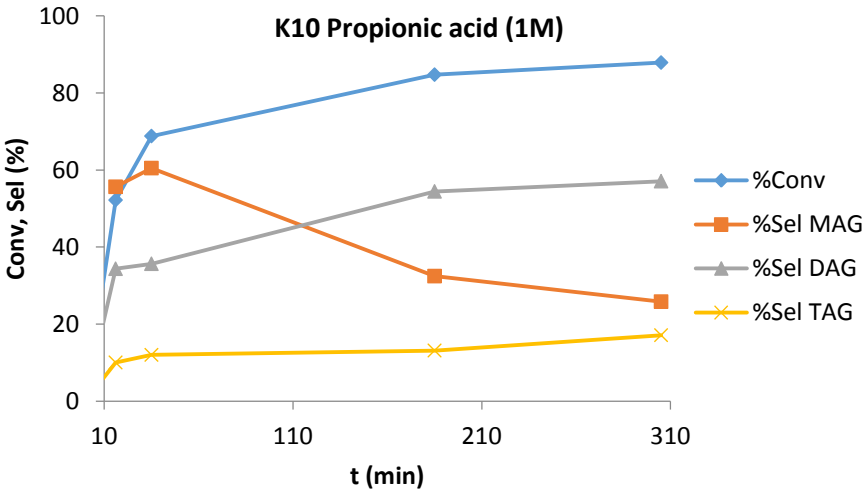
K10 Propionic acid (1M)
Conv, Sel (%)
t (min)
%Conv
%Sel MAG
%Sel DAG
%Sel TAG

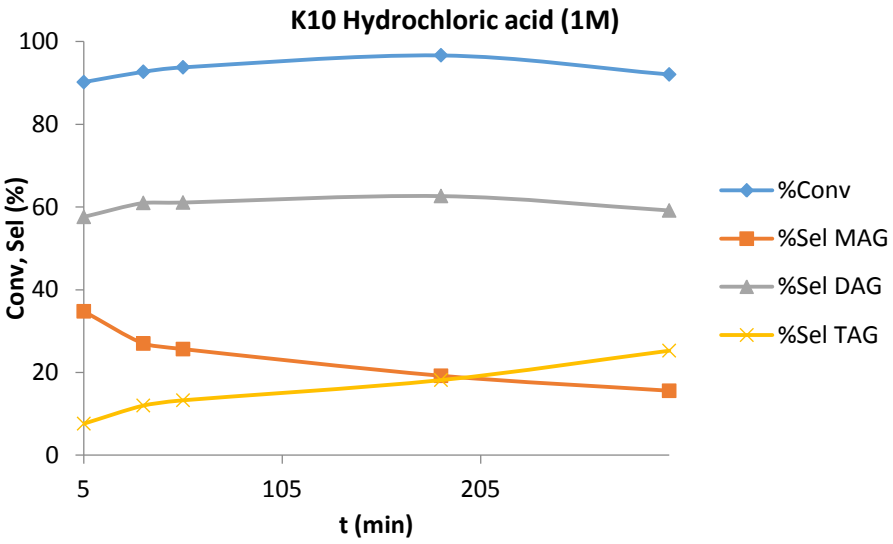
K10 Hydrochloric acid (1M)
100
80
60
40
20
0
Conv, Sel (%)
5
105
205
t (min)
%Conv
%Sel MAG
%Sel DAG
%Sel TAG

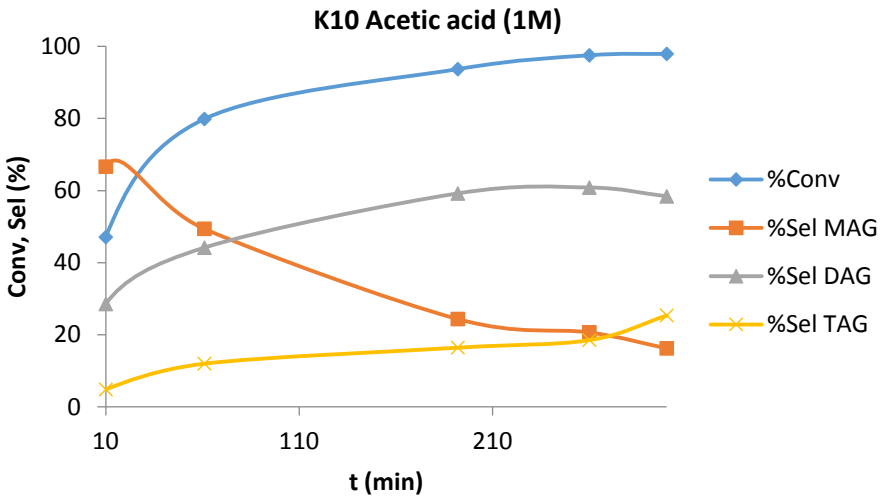
K10 Acetic acid (1M)
100
80
60
40
20
0
Conv, Sel (%)
10
110
210
t (min)
%Conv
%Sel MAG
%Sel DAG
%Sel TAG

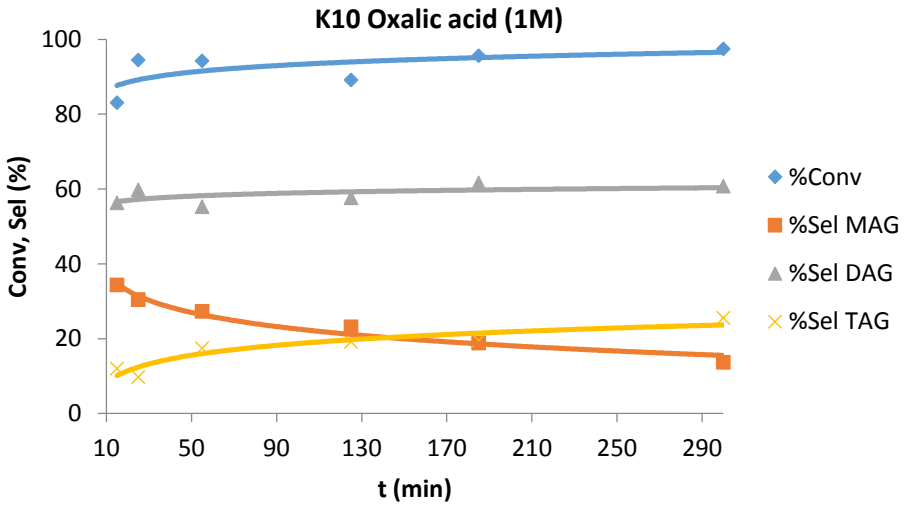
K10 Oxalic acid (1M)
100
80
60
40
20
0
Conv, Sel (%)
10
50
90
130
170
210
250
290
t (min)
%Conv
%Sel MAG
%Sel DAG
%Sel TAG

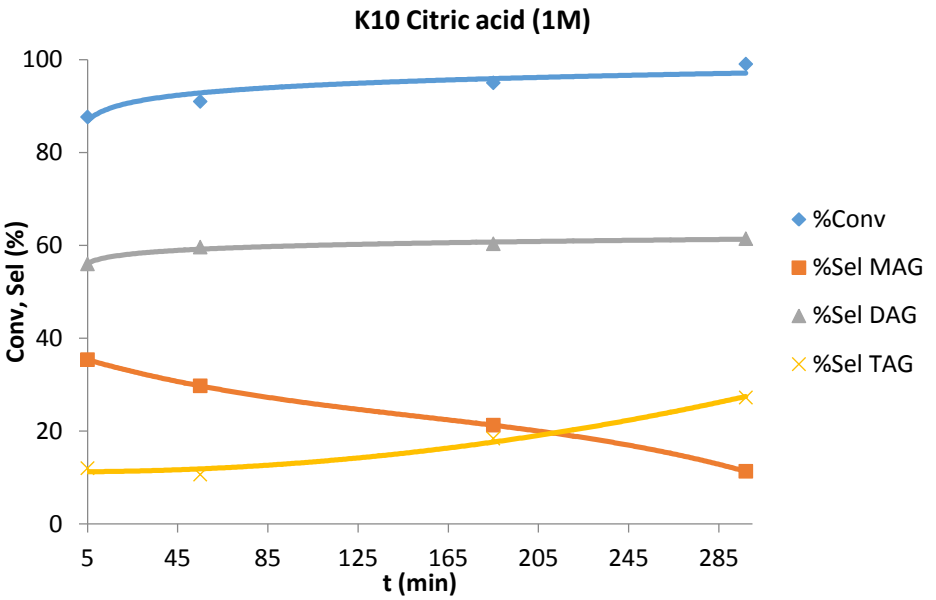
K10 Citric acid (1M)
Conv, Sel (%)
100
80
60
40
20
0
5
45
85
125
165
205
245
285
t (min)
%Conv
%Sel MAG
%Sel DAG
%Sel TAG

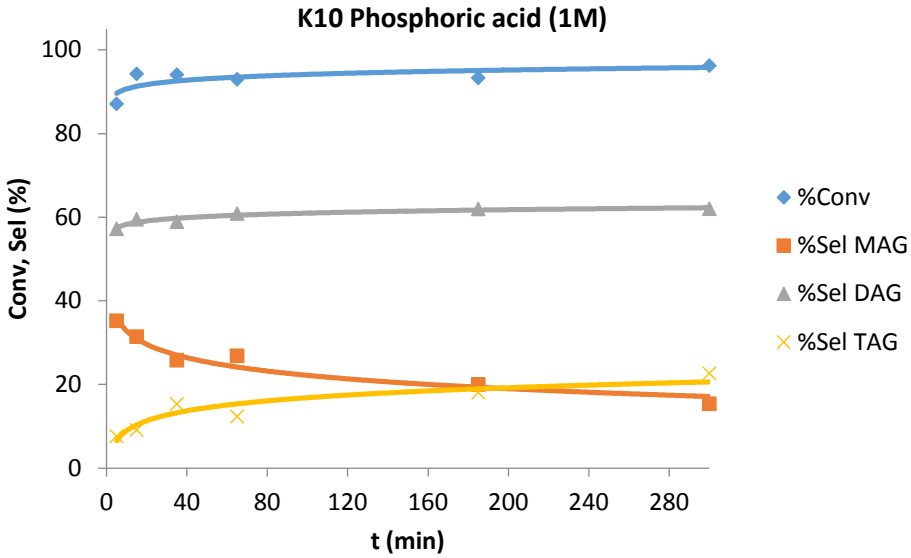
K10 Phosphoric acid (1M)
Conv, Sel (%)
100
80
60
40
20
0
0
40
80
120
160
200
240
280
t (min)
%Conv
%Sel MAG
%Sel DAG
%Sel TAG

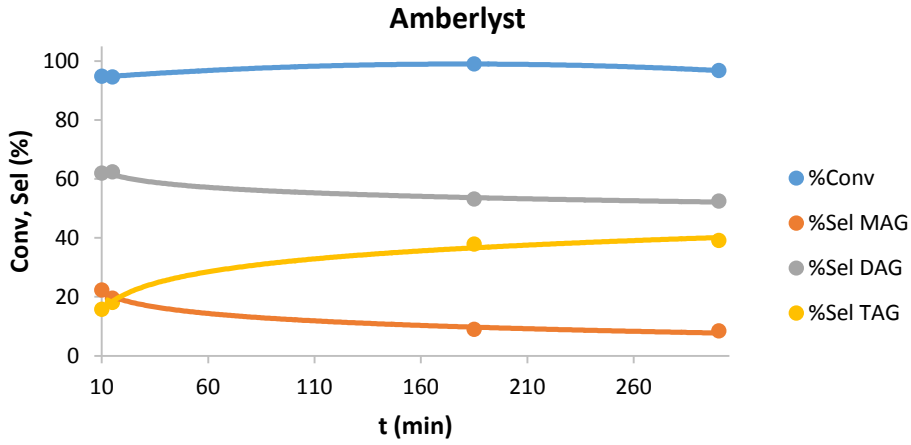
Amberlyst
Conv, Sel (%)
100
80
60
40
20
0
10
60
110
160
210
260
t (min)
%Conv
%Sel MAG
%Sel DAG
%Sel TAG

A6 – Performance of the simulated reaction

Posterior to the economic analysis, the simulated acetylation reaction was performed. On the first step the reaction was carried out with na excess of 9.6:1 of acetic acid to crude glycerin, during 2.5 hours (150 min) using as Catalyst Gly_SO_4 (10 wt% of Glycerin).At the 2.5 hours mar kit was introduced acetic anhydride at 2:1 molar ratio to inicial Glycerin. The results are displayed on the following figure (Figure 50).

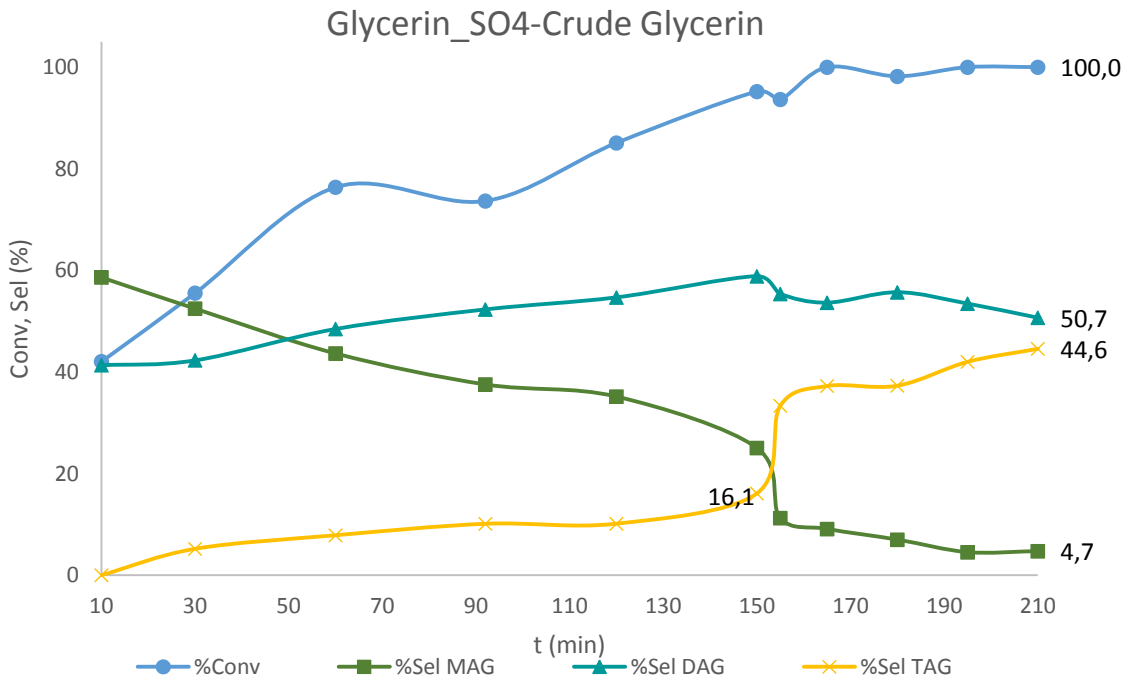

Figure 50 - Acetylation using catalyst Glycerin_SO_4, with a catalyst amount of 10 wt% of Glycerin and a molar ratio of HAc to Gly of 9.6:1, at 125 ºC during 2.5 hours, plus 2:1 of anhydride acetic to glycerin at 150 min.

As can be seen in the figure above, the addition of acetic anhydride caused an acceleration of the formation of TAG. However, due to the fact that there is a substantial amount of water and that acetic anhydride reacts instantly with it, it can be said that almost all the anhydride reacted with this element, forming acetic acid that in turn reacted with MAG and DAG.

Therefore, in the PFD simulation, it would be advantageous that posteriorly to the first reaction a distillate column sould be placed to separate all the water from the acetylated products, followed by the addition of acetc anhydride. At this time, all products would have been acetylated to TAG and this element would be separated from acetic acid in a second column. The remaining acetic acid is then reintroduced in the system. As for the 3rd DC, the triacetin is purified in order to achieve a purity of 99.9 %.

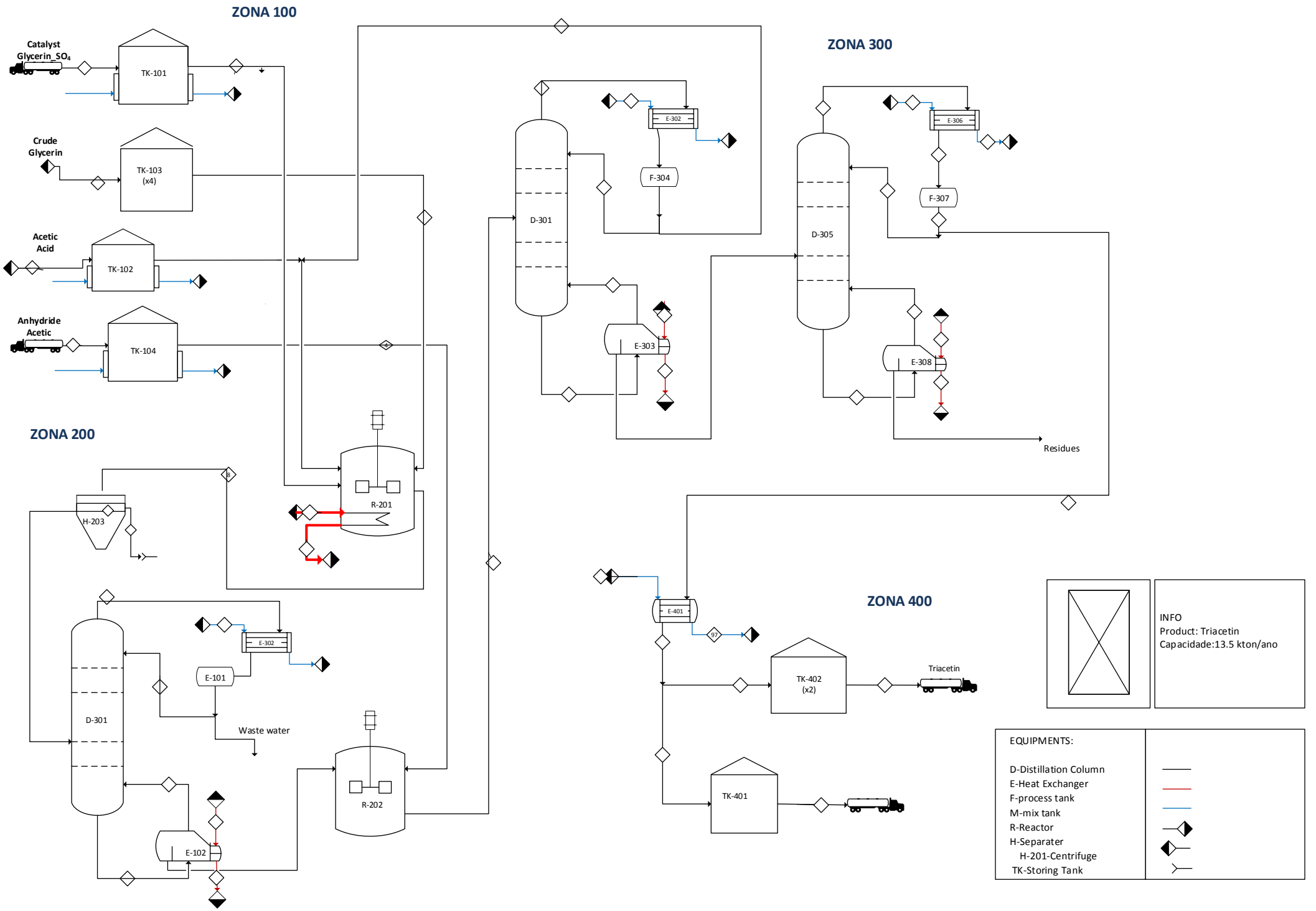
ZONA 100
Catalyst Glycerin_SO4
TK-101
Crude Glycerin
TK-103 (x4)
Acetic Acid
TK-102
Anhydride Acetic
TK-104
ZONA 200
H-203
R-201
E-302
E-101
D-301
Waste water
R-202
E-102
ZONA 300
E-302
F-304
D-301
E-303
E-306
F-307
D-305
E-308
Residues
ZONA 400
E-401
TK-402 (x2)
Triacetin
TK-401
INFO
Product: Triacetin
Capacidade:13.5 kton/ano
EQUIPMENTS:
D-Distillation Column
E-Heat Exchanger
F-process tank
M-mix tank
R-Reactor
H-Separater
H-201-Centrifuge
TK-Storing Tank